INVESTIGATING CONDUCTED MICROVASCULAR RESPONSE TO LOCALIZED OXYGEN DELIVERY *IN VIVO* USING A NOVEL MICRO-DELIVERY APPROACH

(Thesis format: Integrated Article)

by

Nour W. Ghonaim

Graduate Program in Biomedical Engineering

A thesis submitted in partial fulfillment
of the requirements for the degree of
Doctor of Philosophy

The School of Graduate and Postdoctoral Studies
The University of Western Ontario
London, Ontario, Canada

Abstract

Since erythrocytes release the vasodilator adenosine triphosphate (ATP) in an oxygen (O_2) dependent manner, erythrocytes are proposed to play a central role in O_2 regulation. This ATP signaling mechanism is proposed to be most efficient in the capillaries due to the short diffusion distance to the electrically coupled endothelium which communicates directly with arterioles. We hypothesize that capillaries are able to signal upstream arterioles for changes in erythrocyte supply rate in response to changes in capillary erythrocyte O_2 saturation (SO_2) through SO_2-dependent ATP signaling. To test this hypothesis, we have developed a micro-delivery system for controlling the O_2 availability to highly localized regions of the micro-vascular bed within intact tissue (rat Extensor Digitorum Longus). This approach allows for altering the erythrocyte SO_2 level in selected capillaries while simultaneously recording blood flow changes using *in vivo* video microscopy (IVVM). Three designs for the O_2 exchange outlet were tested. Gas with varying levels of O_2 was directly transported to specific locations on the surface of the muscle through a circular micro-outlet (~100 μm in diameter), a square micro-slit (200 μm x 200 μm), or a rectangular micro-slit (1000 μm wide x 200 μm long) patterned in ultrathin glass/plastic sheet using state-of-the-art microfabrication techniques. Video sequences captured during oscillating O_2 levels were processed for changes in capillary hemodynamic parameters and erythrocyte SO_2. Our results indicated that a sufficient number of capillaries need to be affected by local O_2 perturbations in order to elicit micro-vascular responses.. Although erythrocyte SO_2 can be measured in single capillaries flowing over an O_2 micro-outlet down to 100 μm in diameter, at least 3-4 capillaries needed to be stimulated within a branching capillary network in order to induce conducted micro-vascular responses. Since the measured supply rate responses show strong

linear correlation with capillary erythrocyte SO_2, the responses are suggested to be linked to an SO_2-dependent signaling mechanism by the erythrocyte, which further supports our hypothesis. Based on the results, we have successfully designed a novel micro-delivery device for localized O_2 exchange at the microvasculature to understand fundamental mechanisms of micro-vascular regulation of O_2 supply.

Keywords: Adenosine triphosphate (ATP), oxygen saturation (SO_2), *in vivo* video-microscopy (IVVM), microcirculation, microfabrication, O_2 micro-delivery, hemodynamics, conducted microvascular response.

Co-Authorship Statement

Chapter 1 entitled "Understanding oxygen transport and microvascular regulation" was written by Nour W. Ghonaim with input from Dr. Christopher G. Ellis and Dr. Daniel Goldman. Chapter 2 entitled "A Micro-delivery Approach for Studying Microvascular Responses to Localized Oxygen Delivery" was written by Nour W. Ghonaim with input from Dr. Christopher G. Ellis, Dr. Daniel Goldman, and Dr. Jun Yang. The O_2 micro-delivery system was designed by Nour W. Ghonaim, Dr. Leo W.M. Lau, Dr. Daniel Goldman, Dr. Christopher G. Ellis, and Dr. Jun Yang. The micro-fabrication of the O_2 micro-outlets in ultrathin glass was fully conducted by Nour W. Ghonaim at the nanofabrication laboratory at Western University, Canada. The *in vivo* experiments with the O_2 micro-delivery system were fully conducted by Nour W. Ghonaim under the supervision of Ms. Stephanie Milkovich. Data analysis was fully performed by Nour W. Ghonaim with technical assistance by Ms. Stephanie Milkovich and with intellectual input on data interpretation from Dr. Christopher G. Ellis and Dr. Jun Yang. The mathematical model simulating the PO_2 tissue distribution from O_2 micro-outlets was developed by Dr. Daniel Goldman and simulations were run by Nour W. Ghonaim. Also, Dr. Goldman wrote the section titled "Mathematical Modeling of the PO_2 Distribution Profile". Chapter 3 entitled "Modeling steady state SO_2-dependent changes in capillary ATP concentration using novel O_2 micro-delivery methods" was written by Nour W. Ghonaim with input from Dr. Graham M. Fraser, Dr. Christopher G. Ellis, Dr. Jun Yang, and Dr. Daniel Goldman. The computational models that describe O_2 and ATP transport in the capillaries were developed by Dr. Daniel Goldman. Simulations were run by Nour W. Ghonaim. Data analysis was performed by Nour W. Ghonaim and Dr. Graham M. Fraser with intellectual input on data interpretation from Dr. Christopher G. Ellis,

Dr. Daniel Goldman, Dr. Graham Fraser, and Dr. Jun Yang. Chapter 4 entitled "Conducted Microvascular Response to Localized Oxygen Delivery using A Novel Micro-delivery Approach" was written by Nour W. Ghonaim with input from Dr. Christopher G. Ellis and Dr. Jun Yang. The O_2 micro-delivery system was designed by Nour W. Ghonaim, Dr. Leo W.M. Lau, Dr. Daniel Goldman, Dr. Christopher G. Ellis, and Dr. Jun Yang. The micro-fabrication of the O_2 micro-outlets in ultrathin glass was fully conducted by Nour W. Ghonaim at the nanofabrication laboratory at Western University, Canada. The micro-fabrication of the O_2 micro-slit in ultrathin plastic was conducted by Nour W. Ghonaim with the help of Hugo W. Reshef and Mohammad Tauhiduzzaman at the National Research Council, Research Park, London, Ontario. The *in vivo* experiments with the O_2 micro-delivery system were fully conducted by Nour W. Ghonaim. Data analysis was fully performed by Nour W. Ghonaim with intellectual input on data interpretation from Dr. Christopher G. Ellis, Dr. Daniel Goldman, and Dr. Jun Yang. Chapter 5 entitled "General Discussion" was written by Nour W. Ghonaim with input from Dr. Christopher G. Ellis and Dr. Daniel Goldman.

Acknowledgments

First I would like to thank my amazing supervisors Professor Jun Yang and Professor Christopher Ellis for all their guidance and support throughout my Doctoral research. I am grateful for their time and understanding and I appreciate their determination to motivate me to do excellent work. I am very proud to have had the privilege to be their student and trainee. My respect for their intellect and constructive supervision is beyond that of a student to a supervisor. They will always continue to inspire me to be the best researcher and supervisor I can be. Also, I would like to thank my advisory committee members Professor Leo Lau and Professor Daniel Goldman for their advice and guidance.

I would like to thank my lab members, colleagues and technical instructors for being an amazing team and for all the help, training and support. Specifically, I would like to thank Ms. Stephanie Milkovich from Dr. Ellis' laboratory for spending countless hours training and assisting me in running my experimental procedures and data analysis. I also thank Dr. Graham Fraser from Dr. Ellis' laboratory for his help in data analysis and producing figures presented in Chapter 3. I would like to thank the members of the nanofabrication facility at Western University as well as Dr. Mei Liu, Dr. Tingjie Li, and Dr. Charles Guo from Dr. Yang's laboratory for their training and input on microfabrication techniques and microfluidic device design.

Finally, this work would have never been accomplished without the invaluable support and motivation from my parents, my sisters, and my wonderful husband. I cannot thank them more for their kindness and incentive throughout the progression of my PhD work and thesis. I admire my husband, Zaid, for continuing to push me towards success in my career and

throughout my PhD despite the distance that separated us. To my beloved family and husband I dedicate this thesis.

Table of Contents

List of Tables

List of Figures

List of Appendices

List of Abbreviations

Description	Abbreviation
Adenosine triphosphate	ATP
Adenylyl cyclase	AC
Audio Video Interleaved	AVI
Calcium	Ca^{2+}
Capillary	Cap
Cyclic adenosine monophosphate	cAMP
Cystic Fibrosis Trans-membrane Conductance Regulator	CFTR
Dual wavelength *in vivo* video microscopy	DλIVVM
Epoxyeicosanoic acids	EETs
Extensor Digitorum Longus	EDL
Hematocrit	Hct
Hill Coefficient	*n*
In vivo video microscopy	IVVM
Inhibitory regulative G-protein	Gi
Intra-peritoneal	IP
Nitric oxide	NO
O_2 consumption rate	M_0
O_2 diffusion coefficient	D
O_2 solubility	α
One Dimensional	1D
Oxygen	O_2

Oxygen partial pressure (oxygen tension)	PO_2
Oxygen Saturation	SO_2
Phosphodiesterase	PDE3B
PO_2 at 50% SO_2	*P50*
Potassium	K^+
Protein Kinase A	PKA
Purinergic receptors	P_{2y}
Red Blood Cell	RBC
Smooth Muscle Cells	SMCs
S-nitroso group	SNO
Supply Rate	SR
Three Dimensional	3D
Two Dimensional	2D

Chapter 1

1 Understanding oxygen transport and microvascular regulation

1.1 Introduction

The mechanisms regulating oxygen (O_2) supply in microvascular networks to meet tissue O_2 demand comprise one of the most critical physiological regulation systems. The understanding of O_2 transport and regulation is fundamental to the understanding of the pathophysiology underlying several microvascular diseases. The increased diffusion distance of O_2 in sepsis and the compromised vascular reactivity in type II diabetes eventually lead to tissue hypoxia and organ failure (Ellis et al. 2002; 2010, Goldman et al. 2004, Sprague et al. 2006; 2010). In the microcirculation, O_2 is transported by erythrocytes bound to hemoglobin and is unloaded near metabolically active tissue down its partial pressure (PO_2) gradient. The hemoglobin molecule has four subunits each of which contains an O_2 binding site. Hemoglobin binds O_2 in a cooperative manner such that binding of O_2 to one of the subunits facilitates binding by the others. When all four binding sites are occupied by O_2, hemoglobin is in its fully saturated state. Due to the cooperative binding, the hemoglobin O_2 saturation (SO_2) level is related to blood PO_2 in a sigmoidal relationship described by the Hill Equation (Hill 1910):

$$S(P)=P^n/(P^n+P_{50}{}^n)$$

Where, $S(P)$ is the hemoglobin SO_2, P is blood PO_2, $P50$ is blood PO_2 at 50% SO_2, and n is the Hill coefficient, which describes cooperativity of binding.

This chapter provides a summary of the literature describing the theories and mechanisms by which O_2 supply and demand are matched and the possible role of the erythrocyte through O_2 saturation (SO_2)-dependent ATP release. Then, the chapter will present a review of the techniques and mathematical models developed for investigating SO_2-dependent ATP signaling both *in vivo* and *in vitro*. Finally, findings from recent studies suggesting the capillary bed as the site for SO_2-dependent ATP release will be presented.

1.2 Matching oxygen supply and demand: Where is the sensor?

In 1919, over 90 years ago, August Krogh along with his colleague, K. Erlang, developed a mathematical model to describe regulation of O_2 transport to metabolic tissue. According to Krogh's model, O_2 loss only occurs in the capillary bed with each capillary supplying O_2 radially to the surrounding cylindrical tissue volume "the Krogh cylinder" (Krogh, 1919). In this model, both O_2 diffusivity and tissue O_2 consumption rate were assumed to be constant (Krogh, 1919). The model suggested that capillary density has to be constantly adjusted to match O_2 demand (Krogh, 1919).

In 1970, B.R. Duling and R.M. Berne demonstrated that longitudinal O_2 partial pressure (PO_2) gradients exist in the arterioles and that substantial O_2 diffusional loss occurs across the arteriolar wall and other locations along the microvasculature (Duling and Berne 1970). Studies on different animal models and tissue preparations by various groups confirmed these findings and reported the establishment of periarteriolar PO_2 gradients prior to reaching the capillaries, which may be partially due to diffusional exchange of O_2 between micro-vessels (Swain and Pittman 1989, Ellsworth and Pittman

1990, Stein et al. 1993, Ellsworth et al. 1994, Tsai et al. 2003). In arterioles, O_2 diffusional loss across the wall causes the red blood cells (RBCs) nearest the wall to have relatively lower SO_2 than those near the center line (Ellsworth and Pittman 1986, Carvalho and Pittman 2008). Plasma skimming would result in uneven erythrocyte distribution at bifurcations (Pries et al. 1996), which leads to the observed heterogeneity in capillary SO_2 and supply rate (Tyml et al. 1981, Ellis et al. 1994). Since capillary perfusion alone is not indicative of proper O_2 supply, the Krogh model cannot fully account for the complexity of micro-vascular O_2 regulation.

A more sensitive and local O_2 regulation mechanism must exist in order to tightly control the distribution of erythrocytes to capillaries with varying O_2 environments (Ellis et al. 2005; 2012, Ellsworth et al. 2009). Since the myogenic response (leading to changes in vascular wall tension) and the flow response (leading to changes in shear stress) are independent of changes in the local O_2 content, they cannot be proposed in the primary regulation of O_2 supply (Ellis et al. 2012). Also, although changes in tissue metabolism will trigger O_2 supply rate changes, it is unlikely that under normal physiological conditions, the regulatory system will delay its response until the tissue becomes hypoxic (Ellis et al. 2012). The system has to constantly adjust and maintain a homogenous O_2 supply and erythrocyte distribution across the micro-vascular bed. This demands a highly localized sensory mechanism, hence the question investigated by several research groups: "where is the O_2 sensor?"

Some groups have suggested micro-vessels or the cells comprising vascular walls (smooth muscle cells or endothelial cells) might act as vascular O_2 sensors (Pittman and Duling 1973, Duling 1974, Jackson and Duling 1983, Jackson 1987, Ellsworth et al.

1988; 1990; 1994, Hester 1993, Messina et al 1994, Pries et al. 1995). Others have suggested the sensor is localized in the tissue surrounding the micro-vessels (parenchymal cells) (Haddy and Scott 1968, Harder et al. 1996). Recently, it has been proposed that the erythrocyte itself may act as a vascular sensor and a key regulator of O_2 supply. This was based on the observation by Stein et al. (1993), that O_2 content (proportional to SO_2) is more important than PO_2 in generating a micro-vascular response. Since O_2 content reflects the status of hemoglobin, carried by the erythrocytes, which traverse micro-vessels experiencing varying PO_2 environments, the erythrocyte was suggested as the vascular PO_2 sensor and effector (Ellsworth et al. 1995, Jia et al. 1996).

There are three mechanisms suggested by which the erythrocyte may act on the micro-vasculature. Stamler et al. (1997) proposed the S-nitroso (SNO) group in micro-vascular signaling. The low molecular weight nitroso group is carried on the cysteine (cys93) residue of the hemoglobin molecule. Under low PO_2 conditions, the conformational change associated with the desaturation of hemoglobin decreases the binding affinity of SNO to hemoglobin. The released SNO from saturated hemoglobin is proposed to act as a potent vasodilator (Jia et al. 1996, Stamler et al. 1997). The measured venous concentrations of SNOs are much less than in the arterial end which suggests these groups are picked up in the lungs when O_2 levels are high. Despite the presence of some evidence to support the above hypothesis (Liu et al. 2004, Stamler et al. 1997), the role of SNO *in vivo* remains unclear and the accuracy of SNO measurements from biological samples is questionable (Patel et al. 1999, Gladwin and Schechter 2004, Gladwin et al. 2003). Some groups also have suggested that deoxyhemoglobin may act as a nitrite

reductase converting nitrite to NO, which is known to play an important role in micro-vascular signaling (Patel et al. 1999, Cosby et al. 2003, Gladwin et al. 2004). Although this mechanism suggests the erythrocyte may act locally to vasodilate arterioles under low SO_2 conditions, it would lack the temporal resolution required to rapidly and tightly control erythrocyte distribution (Ellsworth et al. 2009). Finally, no evidence has been provided yet to elucidate the involvement of either of the above mentioned mechanisms in conducted micro-vascular response, which would be necessary to integrate the response across the arteriolar tree as well as enable signaling from the capillary bed and venular tree to regulate arteriolar blood flow distribution (Ellsworth et al. 2009).

The third mechanism involves SO_2-dependent adenosine triphosphate (ATP) release from the erythrocyte. ATP is known to be a potent vasodilator and is found in erythrocytes in millimolar concentrations (Miseta et al. 1993). ATP was shown to be released form the erythrocyte under different stimuli including hypoxia and hypercapnia (Bergfeld and Forrester 1992), decrease in pH (Ellsworth et al. 1995), and due to mechanical deformation (Sprague et al. 1996; 1998; 2006). Also, injection of ATP into the vascular lumen was shown to trigger a vaso-dilatory response (McCullough et al. 1997, Collins et al. 1998), which is proposed to be initiated by ATP binding to intraluminal purinergic receptors (P_{2Y}) (Needham et al. 1987, Rubino et al. 1995, Corr and Burnstock 1996, Malmsjo et al. 1999, Wihlborg et al. 2003). In 2001, Jagger et al. (2001) showed that ATP efflux from the erythrocyte is linearly related to hemoglobin SO_2. The optimal response was found to be near the animal's P_{50} (Sprague and Ellsworth 2012); that is PO_2 at 50% SO_2. The linear relationship between ATP efflux and SO_2 lead Jagger et al. to suggested that ATP release is elicited by the conformational change of hemoglobin as it

de-saturates (Jagger et al 2001; Ellsworth et al. 2009). To test this hypothesis, Jagger et al (2001) exposed erythrocytes to zero PO_2 in the presence of sufficient carbon monoxide to keep the hemoglobin molecule in its fully saturated state. With zero O_2 but hemoglobin fully saturated, there was no ATP efflux confirming that the conformational change of hemoglobin elicits the ATP release. The association of hemoglobin SO_2 to ATP release was further confirmed by several human studies (Roach et al. 1999, González-Alonso et al. 2002; 2006). Recently, studies have demonstrated that patients with type II diabetes, a medical condition characterized by micro-vascular dysfunction, suffer defects in the release of ATP (Sprague et al. 2006). Also, erythrocytes from human and animal models of pre-diabetes have been shown to suffer attenuated release of ATP in response to decreased O_2 levels (Hanson et al. 2009, Ellis et al. 2010). The release of ATP by the erythrocyte in response to various stimuli transformed our perspective of the erythrocytes being merely O_2 carriers to being vascular sensors actively involved in the regulation of micro-vascular O_2 supply.

1.3 Erythrocyte SO_2-dependent conducted ATP signaling

The mechanism that links the drop in SO_2 to controlled ATP release from the erythrocyte is not yet fully elucidated (Ellsworth et al. 2009). However, it is suggested that conformational changes in the hemoglobin molecules bound to the erythrocyte membrane as they desaturate (Jagger et al. 2001, Wan et al. 2008; Sridharan et al. 2010b; Forsyth et al. 2011) directly activate the heterotrimetric Gi protein or some other component in the ATP release pathway described by Sprague's group (Olearczyk et al. 2001; 2004,

Sprague et al. 1998; 2002; 2006) (Figure 1.1). Activation of Gi protein is known to increase adenylyl cyclase (AC) activity (Federman et al. 1992, Bayewitch et al. 1998), which was shown to be a component in the ATP release pathway (Sprague et al. 1998; 2001, 2008). Activation of AC increases intracellular cAMP level, which is modulated by phosphodiesterase 3B (PDE3B) activity (Hanson et al. 2008, Adderley et al. 2010a; 2010b). cAMP activates protein kinase A (PKA) (Sprague et al. 2001), which subsequently leads to activation of the cystic fibrosis trans-membrane conductance regulator (CFTR) (Sprague et al. 1998). ATP is suggested to be eventually released from the erythrocyte through the pannexin 1 channel (Sridharan et al. 2010a) (Figure 1.1). The release of ATP from the erythrocyte through the described pathway is shown to be rapid; in the order of 150-500 ms (Dietrich et al. 2000, Wan et al. 2008).

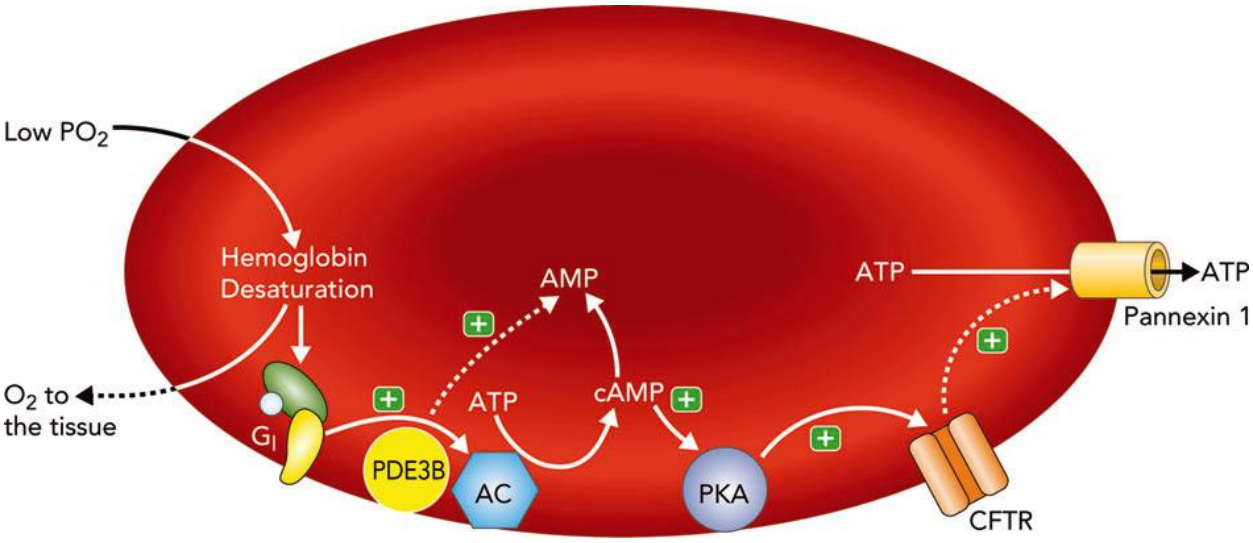

Figure 1.1 Proposed SO_2-dependent ATP release signaling pathway from the erythrocyte. Conformational changes associated with desaturation of membrane-bound hemoglobin mechanically activate the Gi heterotrimetric G protein. Consequently, the Gi

protein activates Adenylyl Cyclase (AC) increasing intracellular cAMP concentrations. The level of cAMP in the cell is modulated by phosphodiesterase function (PDE3B). Increase in cAMP activates protein kinase A (PKA) followed by cystic fibrosis transmembrane conductance regulator (CFTR) activation. ATP is eventually released from the cell through the pannexin 1 channels. Figure is reproduced from Sprague and Ellsworth 2012 with permission.

Released ATP is known to bind to P_{2y} receptors (You et al. 1999, Horiuchi et al. 2001) on the vascular endothelium, which then promotes the release of Ca^{2+} from the endoplasmic reticulum (Campbell et al. 1996) (Figure 1.2). Ca^{2+} release mediates the synthesis and release of vasodilators such as nitric oxide (NO) as well as metabolites of arachidonic acid (You et al. 1997; 1999). In order for the capillary erythrocyte supply rate to be increased in response to released ATP, the signal must be conducted upstream to the arteriolar tree. Epoxyeicosanoic acids (EETs), products of arachidonic acid, are known to activate Ca^{2+} activated K^{+} channels, which results in the hyperpolarization of endothelial and smooth muscle cells (SMCs) (Campbell et al. 1996, Dietrich et al. 1998, Fukao et al. 2001) (Figure 1.2). The hyperpolarization can be conducted to adjacent cells in the endothelium through gap junctions and to SMCs through the myoendothelial junction resulting in local and conducted vasodilation (Segal et al. 1989, Segal and Duling 1989). The ATP signal is proposed to be controlled through negative feedback mechanisms by NO or breakdown products of ATP (Olearczyk et al. 2004b, Wang et al. 2005), or through degradation by ecto-ATPases (Knowles 2011, Melani et al. 2012). The magnitude of the micro-vascular response to ATP signaling is suggested to be related to

the extent of the hyperpolarization signal and to the number of endothelial cells activated (Ellis et al. 2012). Some of the factors that would influence ATP signaling to the vascular endothelium include: the time it takes for ATP to be released following an SO_2 drop, the distance ATP has to travel from the erythrocyte membrane to the P_{2y} receptors, and the time it takes to degrade ATP by ecto-ATPases thus eliminating the signal. In order for SO_2-dependent ATP release to be a key regulator of O_2 supply, the ATP signaling mechanism must be efficient (Ellis et al. 2012).

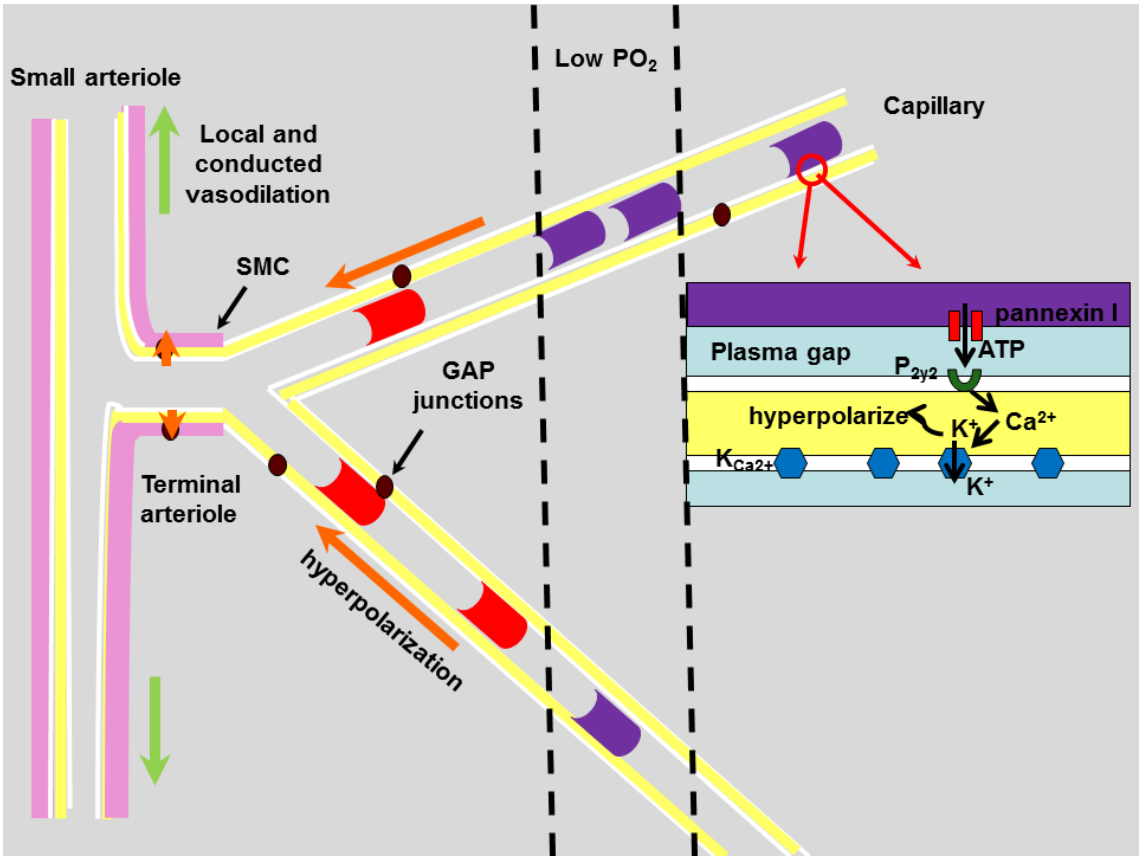

Figure 1.2 ATP-mediated conducted vasodilation response. ATP released from deoxygenated erythrocytes binds and activates purinergic (P_{2y}) receptors on the vascular endothelium. This stimulates Ca^{2+} release from the endoplasmic reticulum which eventually results in the activation of Ca^{2+} activated K^+ channels leading to endothelial hyperpolarization. The hyperpolarization is conducted to adjacent endothelial cell through gap junctions and finally to arteriolar smooth muscle cells through myo-endothelial gap junctions. Hyperpolarization of smooth muscle cells results in local and conducted vasodilation and consequent increases in the supply rate of oxygenated erythrocytes to meet the demand of the hypoxic region.

1.4 The capillary bed as the site for erythrocyte SO_2-dependent ATP release

There is a lot of debate as to the site of ATP release and action (Figure 1.3). It has been suggested that ATP is mainly released in the arterioles such that the activation of endothelial cells would result in immediate vasodilation of adjacent SMCs (Duling and Berne 1970, Duling 1974, Jackson 1987). However, the relatively short erythrocyte transit times would largely compromise the temporal and spatial localization of the signal. Also, due to the parabolic flow profile in arterioles, only those cells nearest the arteriolar wall will experience SO_2 drops and hence be involved in ATP release. Cells flowing through the centerline will experience smaller a SO_2 drop and will participate to a lesser extent in ATP signaling (Ellis et al. 2012). Venules were also suggested to play a role in O_2 regulation. The increase in hematocrit at the venules combined with low SO_2 level would result in a large amount of ATP release and a strong conducted vasodilatory signal as modeled in Arciero et al. (2008). However, since venules collect erythrocytes with a wide range of SO_2 values from various upstream capillaries, the conducted signal would be highly unspecific and may only contribute to controlling regional blood flow rather than to individual capillary networks (Ellis et al. 2012)

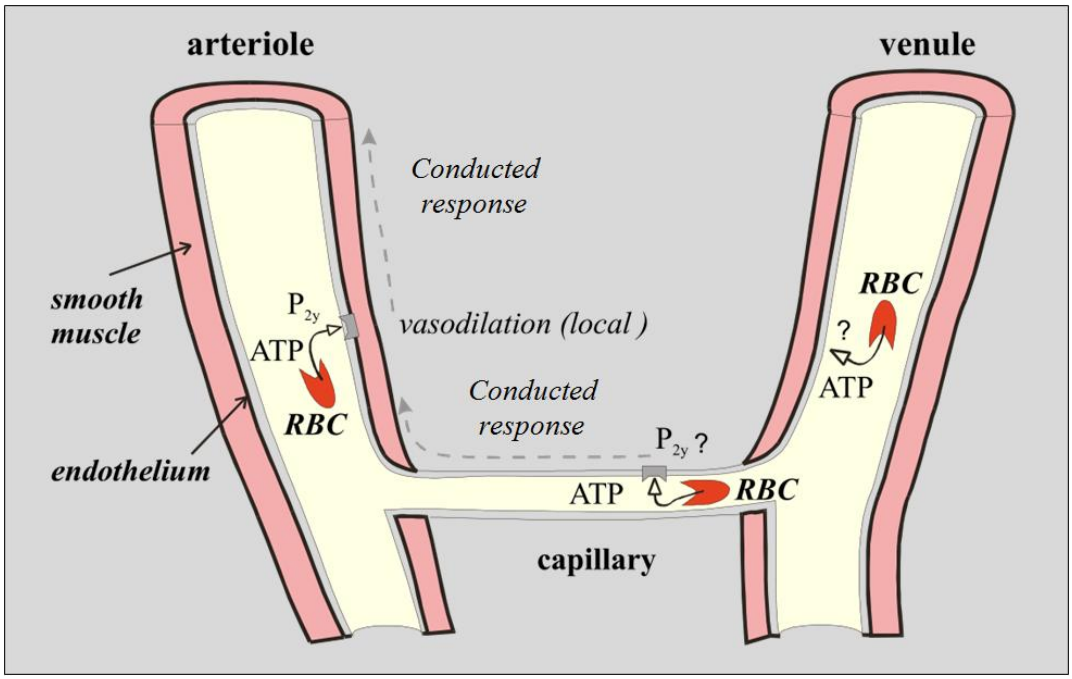

Figure 1.3 Schematic showing possible sites for SO_2-mediated ATP release and action in the microvasculature. Figure reproduced from Ellsworth et al. 1995.

Recently, capillaries have been hypothesized as the major site for SO_2-dependent ATP release and signaling (Ellis et al 2012). Capillaries are composed of endothelial cells which are known to be electrically coupled and communicating (Dietrich, 1989, Dietrich and Tyml, 1992, Song and Tyml 1993, Collins et al., 1998, Bagher and Segal, 2011). Erythrocytes traverse capillaries at relatively longer transit times, which better localizes the ATP signal. Also, the diffusion distance of ATP to the capillary endothelium is < 1 µm. Therefore, depending on the capillary diameter as well as the thickness of the erythrocyte and endothelial coating there might be a direct transfer of ATP from the pannexin 1 channel on the erythrocyte to the P_{2y} receptors on the vascular endothelium (Ellis et al. 2012). This implies more efficient and localized SO_2-dependent ATP

signaling in the capillary bed. It should be noted that in the capillaries, the erythrocyte supply rate (erythrocytes per second) is anticipated to have a great effect on the magnitude of ATP signal (Ellis et al. 2012). At an erythrocyte velocity of 100 μm/sec, each erythrocyte would stimulate the same endothelial cell (~ 104 μm long) for ~1 sec (Ellis et al. 2012). The number of erythrocytes stimulating a single endothelial cell per second would be determined by the supply rate level. For instance, at a supply rate of 10 RBC/sec, approximately 10 erythrocytes would be stimulating the same endothelial cell in 1 sec. At higher velocities, a larger number of endothelial cells would be activated per unit of time, each of which will contribute to the conducted signal (Ellis et al. 2012).

1.5 Techniques developed for investigating micro-vascular response in the capillary bed *in vivo*

Micro-vascular responses to tissue PO_2 perturbations, characterized by changes in the erythrocyte supply rates, have commonly been investigated using *in vivo* video-microscopy (IVVM) techniques (Dewhirst et al. 2000, Varghese et al. 2005, Ellis et al. 2010). IVVM allows for monitoring and recording real-time changes in micro-vascular blood flow properties (Dewhirst et al. 2000, Varghese et al. 2005, Ellis et al. 2010). Typically, studies involved altering PO_2 levels in a superfusion solution equilibrating the surface of a tissue or a vessel (Duling 1974, Jackson and Duling 1983). However, using superfusion solutions may result in washing away substances or signaling molecules from tissue surface, which would affect micro-vascular responses (Ellis et al. 2012). Also, the relatively low solubility of O_2 in saline solution presents another limitation of using

superfusion solutions as a medium for O_2 delivery or removal since erythrocytes flowing in capillaries have a much greater O_2 carrying capacity.

In order to overcome some of the drawbacks of using the superfusion technique, Dr. Chris Ellis' laboratory, at Western University, Canada, developed a gas exchange chamber in which the full bottom surface of the rat extensor digitorum longus (EDL) muscle is exposed to PO_2 perturbations (Jagger et al. 2005, Ellis et al. 2010; 2012, Ghonaim et al. 2011) as shown in Figure 1.4. Using this method, O_2 is delivered to or removed from the tissue surface through a 4 mm x 10 mm outlet covered with fluorosilicone acrylate O_2-permeable membrane of 50 μm in thickness, while maintaining constant CO_2 and temperature. The gas exchange chamber is inserted into the viewing platform of an inverted light microscope and is connected to computer-controlled flow meters. This allows for real-time videos of blood flow changes in the microcirculation to be recorded while simultaneously controlling O_2 levels in the chamber (Figure 1.4). The advantage of using this technique is that O_2 is delivered in a gas mixture bringing the system closer to physiological conditions without washing away other signalling molecules. Furthermore, by setting the minimum chamber O_2 level at 2% (15-mmHg), there should be no or minimal effect on tissue metabolism such that the resulting micro-vascular flow response can be attributed solely to changing O_2 levels. The fluorosilicone acrylate membrane is highly permeable to O_2 (O_2 permeability coefficient = 100 Barrers, where 1 Barrer = 10^{-11} (cm^3 O_2 STP) cm^2 cm^{-3} sec^{-1} $mmHg^{-1}$ (Comyn 1985)) hence, the delivered O_2 would have greater effect on the tissue PO_2 level relative to using liquid media. However, in this setup, the O_2 outlet was designed to have the EDL muscle dimensions, hence the technique measures the collective response of stimulating the full

micro-vascular bed by O_2 delivery or removal. In order to investigate the response to stimulating selected capillaries in the microvasculature, the area of the PO_2 perturbations needs to be limited.

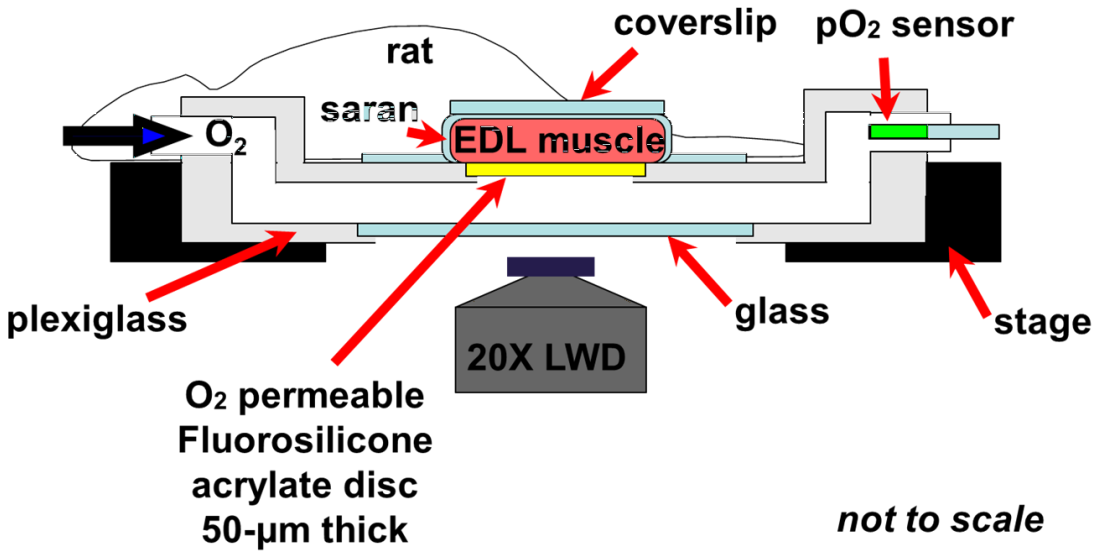

Figure 1.4 *In vivo* video microscopy (IVVM) full gas exchange chamber experimental setup. The chamber is connected to computer controlled flow meters and is inserted into the viewing platform of an inverted microscope. The extensor digitorum longus (EDL) muscle of the rat is surgically exposed and positioned surface down on the viewing platform. Oxygen (O_2) is delivered in a gas mixture to the muscle surface through an outlet with dimensions proportional to the *in situ* dimensions of the EDL muscle. O_2 levels in the chamber are measured and monitored using a fiber-optic oxygen sensor probe. The tissue is trans-illuminated, and hemodynamic responses are recorded and analyzed as O_2 levels are simultaneously oscillated while maintaining constant CO_2 and temperature.

Song and Tyml (1993) investigated the capillary sensory and integrative ability using a micro-pharmacological approach in which micropipettes are filled with either vasoconstrictors or vasodilators. Similarly, Riemann *et al.* (2010) have tried localizing tissue PO_2 perturbations using micropipettes to deliver liquids with low O_2. However, the study was conducted without measuring the impact on tissue O_2 levels or erythrocyte SO_2, which is critical to establish that an SO_2-dependent signal is induced (Jackson and Duling 1983). Until now, no technique has been developed that allows for altering and measuring erythrocyte SO_2 in selected capillaries and to simultaneously record corresponding micro-vascular hemodynamic responses.

1.6 Computational modeling of erythrocyte SO_2-dependent ATP signaling

The O_2 regulatory system in the microcirculation involves a number of integrated signaling processes that harmoniously maintain homogenous O_2 supply in response to the heterogeneity in O_2 demand. The inherent complexities of this system and the lack of current techniques to quantify the release of signaling molecules in response to hypoxia *in vivo* led to the development of theoretical and computational models to investigate micro-vascular O_2 regulation.

A theoretical model presented by Arciero et al. (2008) simulated steady-state ATP release in response to variation in O_2 consumption rates along seven representative micro-vessel segments. It was concluded that high O_2 demand stimulates ATP release from

erythrocytes resulting in conducted vasodilation in resistance vessels and concurrent increase in perfusion. It also indicated that metabolic control overrides shear stress or myogenic control mechanisms in terms of flow regulation.

In 2010, Sprague's group, together with Ellis and Goldman (Sprague et al. 2010), presented a computational model showing that mis-regulation of O_2 supply observed clinically, such as in patients with Type-2 Diabetes, cannot be corrected by regional vasodilation. Regional vasodilation results in uniform increase in flow across all downstream microvascular units rather than directing the flow specifically to undersupplied micro-vascular units. Strong vasodilators would be needed to improve oxygenation of undersupplied capillaries. It was concluded that a local sensory and regulatory mechanism is required to retrieve normal O_2 regulation.

Most recently, Goldman et al. 2012 described a novel multiscale modeling approach to investigate O_2-dependent ATP release and signaling in microcirculation. The model has two components and is based on experimental work. The first component describes ATP release by the erythrocyte through the signaling pathway previously elucidated (Sprague et al. 2001; 2002; 2006, Olearczyk et al 2004a/b, Sridharan, et al. 2010a/b). The second component describes capillary network ATP transport based on realistic *in vivo* measurements of blood flow, O_2 transport, and 3D capillary geometry. The time scales for ATP release calculated in this work were consistent with those calculated experimentally (Dietrich et al. 2000, Wan et al. 2008). This approach was most comprehensive as it allows for simulating dynamic changes in ATP release and for predicting how defects in the signaling pathway may affect O_2 regulation.

1.7 Microfluidic technology

Since microfluidic technology emerged ~40 years ago, it has been undergoing rapid development (Gravesen et al. 1993). Microfluidics refers to the "research discipline dealing with transport phenomena and fluid-based devices at microscopic length scales" (Nguyen and Wereley, 2002). Structures at the micro scale, such as outlets or channels, can be patterned in different types of materials using a variety of micro-fabrication techniques for the purpose of transporting or manipulating fluids (Nguyen and Wereley, 2002). This interdisciplinary field has a broad range of applications in engineering, chemistry, physics, and biotechnology. Since the length scales in microfluidic systems approach those in molecular processes, microfluidics technology has been an especially attractive tool with high impact in biological research (Stone and Kim 2001). Integrating multiple microfluidic components into one device allows for preparing, mixing, as well as screening samples in a single chip (Mark et al. 2010) (also referred to as lab-on-chip systems). Such systems have revolutionized diagnostic methods, blood separation, pathological testing, proteomics, and genomics (Herold and Rasooly 2009a,b, Mark et al. 2010).

Recently, Wan et al. (2008) studied shear-dependent ATP release from erythrocytes using a microfluidic approach. Erythrocytes in a cocktail of luciferin/luciferase were pumped through a narrowing in a micro-channel. Measurement of the light intensity signal generated by the ATP-luciferase reaction following erythrocyte deformation downstream of the narrowing was used to estimate the timescales involved in ATP release. Currently, similar research is being conducted at Dr. Ellis' laboratory to investigate the dynamics of

SO_2-induced ATP released from the erythrocyte. Hence, the use of microfluidic technology is anticipated to provide valuable insights into the timescales and mechanisms involved in the regulation of microvascular blood flow. Also, since microfluidic systems are highly versatile in design and application, they can be used not only in liquid manipulation and analysis but may also serve as an important tool in the limited transport of gaseous substances; for instance, O_2.

1.8 Summary

In summary, a number of theories and hypotheses exist regarding the mechanisms that regulate O_2 transport and erythrocyte distribution in the microcirculation. It is becoming more evident that the regulatory system must allow for local monitoring and sensing of the micro-vascular O_2 environment. A messenger mechanism must also exist for linking the sensory mechanism with the micro-vascular response. Many studies implicate the erythrocyte as actively involved in micro-vascular O_2 regulation. This is mainly due to its ability to release signaling molecules that act to modulate blood flow in response to a drop in internal hemoglobin SO_2. This indicates that the erythrocyte may act as a mobile sensor and effector, with the ability to sense changes in O_2 environment through hemoglobin saturation changes and to respond by the release of vasodilators in an SO_2 dependent manner. Of interest is the potent vasodilator ATP, shown to be released from the erythrocyte not only in response to hypoxia but also to a number of other stimuli. The site where this release mechanism is most efficient is still under investigation. The long erythrocyte transit times in the capillaries and the short diffusion distance of released

ATP to the endothelium suggest the capillary may be the site for O_2 signaling. Due to the inherent complexities of micro-vascular control mechanisms, computational and theoretical models have been developed to provide quantitative estimates of changes in the magnitude of ATP release from the erythrocyte under low SO_2 conditions. Also, a number of techniques have been developed to investigate micro-vascular signaling *in vivo*, however, until now no such technique exists for studying micro-vascular responses to local changes in SO_2, for instance in a few selected capillaries.

1.9 Thesis rationale and objectives

1.9.1 Rationale

Various techniques for exchanging O_2 with tissue surface *in vivo* have been implemented for studying micro-vascular responses to O_2 perturbations. However, none of these reported techniques allows for simultaneously altering and measuring erythrocyte SO_2 in selected capillaries. Limiting the area of O_2 exchange is necessary to investigate the site for major ATP release and signaling in the microvasculature.

In order to address these limitations, a novel micro-fluidic system has been developed for controlling O_2 availability to specific regions on the microvascular bed of intact muscle tissue (rat Extensor Digitorum Longus) (Ghonaim et al. 2011). This approach allows for altering erythrocyte SO_2 in selected capillaries in response to imposed local tissue PO_2 changes. Hemodynamic responses can be recorded simultaneously using IVVM. In this system, an ultrathin glass/plastic sheet micro-fabricated with an O_2 micro-outlet replaces the fluorosilicate acrylate membrane in the original gas exchange chamber (Figure 2).

Three O_2 micro-outlet designs were tested: circular micro-outlet (~100 μm in diameter), a square micro-slit (200 μm x 200 μm) or a rectangular micro-slit (1000 μm wide x 200 μm long).

Due to the complexity involved in studying the microvascular O_2 regulatory system, a computational model was developed based on that presented by Goldman et al. (2012) to describe O_2 exchange across the three proposed outlet designs. The generated 3D tissue PO_2 profiles and ATP vessels maps provided insight into the optimal design for an O_2 micro-outlet. The modeling results suggested that optimal micro-outlet dimensions would allow for activating a sufficient number of capillaries to generate large enough magnitude of ATP signal while maintaining the localization of the signal. Also, the possible contribution of nearby arterioles to the ATP signal was verified.

Experimentally, gas mixture with different concentrations of O_2 was delivered through the micro-outlet to the surface of the muscle. O_2 levels were oscillated using computer controlled flow meters and digitized video sequences were processed for changes in capillary hemodynamic parameters and erythrocyte SO_2. CO_2 levels and temperature were held constant and PO_2 levels were kept above 15 mmHg ensuring that the primary regulatory response are due solely to changes in regulation of the O_2 supply.

1.9.2 Hypothesis

It is hypothesized that capillaries are able to signal upstream arterioles for changes in erythrocyte supply rate in response to changes in capillary erythrocyte SO_2 via SO_2-dependent signaling by the erythrocyte.

1.9.3 Objectives

1. To design a novel O_2 micro-delivery system for altering erythrocyte SO_2 in selected micro-vessels *in vivo* while simultaneously measuring blood flow responses and SO_2 value;
2. To mathematically model spatially limited O_2 delivery to or removal from the capillary bed and the consequent erythrocyte SO_2-dependent ATP release. To determine an optimal dimensions for the O_2 micro-outlet in our novel system; and
3. To experimentally investigate conducted micro-vascular signaling and response to varying capillary SO_2 *in vivo* using our optimized novel O_2 micro-delivery system.

1.10 References

Adderley S.P., Sprague R.S., Stephenson A.H., Hanson M.S. (2010*a*). Regulation of cAMP by phosphodiesterases in erythrocytes. *Pharmacol. Rep.* **62**: 475–482.

Adderley S.P., Sridharan M., Bowles E.A., Stephenson A.H., Ellsworth M.L., Sprague R.S. (2010*b*). Protein kinases A and C regulate receptor-mediated increases in cAMP in rabbit erythrocytes. *Am. J. Physiol. Cell. Physiol.* **298**: C587–C593.

Arciero J. C., Carlson B. E., Secomb T. W. (2008). Theoretical model of metabolic blood flow regulation: roles of ATP release by red blood cells and conducted responses. *Am. J. Physiol. Heart Circ. Physiol.* **295**: H1562–H1571

Bagher P., Segal S.S. (2011) Regulation of blood flow in the microcirculation: role of conducted vasodilation. *Acta. Physiol. (Oxf).* **202**: 271-84

Bayewitch M.L., Avidor-Reiss T., Levy R., Pfeuffer T., Nevo I., Simonds W.F., Vogel Z. (1998) Differential modulation of adenylyl cyclase I and II by various $G_{\beta\gamma}$ subunits. *J. Biol. Chem.* **273:** 2273–2276

Bergfeld G.R., Forrester T. (1992) Release of ATP from human erythrocytes in response to a brief period of hypoxia and hypercapnia. *Cardiovasc. Res.* **26:** 40–47

Campbell W.B., Gebremedhin D., Pratt P.F., Harder D.R. (1996) Identification of epoxyeicosatrienoic acids as endothelium derived hyperpolarizing factors. *Circ. Res.* **78:** 415–423

Carvalho H., Pittman, R.N. (2008) Longitudinal and radial gradients of PO_2 in the hamster cheek pouch microcirculation. *Microcirculation.* **15:** 215–224

Collins D.M., McCullough W.T., Ellsworth M.L. (1998) Conducted vascular responses: communication across the capillary bed. *Microvasc. Res.* **56:** 43–53

Comyn J. Polymer Permeability. New York: Chapman and Hall Inc., 1985, p. 21-23.

Corr, L., Burnstock, G. (1994) Analysis of Pz-purinoceptor subtypes on the smooth muscle and endothelium of rabbit coronary artery. *J. Cardiovasc. Pharmacol.* **23:** 709-715

Cosby K., Partovi K.S., Crawford J.H., Patel R.P., Reiter C.D., Martyr S., Yang B.K., Waclawiw M.A., Zalos G., Xu X., Huang K.T., Shields H., Kim-Shapiro D.B., Schechter A.N., Cannon[3rd] R.O., Gladwin M.T. (2003) Nitrite reduction to nitric oxide by deoxyhemoglobin vasodilates the human circulation. *Nat. Med.* **9:** 1498–1505

Dewhirst M.W., Klitzman B., Braun R.D., Brizel D.M., Haroon Z.A., Secomb T.W. (2000) Review of methods to study oxygen transport at the microcirculatory level. *Int. J. Cancer*. **90:** 237–255

Dietrich H.H. (1989) Effect of locally applied epinephrine and norepinephrine on blood flow and diameter in capillaries of rat mesentery. *Microvasc. Res.* **38**: 125-135

Dietrich H.H., Tyml K. (1992a) Microvascular flow response to localized application of norepinephrine on capillaries in rat and frog skeletal muscle. *Microvasc. Res.* **43**: 73-86

Dietrich H.H., Tyml K. (1992b) Capillary as a communicating medium in the microvasculature. *Microvasc. Res.* **43**: 87-99

Dietrich H.H., Ellsworth M.L., Sprague R.S., Dacey R.G. Jr. (2000) Red blood cell regulation of microvascular tone through adenosine triphosphate. *Am. J. Physiol. Heart. Circ. Physiol.* **278:** H1294–H1298

Dietrich H.H., Horiuchi T., Xiang C., Falck J.R., Hongo K., Dacey R.G. Jr. (2008) Mechanism of ATP-induced local and conducted vasomotor responses in isolated rat cerebral penetrating arterioles. *J. Vasc. Res.* **46:** 253–264

Duling B. (1973) Oxygen sensitivity of vascular smooth muscle. II. In vivo studies. *Am. J. Physiol.* **227:** 42–49

Duling B.R., Berne R.M. (1970) Longitudinal gradients in periarteriolar oxygen tension. A possible mechanism for the participation of oxygen in local regulation of blood flow. *Circ. Res.* **27:** 669-678.

Ellis C.G., Bateman R.M., Sharpe M.D., Sibbald W.J., Gill R. (2002) Effect of a maldistribution of microvascular blood flow on capillary O(2) extraction in sepsis. *Am. J. Physiol. Heart. Circ. Physiol.* **282(1):**H156-64.

Ellis C.G., Goldman D., Hanson M., Stephenson A.H., Milkovich S., Benlamri A., Ellsworth M.L., Sprague R.S. (2010). Defects in oxygen supply to skeletal muscle of prediabetic ZDF rats. *Am. J. Physiol. Heart. Circ. Physiol*. **298:**1661-1670.

Ellis C.G., Jagger J., Sharpe M. (2005) The microcirculation as a functional system. *Crit. Care*. **9(Suppl. 4):** S3–S8

Ellis C.G., Milkovich S.L., Goldman D. (2012) What is the efficiency of ATP signaling from erythrocytes to regulate distribution of O_2 supply within the microvasculature? *Microcirculation*. **5**: 440-450

Ellis C.G., Wrigley S.M., Groom A.C. (1994) Heterogeneity of red blood cell perfusion in capillary networks supplied by a single arteriole in resting skeletal muscle. *Circ. Res.* **75:**357-368.

Ellsworth M.L., Ellis C.G., Goldman D., Stephenson A.H., Dietrich H.H., Sprague R.S. (2009) Erythrocytes: oxygen sensors and modulators of vascular tone. *Physiology*. **24:** 107–116

Ellsworth M.L., Ellis C.G., Popel A.S., Pittman R.N. (1994) Role of microvessels in oxygen-supply to tissue. *News. Physiol. Sci.* **9:**119-123.

Ellsworth M.L., Forrester T., Ellis C.G., Dietrich H.H. (1995) The erythrocyte as a regulator of vascular tone. *Am. J. Physiol. Heart. Circ. Physiol.* **269:** H2155–H2161

Ellsworth M.L., Pittman R.N. (1986) Evaluation of photometric methods for quantifying convective mass transport in microvessels. *Am. J. Physiol. Heart. Circ. Physiol.* **251:** H869–H879

Ellsworth M.L., Pittman R.N. (1990) Arterioles supply oxygen to capillaries by diffusion as well as by convection. *Am. J. Physiol. Heart. Circ. Physiol.* **258:** H1240–H1243

Ellsworth M.L., Popel A.S., Pittman R.N. (1988) Assessment and impact of heterogeneities of convective oxygen transport parameters in capillaries of striated muscle. *Microvasc. Res.* **35:**341–362

Federman A.D., Conklin B.R., Schrader K.A., Reed R.R., Bourne H.R. (1992) Hormonal stimulation of adenylyl cyclase through Gi-protein beta gamma subunits. *Nature.* **356:**159–161

Forsyth A.M., Wan J., Owrutsky P.D., Abkarian M., Stone H.A. (2011). Multiscale approach to link red blood cell dynamics, shear viscosity, and ATP release. *Proc. Natl. Acad. Sci. USA.* **108**:10986–10991.

Fukao M., Mason H.S., Kenyon J.L., Horowitz B., Keef K.D. (2001) Regulation of BK(Ca) channels expressed in human embryonic kidney 293 cells by epoxyeicosatrienoic acid. *Mol. Pharmacol.* **59:**16–23

Gladwin M.T., Crawford J.H., Patel R.P. (2004) The biochemistry of nitric oxide, nitrite, and hemoglobin: role in blood flow regulation. *Free. Radic. Biol. Med.* **36:** 707-717

Gladwin M.T., Lancaster J.R. Jr, Freeman B.A., Schechter A.N. (2003) Nitric oxide's reactions with hemoglobin: a view through the SNOstorm. *Nat. Med.* **9:**496-500

Gladwin M.T., Schechter A.N. (2004) NO contest: nitrite versus Snitroso-hemoglobin. *Circ. Res.* **94:**851-855

Goldman D., Bateman R.M., Ellis C.G. (2004) Effect of sepsis on skeletal muscle oxygen consumption and tissue oxygenation: interpreting capillary oxygen transport data using a mathematical model. *Am. J. Physiol. Heart. Circ. Physiol.* **287(6):**H2535-44.

González-Alonso J., Olsen D.B., Saltin B. (2002) Erythrocyte and the regulation of human skeletal muscle blood flow and oxygen delivery: role of circulating ATP. *Circ. Res.* **91:**1046–1055

González-Alonso J., Mortensen S.P., Dawson E.A., Secher N.H., Damsgaard R. (2006) Erythrocytes and the regulation of human skeletal muscle blood flow and oxygen delivery: role of erythrocyte count and oxygenation state of haemoglobin. *J. Physiol.* **572:** 295–305

Gravesen P., Branebjerg J., Jensen O.S. (1993) Microfluidics - a review. *J. Mioromech. Microeng.* **3:**168-182

Hanson M.S., Ellsworth M.L., Achilleus D., Stephenson A.H., Bowles E.A., Sridharan M., Adderley S., Sprague R.S. (2009) Insulin inhibits low oxygen induced ATP release from human erythrocytes: implication for vascular control. *Microcirculation*. **16:**424–433

Hanson M.S., Stephenson A.H., Bowles E.A., Sridharan M., Adderley S., Sprague R.S. (2008). Phosphodiesterase 3 is present in rabbit and human erythrocytes and its inhibition potentiates iloprost-induced increases in cAMP. *Am. J. Physiol. Heart. Circ. Physiol.* **295**: H786–H793

Haddy F.J., Scott J.B. (1968) Metabolically linked vasoactive chemicals in local regulation of blood flow. *Physiol. Rev.* **48:**688–707

Harder D.R., Narayanan J., Birks E.K., Liard J.F., Imig J.D., Lombard J.H., Lange A.R., Roman R.J. (1996) Identification of a putative microvascular oxygen sensor. *Circ. Res.* **79:** 54–61

Hill A.V. (1910) The possible effects of the aggregation of the molecules of hemoglobin on its dissociation curve. *J. Physiol. (London).* **Iv:**41.

Herold K.E, Rasooly A. Lab-on-a-Chip Technology: Fabrication and Microfluidics. Norfolk: Caister Academic Press., 2009a, p. 125-139

Herold K.E., Rasooly A. Lab-on-a-Chip Technology: Biomolecular Separation and Analysis. Norfolk: Caister Academic Press., 2009b, p. 3-69

Hester R.L. (1993) Uptake of metabolites by postcapillary venules: mechanism for the control of arteriolar diameter. *Microvasc. Res.* **46:** 254–261

Horiuchi T., Dietrich H.H., Tsugane S., Dacey R.G. Jr. (2001) Analysis of purine- and pyrimidine-induced vascular responses in the isolated rat cerebral arteriole. *Am. J. Physiol. Heart. Circ. Physiol.* **280:** H767–H776

Jackson W.F. (1987) Arteriolar oxygen reactivity: where is the sensor. *Am. J. Physiol. Heart. Circ. Physiol.* **253:**H1120–H1126

Jackson W.F., Duling B.R. (1983) The oxygen sensitivity of hamster cheek pouch arterioles. In vitro and in situ studies. *Circ. Res.* **53:** 515–525

Jagger J.E., Bateman R.M., Ellsworth M.L., Ellis C.G. (2001) Role of erythrocyte in regulating local O2 delivery mediated by hemoglobin oxygenation. *Am. J. Physiol. Heart. Circ. Physiol.* **280:** H2833–H2839

Jagger J.E., Ellis C.G. (2005) Effect of varying oxygen levels on hemodynamic and oxygen transport parameters in the EDL muscle of the rat. *FASEB. J.* **19** (Suppl 4): A731-A731

Jia L., Bonaventura C., Bonaventura J., Stamler J.S. (1996) S-nitrosohaemoglobin: a dynamic activity of blood involved in vascular control. *Nature.* **380:** 221–226

Knowles A.F. (2011) The GDA1_CD39 superfamily: NTPDases with diverse functions. *Purinergic. Signal.* **7:** 21–45

Krogh A. (1919) The number and the distribution of capillaries in muscle with the calculation of the oxygen pressure necessary for supplying tissue. *J. Physiol. (Lond).* **52:**409-515.

Liu L., Yan Y., Zeng M., Zhang J., Hanes M.A., Ahearn G., McMahon T.J., Dickfeld T., Marshall H.E., Que L.G., Stamler J.S. (2004) Essential roles of S-nitrosothiols in vascular homeostasis and endotoxic shock. *Cell.* **116:** 617–628

Malmsjo M., Erlinge D., Hogestatt E.D., Zygmunt P.M. (1999) Endothelial P2Y receptors induce hyperpolarisation of vascular smooth muscle by release of endothelium-derived hyperpolarising factor. *Eur. J. Pharmacol.* **364:**169-173

Mark D., Haeberle S., Roth G., von Stetten F., Zengerle R. (2010) Microfluidic lab-on-a-chip platforms: requirements, characteristics and applications. *Chem. Soc. Rev.* **39:**1153-82

McCullough W.T., Collins D.M., Ellsworth M.L. (1997) Arteriolar responses to extracellular ATP in striated muscle. *Am. J. Physiol. Heart. Circ. Physiol.* **272:** H1886–H1891

Melani A., Corti F., Stephan H., Muller C.E., Donati C., Bruni P., Vannucchi M.G., Pedata F. (2012) Ecto-ATPase inhibition: ATP and adenosine release under physiological and ischemic *in vivo* conditions in the rat striatum. *Exp. Neurol.* **233:** 193–204

Messina E.J., Sun D., Koller A., Wolin M.S., Kaley G. (1994) Increases in oxygen tension evoke arteriolar constriction by inhibiting endothelial prostaglandin synthesis. *Microvasc. Res.* **48:**151–160

Miseta A., Bogner P., Berenyi E., Kellermayer M., Galambos C., Wheatley D., Cameron I. (1993) Relationship between cellular ATP, potassium, sodium and magnesium concentrations in mammalian and avian erythrocytes. *Biochim. Biophys. Acta.* **1175:**133–139

Needham L., Cusack N.J., Pearson J.D., Gordon J.L: (1987) Characteristics of the P2 purinoceptor that mediates prostacyclin production by pig aortic endothelial cells. *Eur. J. Pharmacol.* **134:**199-209

Nguyen N-T, Wereley S.T. Fundamentals and Applications of Microfluidics. Norwood: Artech House, Inc., 2002, p. 1-129

Olearczyk J., Stephenson A.H., Lonigro A.J., Sprague R.S. (2001) Receptor-mediated activation of the heterotrimeric G.-protein Gs results in ATP release from erythrocytes. *Med. Sci. Monit.* **7:**669–674

Olearczyk J.J., Stephenson A.H., Lonigro A.J., Sprague R.S. (2004a) Heterotrimeric G protein Gi is involved in a signal transduction pathway for ATP release from erythrocytes. *Am. J. Physiol. Heart. Circ. Physiol.* **286:** H940–H945

Olearczyk J.J., Stephenson A.H., Lonigro A.J., Sprague R.S. (2004b) NO inhibits signal transduction pathway for ATP release from erythrocytes via its action on heterotrimeric G protein Gi. *Am. J. Physiol. Heart. Circ. Physiol.* **287:** H748–H754

Patel R.P., Hogg N., Spencer N.Y., Kalyanaraman B., Matalon S., Darley-Usmar V.M. (1999) Biochemical characterization of human Snitrosohemoglobin. Effects on oxygen binding and transnitrosation. *J. Biol. Chem* . **274:**15487-15492

Pittman R.N., Duling B.R. (1973) Oxygen sensitivity of vascular smooth muscle. *Microvasc. Res.* **6:** 202–211

Pries A.R., Heide J., Ley K., Klotz K.F., Gaehtgens P. (1995) Effect of oxygen tension on regulation of arteriolar diameter in skeletal muscle in situ. *Microvasc. Res.* **49:** 289–299

Pries A.R., Secomb T.W., Gaehtgens P. (1996) Biophysical aspects of blood flow in the microvasculature. *Cardiovasc. Res.* **32:**654-667.

Riemann M., Rai A., Ngo A.T., Dziegiel M.H., Holstein-Rathlou N-H, Torp-Pedersen C. (2010). Oxygen-dependant vasomotor responses are conducted upstream in the mouse cremaster microcirculation. *J. Vac. Res.* **48:**79-89.

Roach R.C., Koskolou M.D., Jose A.L.C., Saltin B. (1999) Arterial O2 content and tension in regulation of cardiac output and leg blood flow during exercise in humans. *Am. J. Physiol. Heart. Circ. Physiol.* **276:** H438–H445

Rubino A., Ralevic V., Burnstock G. (1995) Contribution of P1-(A2b subtype) and P2-purinoceptors to the control of vascular tone in the rat isolated mesenteric arterial bed. *Br. J. Pharmacol*. **115:**648-652.

Segal S.S., Damon D.N., Duling B.R. (1989) Propagation of vasomotor responses coordinates arteriolar resistances. *Am. J. Physiol. Heart. Circ. Physiol.* **256:** H832–H837

Segal S.S., Duling B.R. (1989) Conduction of vasomotor responses in arterioles:a role for cell-to-cell coupling? *Am. J. Physiol. Heart. Circ. Physiol.* **256:** H838–H845

Song H., Tyml K. (1993) Evidence for sensing and integration of biological signals by the capillary network. *Am. J. Physiol.* **265**: H1235-H1242

Sprague R.S., Ellsworth M.L., Stephenson A.H., Lonigro A.J. (1996) ATP: the red blood cell link to NO and local control of the pulmonary circulation. *Am. J. Physiol. Heart. Circ. Physiol*. **271:**H2717–H2722

Sprague R.S., Ellsworth M.L., Stephenson A.H., Kleinhenz M., Lonigro A. (1998) Deformation-induced ATP release from red blood cells requires cystic fibrosis transmembrane conductance regulator activity. *Am. J. Physiol. Heart. Circ. Physiol.* **275:** H1726–H1732

Sprague R.S., Ellsworth M.L., Stephenson A.H., Lonigro A.J. (2001) Participation of cAMP in a signal-transduction pathway relating erythrocyte deformation to ATP Release. *Am. J. Physiol. Cell. Physiol.* **281**: C1158–C1164.

Sprague R.S., Bowles E.A., Olearczyk J.J., Stephenson A.H., Lonigro A.J. (2002) The role of G *protein* subunits in the release of ATP from human erythrocytes. *J. Physiol. Pharmacol.* **53:**667–674

Sprague R.S., Stephenson A.H., Bowles E.A., Stumpf M.S., Lonigro A.J. (2006) Reduced expression of Gi in erythrocytes of humans with Type 2 diabetes is associated with impairment of both cAMP generation and ATP release. *Diabetes.* **55:** 33588–33593

Sprague R.S., Bowles E.A., Hanson M.S., DuFaux E., Sridharan M., Adderley S., Ellsworth M.L., Stephenson A.H. (2008) Prostacyclin analogues stimulate receptor-mediated cAMP synthesis and ATP release from rabbit and human erythrocytes. *Microcirculation.* **15**:461–471

Sprague R.S., Goldman D., Bowles E.A., Achilleus D., Stephenson A.H., Ellis C.G., Ellsworth M.L. (2010) Divergent effects of low-O(2) tension and iloprost on ATP release from erythrocytes of humans with type 2 diabetes: implications for O(2) supply to skeletal muscle. *Am. J. Physiol. Heart. Circ. Physiol.* **299(2):**H566-73.

Sprague R.S., Ellsworth M.L. (2012) Erythrocyte-derived ATP and perfusion distribution: Role of intracellular and intercellular communication. *Microcirculation.* **5:**430-439

Sridharan M., Adderley S.P., Bowles E.A., Egan T.M., Stephenson A.H., Ellsworth M.L., Sprague R.S. (2010a) Pannexin 1 is the conduit for low oxygen tension-induced ATP release from human erythrocytes. *Am. J. Physiol. Heart. Circ. Physiol.* **299**:H1146–H1152.

Sridharan M., Sprague R.S., Adderley S.P., Bowles E.A., Ellsworth M.L., Stephenson A.H. (2010b) Diamide decreases deformability of rabbit erythrocytes and attenuates low oxygen tension-induced ATP release. *Exp. Biol. Med. (Maywood).* **235**: 1142–1148

Stamler J.S., Jia L., Eu J.P., McMahon T.J., Demchenko I.T., Bonaventura J., Gernert K., Piantadosi C.A. (1997) Blood flow regulation by S-nitrosohemoglobin in the physiological oxygen gradient. *Science.* **276:**2034–2037

Stein J.C., Ellis C.G., Ellsworth M.L. (1993) Relationship between capillary and systemic venous PO_2 during nonhypoxic and hypoxic ventilation. *Am. J. Physiol.* **265:**H537-H542

Stone H.A., Kim S. (2001) Microfluidics: Basic Issues, Applications, and Challenges. *AIChE. J.* **48:**1250-1254

Swain D.P., Pittman R.N. (1989) Oxygen exchange in the microcirculation of hamster retractor muscle. *Am. J. Physiol. Heart. Circ. Physiol*. **256:**H247-H255

Tsai A.G., Johnson P.C., Intaglietta M. (2003) Oxygen gradients in the microcirculation. *Physiol. Rev*. **83:**933-963.

Tyml K., Ellis C.G., Safranyos R.G., Fraser S., Groom A.C. (1981) Temporal and spatial distributions of red cell velocity in capillaries of resting skeletal muscle, including estimates of red cell transit times. *Microvasc. Res.* **22:**14-31.

Varghese H.J., MacKenzie L.T., Groom A.C., Ellis C.G., Chambers A.F., MacDonald I.C. (2005) Mapping of the functional microcirculation in vital organs using contrast-enhanced *in vivo* video microscopy. *Am. J. Physiol. Heart. Circ. Physiol.* **288:**185-193.

Wan J., Ristenpart W.D., Stone H.A. (2008) Dynamics of shear-induced ATP release from red blood cells. Proc. *Natl. Acad. Sci. USA.* **105:**16432–16437

Wang L., Olivecrona G., Gotberg M., Olsson M.L., Winzell M.S., Erlang D. (2005) Acting on P2Y13 ADP receptors is a negative feedback pathway for ATP release from human red blood cells. *Circ. Res.* **96:**189–196

Wihlborg A-K., Malmsjo M., Eyjolfsson A., Gustafsson R., Jacobson K., Erlinge D. (2003) Extracellular nucleotides induce vasodilatation inhuman arteries via prostaglandins, nitric oxide and endothelium- derived hyperpolarising factor. *Br. J. Pharmacol.* **138:**1451-1458.

You J., Johnson T.D., Childres W.F., Bryan R.M. Jr. (1997) Endothelial-mediated dilations of rat middle cerebral arteries by ATP and ADP. *Am. J. Physiol. Heart. Circ. Physiol.* **273:**H1472–H1477

You J.P., Johnson T.D., Marrelli S.P., Bryan R.M.Jr. (1999) Functional heterogeneity of endothelial P2 purinoceptors in the cerebrovascular tree of the rat. *Am. J. Physiol. Heart. Circ. Physiol.* **277:**H893–H900

Chapter 2

2 A micro-delivery approach for studying microvascular responses to localized oxygen delivery[1]

[1] Research article published in Microcirculation (2011) 18 (8), 646-654

2.1 Introduction

Several medical conditions that are characterized by microvascular dysfunction lead to more critical problems such as tissue hypoxia and organ failure (Ellis et al. 2005). The understanding of the pathophysiology underlying these conditions depends on the understanding of oxygen (O_2) transport and its regulation under physiological conditions. Previous studies have demonstrated that red blood cells (RBCs) have an O_2-dependent release of adenosine triphosphate (ATP), which is directly correlated to the oxygen saturation (SO_2) level of haemoglobin (Ellsworth et al. 1995, 2009, Jagger et al. 2001). Under hypoxic conditions, a signal transduction pathway is modulated in RBCs, which results in increased ATP release and purinergic receptor activation on the vascular endothelium (Ellsworth et al. 2009). In arterioles, this leads to the production of signaling molecules, such as nitric oxide (NO) in the endothelium, that cause local vascular smooth muscle dilation. In addition, activation of P2Y2 receptors initiates conducted signaling along the vascular endothelium in both arterioles and capillaries resulting in upstream vascular dilation to increase the supply of O_2-carrying red blood cells (Ellsworth et al. 2009). Type-II diabetes is a medical condition associated with peripheral vascular

dysfunction and impaired tissue oxygenation. Interestingly, it has recently been shown that RBCs from type II diabetes patients suffer defects in the release of ATP (Sprague et al. 2006) and that RBCs from humans and animal models of prediabetes have attenuated release of ATP in response to a decrease in O_2 levels (Hanson et al. 2009, Ellis et al. 2010).

In vivo video-microscopy (IVVM) techniques, which allow for monitoring and recording real-time changes in blood flow properties within the microcirculation (Dewhirst et al. 2000, Ellis et al. 2010, Varghese et al. 2005), have been used to study the blood flow characteristics as a function of local O_2 concentration in capillary microcirculatory networks. The classical setup involves altering O_2 partial pressure (PO_2) levels in the superfusion solution equilibrating the surface of a tissue or a vessel (Duling 1974, Jackson and Duling 1983). However, the use of a superfusion solution may alter the physiological environment by continuously washing away substances from the surface of the tissue and can potentially affect the microvascular response by depleting the tissue of molecules involved in microvascular signalling. Another limitation of using superfusion solution as a medium for O_2 delivery is the relatively low solubility of O_2 in saline solution.

The IVVM setup currently used in our lab involves varying the levels of O_2 transported to the surface of the rat Extensor Digitorum Longus (EDL) muscle using a gas exchange chamber positioned on the viewing platform of an inverted microscope (see Figure 2.1). More specifically, O_2 is delivered through a 4 mm × 10 mm window covered with fluorosilicone acrylate O_2 permeable membrane of 50 μm thickness. The tissue is trans-illuminated and real-time videos of blood flow changes in the microcirculation are

recorded while simultaneously controlling local O_2 levels in the chamber using computer-controlled flow meters. Direct O_2 delivery through a highly O_2 permeable membrane such as fluorosilicone acrylate (O_2 permeability coefficient = 100 Barrers, where 1 Barrer = 10^{-11} (cm^3 O_2 STP) cm^2 cm^{-3} sec^{-1} $mmHg^{-1}$ (Comyn 1985)) has a greater effect on tissue PO_2 levels than when using liquid media. Also, this setup offers minimal disturbance to the tissue's physiological environment. However, the dimensions of the O_2 delivery window are proportional to the *in situ* dimensions of the EDL muscle. Hence, the current IVVM setup measures the collective response of stimulating a very large area of the microvascular network at the muscle surface (Figure 2.1). Riemann *et al*. (2010) have recently tried to limit the area affected by O_2 using micropipettes for infusing liquids with low O_2 but without measurement of the impact on tissue O_2 levels or RBC saturation. The ability to measure RBC SO_2 is critical to establish that an SO_2 dependent microvascular signal is induced (Jackson and Duling 1983).

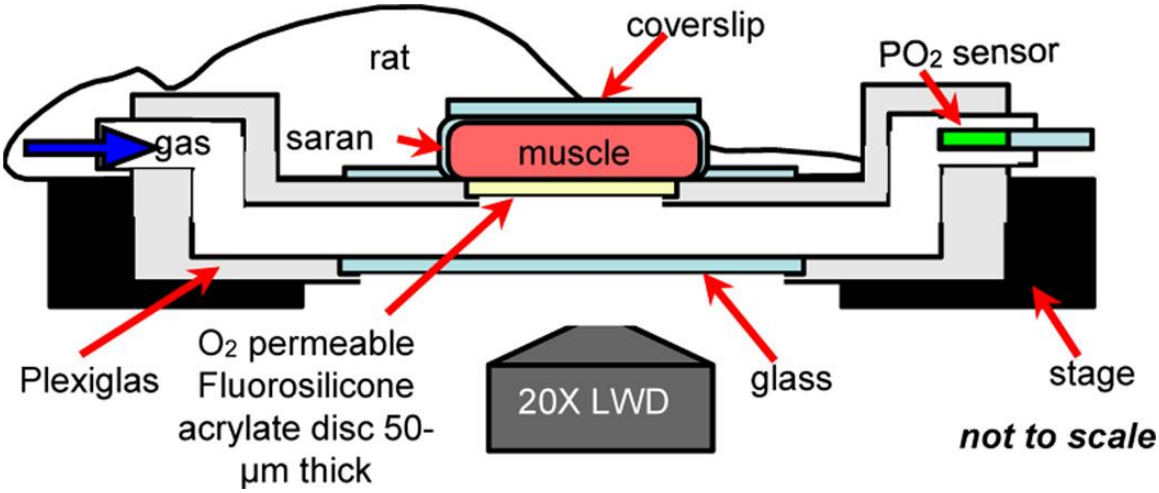

Figure 2.1 Classical IVVM experimental setup. Extensor Digitorum Longus (EDL) muscle of the rat is surgically exposed and positioned surface down on the viewing platform of an inverted light microscope. O_2 is delivered to the muscle using a gas exchange chamber connected to computer-controlled flow meters. O_2 levels in the chamber are measured and monitored using a fibre optic O_2 sensor probe. The tissue is trans-illuminated and blood flow responses are recorded and analyzed as O_2 levels are simultaneously oscillated.

In this study, a micro-delivery approach was developed for investigating localized microvascular signaling and response to varying tissue PO_2 levels. We have limited the area of O_2 perturbation at the microvascular bed within live muscle tissue (rat EDL) by 40 fold relative to the original gas exchange chamber setup. Gas with varying levels of O_2 was directly transported to the surface of the EDL muscle through a set of micro-outlets (~100 µm in diameter) patterned in an ultrathin glass sheet using state-of-the-art microfabrication techniques. RBC SO_2 changes due to O_2 level oscillations were measured and recorded while simultaneously controlling local O_2 levels. This novel

approach aims to provide greater insight into the underlying mechanisms of microvascular control.

2.2 Materials and Methods

2.2.1 Mathematical modeling of the PO_2 distribution profile

The oxygen partial pressure (PO_2) distribution profile through an O_2 delivery micro-outlet interfaced directly with live tissue was modeled using an O_2 transport code written in MATLAB (Mathworks, Natick, MA). The model simulates O_2 diffusing through varying sized outlets (20 μm, 50 μm, 100 μm, and 200 μm in diameter) patterned in a zero thickness material into tissue that consumes O_2 and also has a continuous distribution of capillary O_2 sources. We have shown previously that O_2 transport through tissue of this type differs from O_2 transport through a purely diffusive medium (Goldman 2008). In the present case, a finite-difference method is used to solve the axisymmetric 3-D problem of axial and radial diffusion, for instance, from a 100 μm outlet (x=0, r≤50 μm) into the overlying tissue ($0 < x \leq 500$ μm, 0 μm $< r \leq 500$ μm) with no-flux boundary conditions at r=500 μm, x=500 μm and x=0 for r>50 μm. The micro-outlet PO_2 was set to be 205 mmHg (27% O_2) and the far-field tissue PO_2 (P_∞) was set to be 42 mmHg (typical tissue PO_2 under normal resting conditions). As described in Goldman (2008), the other parameters needed for the O_2 transport model were the tissue O_2 diffusion coefficient (D=2.41×10^{-5}cm^2/s), O_2 solubility (α=3.89×10^{-5} ml O_2/ml/mmHg), O_2 consumption rate (M_0=1.5 10^{-4} ml O_2/ml/s), and the mean capillary PO_2 (P^*=48 mmHg), Note that P_∞ and

P^* represent, respectively, average tissue and capillary values far from the outlet, and hence should not be affected by the outlet PO_2.

2.2.2 Microfabrication

Oxygen delivery micro-outlets with a diameter of ~100 μm and a pitch of ~277 μm (center-to-center) were patterned in 30 μm thick D263C borosilicate glass substrate (SCHOTT North America) by photolithography and subsequent wet etching in hydrogen fluoride. The photolithography and wet etching steps were carried out similar to previously described procedures (Ilie et al. 2003, Srivastava et al. 2005). Since the etching is isotropic, there is a certain degree of undercutting beneath the masking layers (Ilie et al. 2003). This results in the pattern to be larger on the glass relative to the photomask. Also, due to the undercutting, the micro-outlet would be cone-shaped rather than cylindrically shaped, which means that the diameter is larger right beneath the masking layer. All pattern dimensions were optically measured at the top glass surface (glass surface directly beneath the masking layers) using QCapture Pro™ 6.0 software. The patterned ultrathin glass substrate replaced the O_2 permeable fluorosilicone acrylate in the original IVVM setup (Figure 2.1).

2.2.3 *In vivo* video microscopy

RBC SO_2 levels in response to O_2 delivery through the micro-outlets were measured using IVVM techniques. These measurements were used to assess the tissue response time for O_2 delivery from the micro-outlets as well as to validate the model results.

2.2.3.1 Animal preparation

All procedures described are approved from the University of Western Ontario's Animal Care and Use Committee. Male Sprague-Dawley rats (Charles River Laboratories, Wilmington, MA) (150–200 g) were anesthetized with pentobarbital sodium (6.5 mg/100 g body wt IP) and were subjected to a preparatory surgery as described (Ellis et al. 2002, 2010). The animals were mechanically ventilated at 30% O_2 (70% Nitrogen), and the inspired O_2 level (Oxychek) and blood pressure (MicroMed) were constantly monitored and recorded (Ellis et al. 2010). The Extensor Digitorum Longus (EDL) muscle of the hind limb was identified and prepared for *in vivo* video microscopy as described by Tyml and Budreau (1991). The muscle was extended along the viewing platform of a Nikon inverted microscope equipped with long-working distance 10X and 20X objectives and a beam splitter for dual video cameras (DAGE-MTI CCD cameras). A suture attached to the edge of the muscle was taped to the platform. The muscle was covered with Saran Wrap (Dow Corning) and a cover slip to isolate it from room air and to preserve moisture. The tissue was trans-illuminated with a 100-W xenon lamp and viewed using the dual video camera system as previously described (Ellis et al. 2010).

2.2.3.2 Dual video camera intravital microscopy system

Real-time video recordings (640 × 480, 30 frames/second) of RBC flow through capillaries were simultaneously obtained at two wavelengths, 431 nm, an O_2 sensitive wavelength for hemoglobin, and 420 nm, an isosbestic or O_2 insensitive wavelength (Ellsworth et al. 1987) using the dual video camera intravital microscopy system (Ellis et al. 2010). Live video sequences were digitized and stored as uncompressed AVI movie

files using custom acquisition software from Neovision (Ellis et al. 2010) for post-processing. Geometric, spatiotemporal, and photometric off-line analyses of the AVI files (for both 420 nm and 431 nm wavelengths) were conducted as described by Ellis et al. (Ellis et al.. 1990, 1992) and Japee et al. (Japee et al. 2004, 2005) using algorithms written in MATLAB (Mathworks, Natick, MA) to quantify changes in capillary hemodynamic parameters and erythrocyte SO_2. Parameters measured include average RBC velocity, supply rate, lineal density, and RBC SO_2(Ellis et al.. 1990, 1992, Japee et al. 2004, 2005).

2.3 Results

2.3.1 Mathematical modeling of the PO_2 distribution profile

Microvascular responses to variations of local tissue PO_2 levels were examined by delivering or removing O_2 at specific locations on the surface of the rat EDL muscle through a set of micro-outlets patterned in ultrathin glass. Prior to the microfabrication step (see Materials and Methods), the desired micro-outlet diameter was estimated by computational modeling in MATLAB (Mathworks, Natick, MA). The criteria guiding the modeling and final selection of micro-outlet geometry were determined by the maximum depth a capillary can be into the tissue for accurate analysis with our current microscopy techniques (50–60 μm) and the average dimensions of a microvascular unit (150 μm × 400 μm). Also, the separation between adjacent micro-outlets must be great enough for the PO_2 stimuli from each to be independent. Thus, in the simulation, the micro-outlet diameter was selected based on the depth of O_2 penetration into the tissue and the degree of radial diffusion away from the center of the outlet. Optimal micro-outlet dimensions

would allow for limiting the amount of radial diffusion of O_2 away from the center of an outlet, which maximizes the amplitude of O_2 diffusion into the tissue. The PO_2 distribution model for micro-outlets of 20 μm, 50 μm, 100 μm, and 200 μm in diameter (see Materials and Methods) showed an increase in the depth of penetration with increasing micro-outlet diameter; however, the degree of radial diffusion was unaffected by the size of the micro-outlet (Figure 2.2). The simulation suggested a limited amount of radial diffusion extending to about 25% of the micro-outlet diameter. The model indicated that below a 100 μm outlet diameter, the depth of PO_2 transport into the tissue is too small to ensure that capillary oxygenation will be affected. Above 100 μm, the depth of PO_2 transport increases; yet accompanied by a concurrent increase in the area of the tissue influenced by local PO_2 changes. For a 100 μm diameter outlet, we could affect an area ~150 μm in diameter with a depth of penetration of ~55 μm per outlet (Figure 2.2). Thus, a 100 μm micro-outlet was chosen as the minimum desired size since it would allow for altering the O_2 level of a specific region within a microvascular unit to the depth of our ability to analyze. The original O_2 delivery system was modeled as 1D diffusion resulting in the depth of penetration of ~100 μm (Goldman 2008). With the micro-outlets, the diffusion is physically 3D (mathematically 2D due to axisymmetry) and as expected the depth of penetration is less.

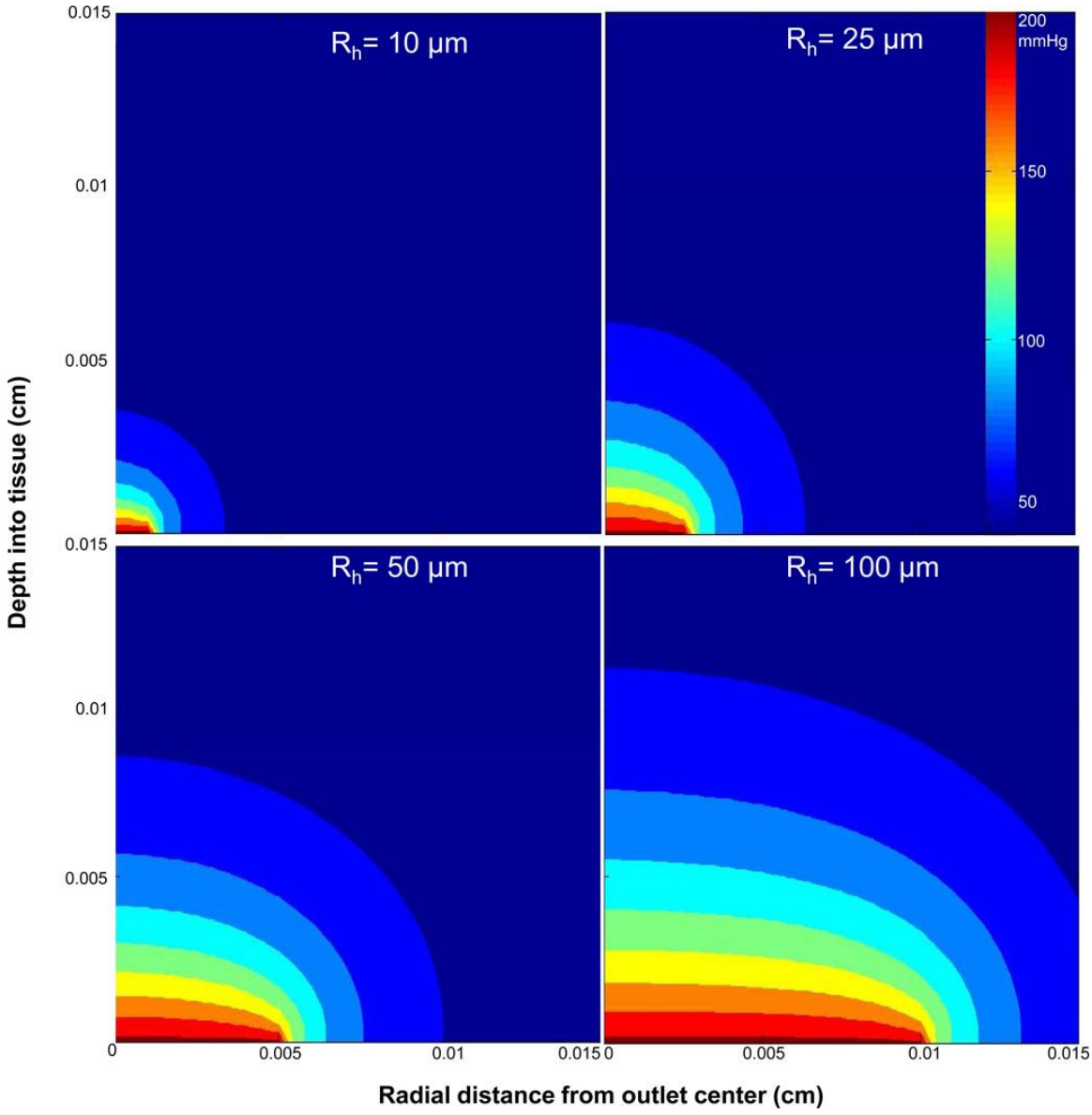

Figure 2.2 Calculated PO_2 distribution for O_2 delivery into live metabolic tissue through micro-outlets of various sizes (10 µm, 25 µm, 50 µm, and 100 µm in radius (R_h)). Using $P_{norm}(r,x) = (P(r,x)-P_\infty)/ (P_{outlet} - P_\infty)$ and a cut-off of P_{norm}=0.25, the radius of lateral O_2 diffusion from the center of the micro-outlet is constant at ~150% of the radius while the depth of penetration increases with increasing outlet radius. The width of the tissue in this model (Rt) was set to 500 µm, however, the maximum value on the x-axis in the PO_2

distribution plots was set to 150 μm for clarity. Computational modelling was conducted using algorithms written in MATLAB (Mathworks, Natick, MA).

2.3.2 Microfabrication

Oxygen delivery micro-outlets were patterned in ultrathin D263T borosilicate glass substrate (SCHOTT North America) based on the mathematical PO_2 distribution model described before. To test microvascular responses at different areas on the surface of the EDL muscle, multiple micro-outlets were patterned in ultrathin glass with a diameter of ~100 μm separated by ~277 μm center-to-center distance (Figure 2.3). The area simultaneously examined could be within a single microvascular network unit (~150 μm × 400 μm) or could be located at adjacent units.

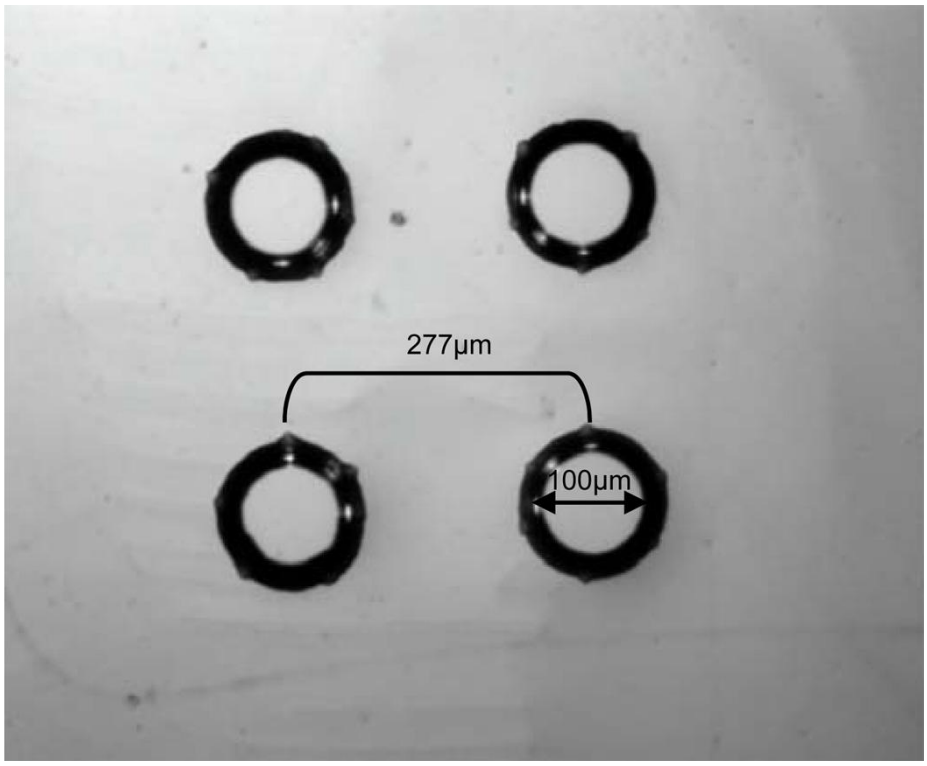

Figure 2.3 Oxygen delivery micro-outlets ~100 µm in diameter separated by ~277 µm distance (center-to center) patterned in D263T borosilicate ultrathin glass substrate as they appear under an upright light microscope at 10x objective. The micro-outlets were microfabricated using photolithography and subsequent wet etching in hydrogen fluoride.

2.3.3 Micro-delivery system *in vivo* validation

Prior to *in vivo* analysis, O_2 delivery through the designed micro-outlets was verified *in vitro* using the NeoFox® Phase Measurement System (O_2 sensing cover slip, FOXY sensor formulation, Ocean Optics, Inc.). Parameters examined included the PO_2 level changes associated with the micro-outlets and the response time. Following the *in vitro* validation, the effects of O_2 delivery through the micro-outlets were tested on live tissue (rat EDL muscle) using IVVM (see Materials and Methods).

2.3.3.1 Sine wave oscillations

With the aid of an inverted microscope, selected capillaries, designated as Cap1 and Cap2, on the surface of the EDL muscle were positioned on top of an O_2 delivery micro-outlet (Figure 2.4). The edge of the micro-outlet could be clearly viewed when focussing away from the tissue at 20X objective (Figure 2.4). The PO_2 level in the chamber was oscillated in a sine wave patteren (period 120 seconds) and a six minute video sequence was captured to examine RBC SO_2 changes within the selected capillaries. Analysis of the postprocessed video sequence shows a close association between the oscillated chamber PO_2 levels and the RBC SO_2 changes in both Cap1 and Cap2 with a lag time of approximately 10 seconds (Figure 2.4). The shape of the SO_2 time series is flattened at high O_2 saturations and steeper at low O_2 saturations, which is consistent with the sigmoidal shape of the hemoglobin O_2 saturation curve (Hill 1910). This was further confirmed by comparing the measured RBC SO_2 time series to the SO_2 curve calculated using Hill's equation and the measured chamber PO_2 values (Figure 2.4) (Hill 1910). As expected, the range of SO_2 values are greater in the calculated SO_2 curve and the lag time is absent when compared to the measured SO_2 data (Figure 2.4). Analysis of hemodynamic data indicated that the mean supply rate in Cap1 was higher (~13.2 ± 5.2 cells/sec, N=360) than in Cap2 (~4.3 ± 3.2 cells/sec, N=360).

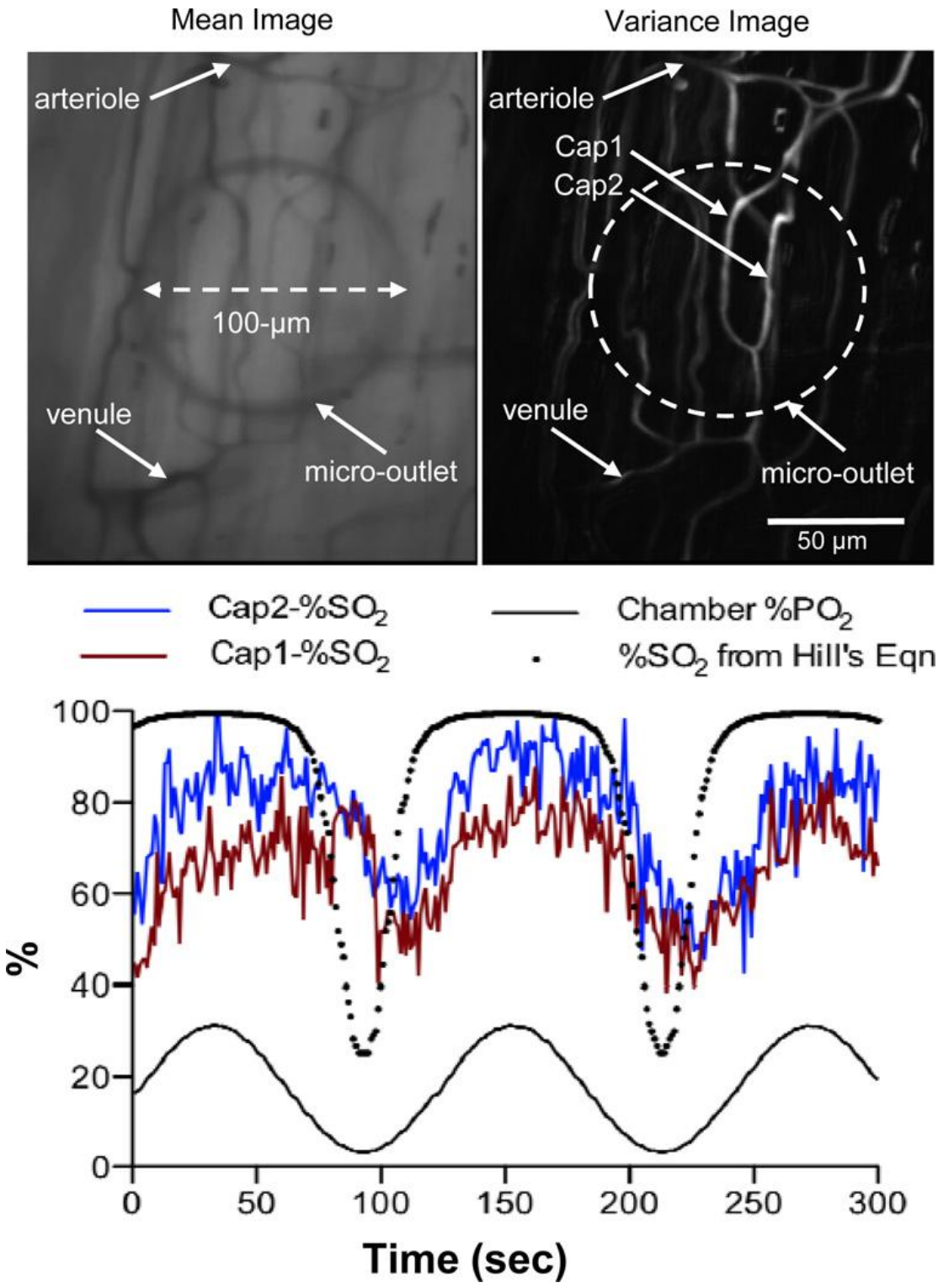

Figure 2.4 Muscle preparation with transparent micro-outlets positioned under the muscle. The edge of the micro-outlet is clearly visible in the 20X Mean Image showing

the outlet positioned under the capillary network between the arteriole and venule. In focus capillaries for analysis are visible in the Variance Image of the same field of view. Selected capillaries Cap1 and Cap2 were analyzed for RBC SO_2 changes as O_2 levels delivered through the micro-outlet were oscillated in a sine wave (of 120 second period). Videos of the selected region were simultaneously recorded at both 431 nm and 420 nm wavelengths using the dual video camera intravital microscopy system. The video sequences were digitized and postprocessed off-line using algorithms written in MATLAB to quantify changes in the RBC SO_2. The RBC SO_2 profiles of both capillaries are closely associated with the local O_2 oscillations. The shape of the SO_2 profiles for the selected capillaries also follows that of the SO_2 curve calculated using the Hill's equations and the measured chamber PO_2 values. The difference in the measured baseline SO_2 values between Cap 1 and Cap2 is likely due to the difference in their mean supply rates with Cap1 having higher supply rate (~13.2 ± 5.2 cells/sec, N=360) than Cap2 (~4.3 ± 3.2 cells/sec, N=360).

2.3.3.2 Square wave oscillations

A selected capillary, designated as Cap3, on the surface of the EDL muscle was positioned on top of a micro-outlet (Figure 2.5). The PO_2 level in the chamber was decreased from 22% (~167 mmHg) to 1.4% (~10.6 mmHg) for a 120 second hypoxic challenge and back to 22%. A video sequence was recorded over a six minute period beginning 2 minutes before the hypoxic challenge. The video was postprocessed for changes in capillary hemodynamic parameters and erythrocyte SO_2. Similar to our observations with induced sine oscillations of tissue PO_2 levels (Figure 2.4), RBC SO_2

changes were closely associated with the chamber PO_2 level with a lag time of approximately 7 seconds (Figure 2.5). The mean supply rate for Cap3 was measured to be ~9.4±3.4 cells/sec, N=220.

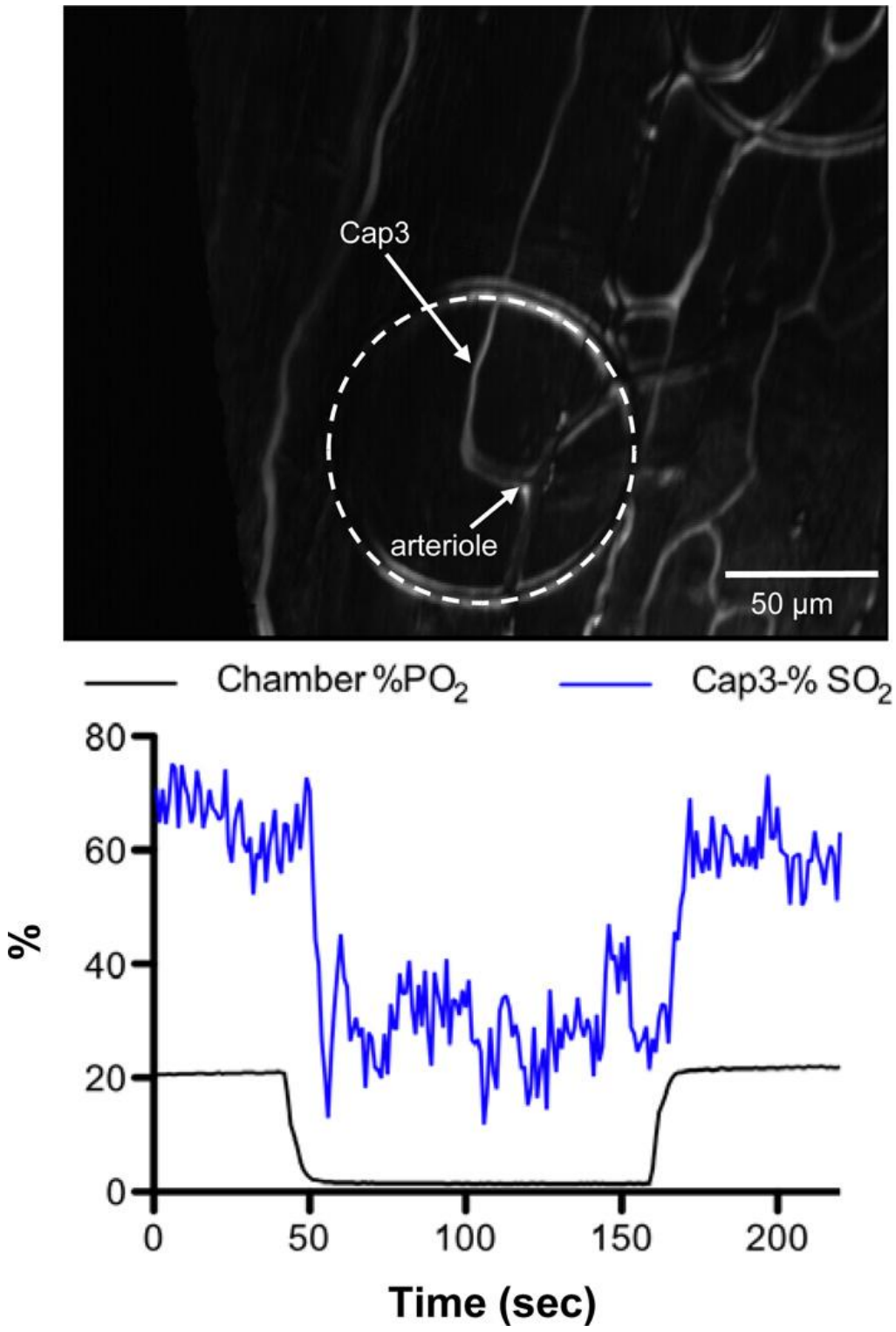

Figure 2.5 Selected capillary Cap3 was analyzed for RBC SO_2 changes as O_2 levels delivered through the micro-outlet were oscillated in a square wave. The PO_2 level in the

chamber was decreased from 22% (~167 mmHg) to 1.4% (~10.6 mmHg) for a 120 second hypoxic challenge and back to 22%. A six minute video sequence was captured beginning 2 minutes before the hypoxic challenge. The RBC SO_2 profile is closely associated with the chamber PO_2 level. The mean supply rate for Cap3 was measured to be ~9.4±3.4 cells/sec, N=220.

2.3.4 *In vivo* examination of radial diffusion

Following *in vivo* validation of O_2 delivery through the micro-outlets, the extent of radial diffusion from the center of the micro-outlet was examined *in vivo*. Selected capillaries, designated as Cap4 and Cap5, were positioned adjacent to a micro-outlet with the aid of the inverted microscope (Figure 2.6, panel A). The average distance of the selected capillaries from the center of the micro-outlet were calculated to be 62.2 μm and 73.2 μm, respectively. The PO_2 level in the chamber was decreased from 16.2% (~123 mmHg) to 0.2% (~1.5 mmHg) for a 120 second hypoxic challenge and back to 16.2%. A video sequence was recorded over a six minute period beginning 2 minutes before the hypoxic challenge. The video was postprocessed for changes in hemodynamic parameters and capillary erythrocyte SO_2. The mean SO_2 was calculated over a 40 second period prior to inducing local hypoxia (t=50–90 seconds) and over a 40 second period during the hypoxic challenge (t=160–200 seconds) for both Cap4 and Cap5. The difference in the means was calculated to be 28.0% for Cap4 and 15.1% for Cap5. The tissue PO_2 distribution profile was modelled (Figure 2.6, panel B) and the surface (depth=0 cm) PO_2 contour lines were superimposed on top of the image showing the micro-outlet and the selected capillaries (Figure 2,6, panel C). The RBC SO_2 at various depths into the tissue

(z=0 μm, 10 μm, 30 μm, and 50 μm) were calculated from the PO_2 values predicted by the model using Hill's equation (Hill 1910). The calculated SO_2 values were then plotted against the radial distance from the center of the micro-outlet (Figure 2.6, panel D). The SO_2 plots calculated based on the PO_2 distribution model into the tissue at baseline (SO_2 decreasing with radial position) or during hypoxia (SO_2 increasing with radial position) all converge to a value of 60% which corresponds to the tissue PO_2 level set in the model (~42 mmHg). Experimentally measured SO_2 mean values for Cap4 and Cap5 at baseline and during hypoxia were plotted and compared with the predicted SO_2 against the capillaries' measured distance from the center of the micro-outlet (Figure 2.6, panel D). The maximum mean SO_2 values for both Cap 4 and Cap5 fall between the model predicted SO_2 plots for 30 μm and 50 μm depth into the tissue. However, the minimum mean SO_2 values for both Cap 4 and Cap5 lay above the SO_2 values predicted for 50 μm depth into the tissue.

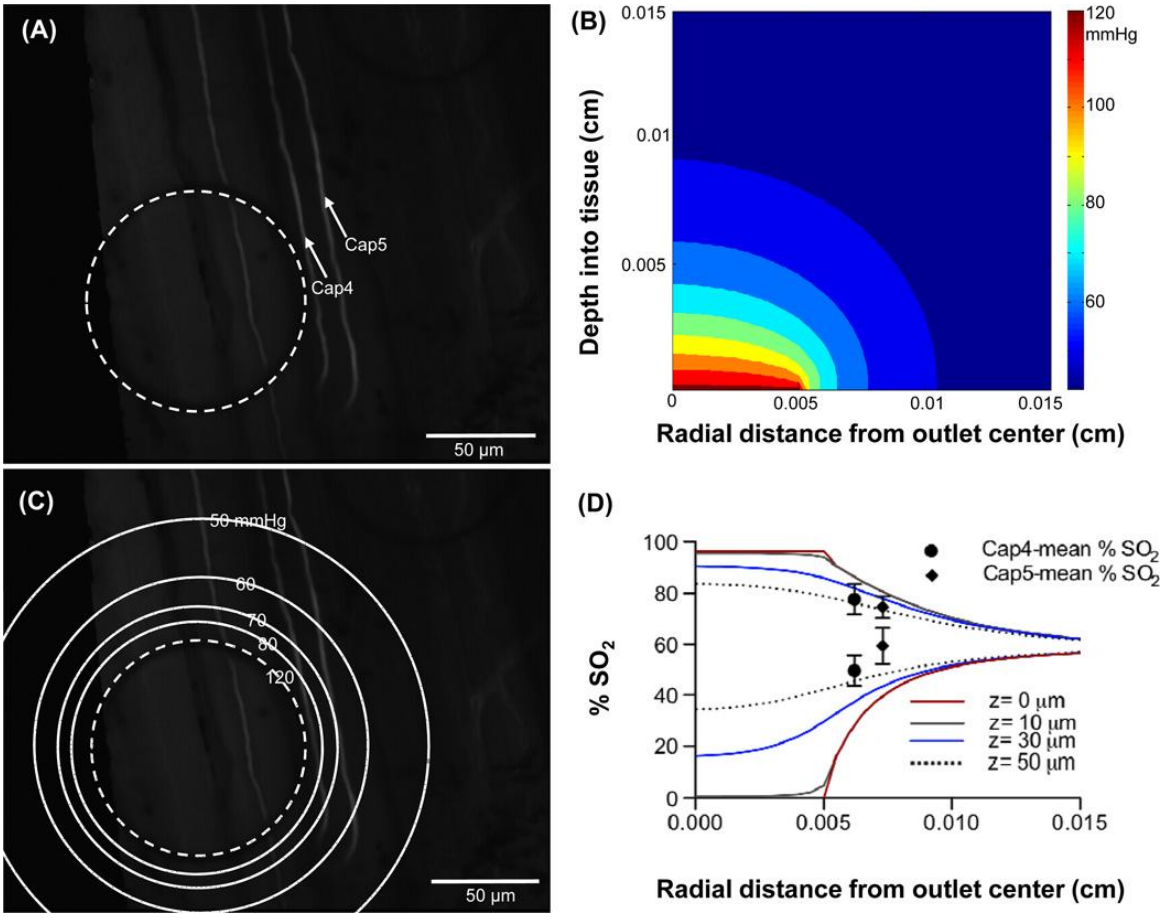

Figure 2.6 Selected capillaries Cap4 and Cap5 shown in panel A were analyzed for RBC SO_2 changes as O_2 levels delivered through the micro-outlet were oscillated in a square wave. The PO_2 level in the chamber was decreased from 16.2% (~123 mmHg) to 0.2% (~1.5 mmHg) for a 120 second hypoxic challenge and back to 16.2%. A six minute video sequence was captured beginning 2 minutes before the hypoxic challenge. The PO_2 distribution profile into the tissue was modelled. Panel B shows a 2D contour plot for a micro-outlet PO_2 value of 123 mmHg. Panel C shows the surface (depth=0 cm) PO_2 contour lines superimposed on top of the image showing the micro-outlet and the selected capillaries. The radial change in RBC SO_2 at various depths into the tissue (z=0 µm, 10 µm, 30 µm, and 50 µm) were calculated from the modelled PO_2 values using Hill's

equation then plotted against the radial distance from the center of the micro-outlet for a micro-outlet PO_2 values of 123 mmHg (upper set of lines, panel D) and 1.5 mmHg (lower set of lines, panel D). Experimentally calculated SO_2 mean values for Cap4 and Cap5 prior to and during hypoxia were plotted versus capillary location (upper and lower pair of symbols respectively, panel D).

2.4 Discussion

The aim of this research was to develop a micro-delivery approach for investigating localized microvascular signalling and response to varying PO_2 levels in live tissue. This was accomplished by designing O_2 delivery micro-outlets in ultrathin glass using microfabrication techniques. The proposed dimensions of the patterned micro-outlets were estimated by mathematically modelling the PO_2 distribution profile for micro-outlets of varying sizes in live tissue using a numerical simulation code written in MATLAB (Figure 2.2) (Mathworks, Natick, MA). O_2 delivered to the microcirculation alters the SO_2 levels of RBCs but is also partly consumed by the surrounding metabolic tissue. The microcirculation system constantly fine tunes the local hemodynamic and geometrical properties in response to changes in the RBC SO_2 levels (Ellis et al. 2005, Ellsworth et al. 2009). This is the mechanism by which the microvasculature matches O_2 supply into the tissue with the metabolic demand. Just like any stimulus-response mechanism, the system is sensitive to a specific threshold of applied stimulus. Hence, an optimal outlet diameter should deliver enough O_2 into the tissue to stimulate a microvascular response. Yet, this should not compromise the accurate localization of the stimulus. In other words, radial diffusion away from the center of the micro-outlet must

be limited to create enough contrast between the area stimulated and nearby regions of the microvascular bed. Also, when choosing the dimensions of the O_2 delivery micro-outlet, the microvascular geometry, specifically the dimensions of a single microvascular unit must be considered. The size of a microvascular unit within the rat skeletal muscle is approximately 150 μm × 400 μm. To better understand the microvascular response mechanism, the size of the micro-outlet must allow us to examine specific locations within a single microvascular unit. For instance, it would be insightful to investigate the effects of inducing local hypoxia at the venular end as opposed to the arteriolar end, or to examine the effects of stimulating a single or multiple capillaries. Hence, a proposed micro-outlet diameter of ~100 μm was selected based on the computational model and the above considerations. Note that the computational model assumes a continuous distribution of capillaries throughout the tissue region of interest. Since this is an approximation whose accuracy will depend on local properties (e.g., capillary spacing and whether or not the micro-outlet directly overlays surface capillaries), the predictions of the model need to be validated by experimental observations.

The O_2 permeable fluorosilicone acrylate membrane in the original IVVM setup was replaced by the ultrathin glass substrate patterned with the O_2 delivery micro-outlets (Figure 2.1). O_2 levels transported through the outlets could be oscillated using computer controlled flow meters connected to the gas exchange chamber. Therefore, it was essential to validate the relationship between the chamber PO_2 oscillations and those delivered through the micro-outlets. This was done *in vivo* by testing the response to O_2 delivery through the micro-outlets to interfaced live tissue (rat EDL muscle) using IVVM. The RBC SO_2 levels altered in response to oscillating the tissue PO_2 levels using

the micro-outlets for O_2 delivery. The RBC SO_2 changes were closely associated with the oscillated chamber PO_2 levels during both sine wave and square wave oscillations, however, with a certain time lag in both cases (Figure 2.4 and Figure 2.5). It is critical to note the absence of such a response delay between sensed and chamber PO_2 levels when testing for O_2 delivery through the micro-outlets *in vitro* (data not shown). Hence, the time lag observed between the measured RBC SO_2s (essentially sensed PO_2) and the chamber PO_2 oscillations *in vivo* cannot be attributed to a systematic error. Rather, the delay in tissue response is probably due to O_2 diffusion through the tissue to the RBCs.

For the sine wave oscillation data, similar to the measured RBC SO_2 profile, the SO_2 curve estimated from the measured chamber PO_2 data using Hill's equation (Hill 1910) shows a rapid change at lower PO_2 levels and plateaus as the PO_2 reaches peak levels (Figure 2.4). This typical relationship between PO_2 and RBC SO_2 is due to the cooperative binding of hemoglobin to O_2 (Hill 1910). The difference observed between the estimated and measured SO_2 minima indicates that the RBCs in the selected capillaries were experiencing a narrower range of PO_2 oscillations than what was measured in the chamber. The decrease in the amplitude of PO_2 oscillations experienced by the selected capillaries is proportional to the depth within the tissue (Goldman 2008). The lower saturation values at the peak of the oscillation measured for Cap1 relative to Cap2 can be attributed to the relatively higher mean supply rate for Cap1. The higher the supply rate, the less time the RBCs have to pick up O_2 as they flow across the micro-outlet, which results in lower mean SO_2 values.

Following validation of O_2 delivery through the micro-outlets against controlled chamber PO_2 oscillations, the degree of radial O_2 diffusion from the center of the micro-outlet was

estimated *in vivo*. This was done by measuring the RBC SO_2in selected capillaries (Cap4 and Cap5, Figure 2.6, panel A) at measured distances from the edge of the micro-outlet and comparing the results to the model calculations. Figure 2.6 (panel D) shows the model's predicted steady state O_2 saturations for the same high and low micro-oultlet PO_2 levels used during the *in vivo* measurements. The model shows that the magnitude of the SO_2 perturbation decreases rapidly with radial distance from the edge of the outlet and with depth into the tissue. The diminished effect of the outlet is reflected in the measured SO_2 values for the two capillaries. Although the precise depth of the capillaries were not measured *in vivo*, the approximate depth of 40–50 μm suggested by comparing the measured values to the simulation for 123 mmHg PO_2 in the outlet is close to the expected depth. The paired measurements with 1.5 mmHg in the micro-outlet are higher than predicted by the model for this depth into the tissue but the result is not unexpected. With high PO_2 in the tissue the RBC SO_2 under steady state conditions should equilibrate with the surrounding tissue, i.e. the simulation and experiment should match. With low PO_2 in the tissue, the RBCs should be offloading O_2 to the tissue and hence the RBC SO_2 should correspond to a higher PO_2 than the PO_2 in surrounding tissue. These results highlight that the impact of changing O_2 levels in the micro-outlet are limited to the immediate vicinity of the outlet thus meeting our objective of designing a device to investigate local regulation of O_2 supply *in vivo*.

The *in vivo* data presented verify that the 100 μm diameter micro-outlets were indeed able to alter SO_2 levels of RBCs in capillaries flowing either directly over or even in close proximity to the outlet. Experimentally measured RBC SO_2 levels fit with our computational model of the PO_2 distribution into the tissue from an interfaced O_2 delivery

micro-outlet. These results delineate an important step towards designing a novel microfluidic device for O_2 delivery to microvascular networks to further investigate regulation of O_2 supply *in vivo*. This device would also allow us to examine the physiological level of O_2 supply set by the microvasculature in the same tissue preparation by recording images at un-stimulated regions distal from the micro-outlets; a goal not feasible with current techniques.

2.5 References

Comyn J. Polymer Permeability. New York: Chapman and Hall Inc.; 1985. pp. 21–23.

Dewhirst M.W., Klitzman B., Braun R.D., Brizel D.M., Haroon Z.A., Secomb T.W. (2000) Review of methods to study oxygen transport at the microcirculatory level. *Int. J. Cancer*. **90:**237–255.

Duling B.R. (1974) Oxygen sensitivity of vascular smooth muscle. II. *In vivo* studies. *Am. J. Physiol.* **227:**42–49.

Ellis C.G., Goldman D., Hanson M., Stephenson A.H., Milkovich S., Benlamri A., Ellsworth M.L., Sprague R.S. (2010) Defects in oxygen supply to skeletal muscle of prediabetic ZDF rats. *Am. J. Physiol. Heart. Circ. Physiol.* **298:**1661–1670.

Ellis C.G., Jagger J., Sharpe M. (2005) The microcirculation as a functional system. *Critical. Care.* **9:**S3–S8.

Ellis C.G., Bateman R.M., Sharpe M.D., Sibbald W.J., Gill R. (2002) Effect of a maldistribution of microvascular blood flow on capillary O_2 extraction in sepsis. *Am. J. Physiol. Heart. Circ. Physiol.* **282:**156–164.

Ellis C.G., Ellsworth M.L., Pittman R.N., Burgess W.L. (1992) Application of image analysis for evaluation of red blood cell dynamics in capillaries. *Microvasc. Res.* **44:**214–225.

Ellis C.G., Ellsworth M.L., Pittman R.N. (1990) Determination of red blood cell oxygenation in vivo by dual video densitometric image analysis. *Am. J. Physiol. Heart. Circ. Physiol.* **258:**H1216–H1223.

Ellsworth M.L., Ellis C.G., Goldman D., Stephenson A.H., Dietrich H.H., Sprague R.S. (2009) Erythrocytes: Oxygen Sensors and Modulators of Vascular Tone. *Physiology.* **24:**107–116.

Ellsworth M.L., Forrester T., Ellis C.G., Dietrich H.H. (1995) The erythrocyte as a regulator of vascular tone. *Am. J. Physiol.* **269:**H2155–H2161.

Ellsworth M.L., Pittman R.N., Ellis C.G. (1987) Measurement of hemoglobin oxygen saturation in capillaries. Am. J. Physiol. **252:**H1031–H1040.

Goldman D. (2008) A Mathematical Model of Oxygen Transport in Intact Muscle with Imposed Surface Oscillations. *Math. Biosci.* **213(1):**18–28.

Hanson M.S., Ellsworth M.L., Achilleus D., Stephenson A.H., Bowles E.A., Sridharan M., Adderley S., Sprague R.S. (2009) Insulin inhibits low oxygen induced ATP release

from human erythrocytes: implication for vascular control. *Microcirculation.* **16:**424–433.

Hill A.V. (1910) The possible effects of the aggregation of the molecules of hemoglobin on its dissociation curve. *J. Physiol. (London).* **Iv:**41.

Ilie M., Foglietti V., Cianci E., Minotti A. (2003) Optimized deep wet etching of borosilicate glass through Cr-Au-resist mask. *SPIE*. **5227:**318–322.

Jackson W.F., Duling B.R. (1983) The oxygen sensitivity of hamster cheek pouch arterioles. In vitro and in situ studies. *Circ. Res*. **53**:515–525.

Jagger J.E, Bateman R.M., Ellsworth M.L., Ellis C.G. Role of erythrocyte in regulating local O_2 delivery mediated by haemoglobin oxygenation. (2001) *Am. J. Physiol. Heart. Circ. Physiol.* **280:**H2833–H2839.

Japee S.A., Pittman R.N., Ellis C.G. (2005) A new video image analysis system to study red blood cell dynamics and oxygenation in capillary networks. *Microcirculation.* **12:**489–506.

Japee S.A., Ellis C.G., Pittman R.N. (2004) Flow visualization tools for image analysis of capillary networks. *Microcirculation.* **11:**39–54.

Riemann M., Rai A., Ngo A.T., Dziegiel M.H., Holstein-Rathlou N-H., Torp-Pedersen C. (2010) Oxygen-dependant vasomotor responses are conducted upstream in the mouse cremaster microcirculation. *J. Vac. Res.* **48:**79–89.

Sprague R.S., Stephenson A.H., Bowles E.A., Stumpf M.S., Lonigro A.J. (2006) Reduced expression of Gi in erythrocytes of humans with Type 2 Diabetes is associated with impairment of both cAMP generation and ATP release. *Diabetes.* **55:**3588–3359.

Srivastava N., Davenport R.D., Burns M.A. (2005) Nanoliter viscometer for analyzing blood plasma and other liquid samples. *Anal. Chem.* **77:**383–392.

Tyml K., Budreau C.H. (1991) A new preparation of rat extensor digitorum longus muscle for intravital investigation of the microcirculation. *Int. J. Microcirc. Clin. Exp.* **10:**335–343.

Varghese H.J., MacKenzie L.T., Groom A.C., Ellis C.G., Chambers A.F., MacDonald I.C. (2005) Mapping of the functional microcirculation in vital organs using contrast-enhanced in vivo video microscopy. *Am. J. Physiol. Heart. Circ. Physiol.* **288:**185–193.

Chapter 3

3 Modeling steady state SO_2-dependent changes in capillary ATP concentration using novel O_2 micro-delivery methods[1]

[1] Research article published in Frontiers in Physiology (2013) 4:260

3.1 Introduction

The microcirculation plays the important role of delivering and regulating the exchange of oxygen (O_2) and nutrients to surrounding live metabolic tissue. The transport processes in the microcirculation are tightly controlled and highly integrated. Since proper O_2 supply to tissue is critical for cellular function and survival, the mechanisms underlying O_2 transport and distribution have been under thorough investigation. The microvasculature has to continuously adjust erythrocyte distribution and hence O_2 supply to meet the varying demand of metabolic tissue. During exercise, erythrocyte supply rate increases delivering more O_2 carrying erythrocytes to the microvasculature. The highly regulated system implies the presence of signalling components that link tissue O_2 demand with blood flow and microvascular function.

A great amount of evidence suggests the involvement of the erythrocyte as a sensor and a key player in this regulation mechanism (Stein and Ellsworth, 1993, Ellsworth et al., 1995, Ellsworth et al., 2008). Erythrocytes are the carriers of O_2, bound to hemoglobin, in the microcirculation. Erythrocytes also contain large amounts of adenosine triphosphate (ATP) (Miseta et al., 1993), a potent vasodilator, and are known to release it under

hypoxic conditions (Bergfeld and Forrester, 1992, Jagger et al., 2001, González-Alonso et al., 2002). Once ATP is released, it binds to purinergic receptors (P2Y) on the vascular endothelium eliciting a vaso-dilatory signal which is conducted upstream in the arteriolar tree (Ellsworth et al., 2008). The resulting vaso-relaxation of smooth muscle cells (SMCs) surrounding upstream arterioles increases erythrocyte supply rate to meet the metabolic demand of the hypoxic region downstream that initiated the release of ATP from erythrocytes.

For a long time, arterioles have been investigated as a major site of microvascular signalling (Dulling and Berne, 1970, Duling, 1974, Jackson, 1987). This has been assumed, mainly, due to the large longitudinal PO_2 gradients that exist at the arteriolar level. In terms of ATP-mediated signalling, the presence of SMCs implies that the released ATP will act locally and will instantaneously elicit a signal. However, the relatively short erythrocyte transit times in arterioles are anticipated to largely compromise the localization of this ATP signal, while the parabolic flow profile in the arteriole means only those cells closest to the wall experience the largest change in O_2 saturation (SO_2) and hence contribute to the signal. Cells flowing in the centerline will be experiencing a lesser drop in SO_2 and any released ATP will be carried downstream (Ellis et al., 2012).

Venules may also be involved in the regulation of O_2 supply since they act as the collectors of large populations of deoxygenated ATP-releasing erythrocytes. However, the diversity in the erythrocyte SO_2 levels as they drain from various upstream capillaries indicates that venules may only contribute to the overall vaso-dilatory signal (Ellis et al., 2012). Finely tuned regulation of O_2 distribution to specific capillaries or microvascular

units in the microcirculation demands the signal be highly localized. This may only be achieved at the capillary level. Erythrocytes traverse capillaries with long transit times and are in almost direct contact with the capillary endothelium. Hence, released ATP, mediated by erythrocyte deoxygenation, will effectively be transferred to purinergic receptors on the endothelium. Many studies have shown that the capillary endothelium is conductive when locally stimulated by vasodilators (Dietrich, 1989, Dietrich and Tyml, 1992a,b, Song and Tyml, 1993, Collins et al., 1998, Bagher and Segal, 2011)**.** Therefore, we hypothesize that capillaries are able to signal upstream arterioles for changes in erythrocyte supply rate in response to changes in capillary SO_2 level via SO_2 dependent ATP signaling by the erythrocyte (Ellis et al., 2012).

To test this hypothesis, we have been examining the micro-vascular response to local perturbations in tissue O_2 partial pressure (PO_2) using a novel O_2 micro-delivery tool (Ghonaim et al., 2011). We have created an O_2 micro-delivery (and removal) system that allows for altering local tissue PO_2 and hence erythrocyte SO_2 in a few selected capillaries at the surface of the Extensor Digitorum Longus (EDL) muscle of the rat (Figure 3.1A). This system replaces the gas exchange chamber originally used in our group to alter surface tissue PO_2 of the entire bottom surface of the muscle (Ellis et al., 2012, Ghonaim et al., 2011). The chamber is positioned in the platform of an inverted microscope and is connected to computer controlled gas flow meters, which allows for capturing video images of the microvascular response to PO_2 perturbations while simultaneously controlling chamber PO_2 levels. Erythrocyte SO_2 values are calculated based on a dual-wavelength image capture system and video sequences are post-

processed to extract functional images and hemodynamic information as previously described (Ellis et al., 1990, Ellis et al., 1992, Japee et al., 2004, Japee et al., 2005a,b).

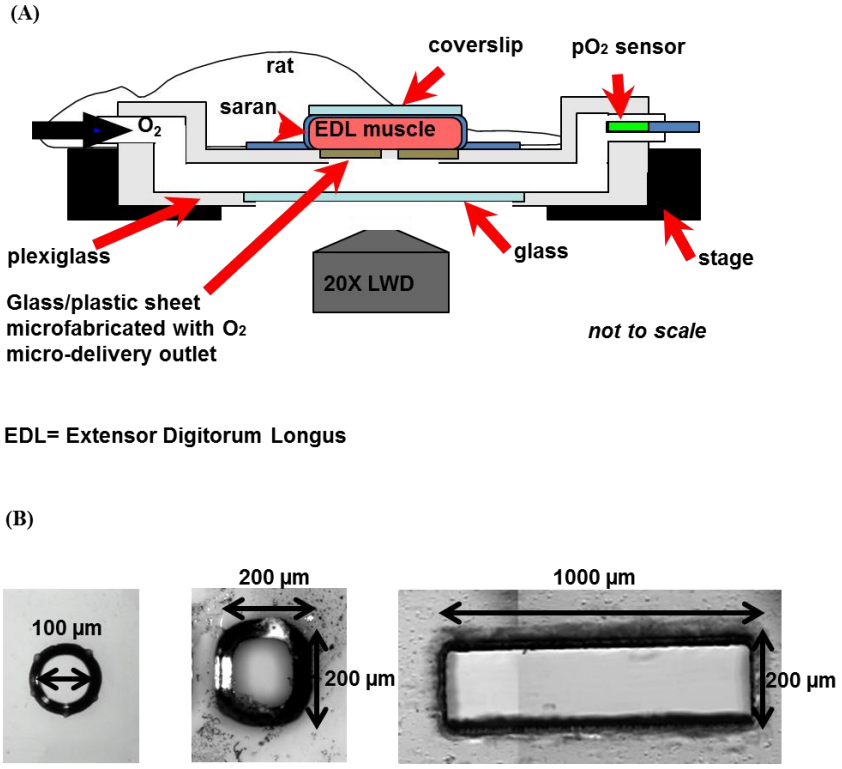

Figure 3.1 (A) The novel O_2 micro-delivery approach. The Extensor Digitorum Longus (EDL) rat muscle is surgically exposed and positioned on the viewing platform of an inverted microscope. O_2 is delivered to the surface of the muscle through a micro-outlet patterned in ultrathin glass/plastic sheet (Ghonaim et al., 2011). O_2 levels in the gas exchange chamber near the muscle surface are oscillated using computer controlled flow meters. Real-time videos of the trans-illuminated tissue are monitored and recorded using a dual-wavelength video microscopy system (Ellis et al., 1990, 1992; Japee et al., 2004, 2005a,b) (B) Three designs of the oxygen micro-delivery outlet being tested: circular micro-outlet (~100 µm in diameter), a square micro-slit (200 µm x 200 µm), and a rectangular micro-slit (1000 µm wide x 200 µm long).

In our novel O_2 micro-delivery setup, ultrathin plastic/glass sheet patterned with an O_2 delivery micro-outlet replaces the gas permeable membrane in the original chamber (Ellis et al., 2012, Ghonaim et al., 2011). Data presented earlier (Ghonaim et al., 2011) show that circular micro-delivery outlets (100 μm in diameter) can alter SO_2 in single capillaries flowing directly over the outlet. However, in order to elicit microvascular responses, the optimal outlet dimensions should allow for a sufficient number of capillaries within a network to be stimulated to produce a large enough ATP signal. This should be accomplished while ensuring the high localization of the stimulus to affect only the desired capillaries. This requires testing with various O_2 outlet sizes and dimensions. Combining the possible technical challenges involved in creating multiple designs of the O_2 micro-delivery device with the inherent complexities of the O_2 regulation system led us to develop a computational model for the system under investigation.

Recently, Goldman et al (2012) presented a theoretical mathematical model based on previous work by Goldman and Popel (1999) and Arciero et al (2008) to describe O_2 and ATP transport in the rat EDL microcirculation when using the original O_2 exchange chamber. In this study, we employ the same approach with the objective of calculating SO_2 and ATP changes in selected capillaries flowing over an O_2 delivery outlet of specific dimensions. Three designs of the O_2-delivery micro-outlet were tested: circular outlet (100 μm in diameter) (Ghonaim et al. 2011), square outlet (200μm x 200μm), and rectangular slit (200μm long x 1000μm wide) (Figure 3.1B). Average capillary SO_2 and ATP level at steady-state were calculated at various chamber PO_2 levels (15, 40 and 150 mmHg) relative to a zero flux boundary condition. In order to simplify the system under investigation, an idealized three dimensional (3D) parallel array capillary geometry has

been used. Simulations were also run on a 3D idealized array geometry in which a terminal arteriole (9 μm in diameter) replaced 4 capillaries and was positioned 30 μm from the bottom tissue surface. These simulations allowed for investigating the potential role of the terminal arteriole in O_2 regulation. Confirming previous findings (Ghonaim et al., 2011), the results indicated that the maximum amount of radial O_2 diffusion from an O_2 delivery micro-outlet is limited to ~50 μm beyond the outlet edge, while axial diffusion affects ~100 μm of tissue. The rectangular slit has the important property of ensuring that capillaries surrounding the network of interest are all experiencing the same PO_2 drop, which minimizes re-oxygenation and emphasizes the ATP signal. This design also produces sufficient ATP release in multiple capillaries such that it should be able to consistently elicit micro-vascular responses, although this remains to be confirmed experimentally. The results presented here also predict minimal contribution of terminal arterioles to the net magnitude of ATP emerging from the capillary network although they would participate as O_2 sources and hence influence the O_2 distribution. In the future, 3D capillary networks reconstructed from experimental data can be modeled which will provide more realistic data and help to more closely predict changes in various parameters.

3.2 Materials and Methods

3.2.1 Oxygen transport model

In this work, O_2 transport and ATP transport were modeled in an idealized 3D capillary network consisting of an array of parallel capillaries (oriented in the *y* direction). The

computational model of O_2 transport was based on a finite-difference model described by Goldman and Popel (1999, 2000, 2001). In the model, the reaction-diffusion equation below was used to describe time-dependent tissue PO_2 *P(x,y,z,t)*:

$$\frac{\partial P}{\partial t} = \left[1 + \frac{c_{Mb}}{\alpha}\frac{dS_{Mb}}{dP}\right]^{-1}\left\{D\nabla^2 P - \frac{1}{\alpha}M(P) + \frac{1}{\alpha}D_{Mb}c_{Mb}\nabla\cdot\left(\frac{dS_{Mb}}{dP}\nabla P\right)\right\} \quad (1)$$

where *D* is the tissue O_2 diffusion coefficient, α is the tissue O_2 solubility, and *M(P)* is consumption rate of O_2 in tissue (Table 1). O_2 transport in tissue was facilitated by the presence of myoglobin where c_{Mb} is the myoglobin concentration, D_{Mb} is the myoglobin diffusion coefficient, and $S_{Mb}(P)=P/(P+P_{50,Mb})$ is the myoglobin SO_2. Convective transport of O_2 in the micro-vessels at each axial location *y* was described using the following time-dependent mass balance equation for capillary SO_2, *S(y,t)*:

$$\frac{\partial S}{\partial t} = -\left[C + \alpha_b\frac{dP_b}{dS}\right]^{-1}\left\{-u\left[\tilde{C} + \tilde{\alpha}_b\frac{dP_b}{dS}\right]\frac{\partial S}{\partial y} - \frac{1}{\pi R}\oint j\cdot d\theta\right\} \quad (2)$$

where *u* is the mean blood velocity, *R* is the capillary radius, *j* is the O_2 flux at (y,θ) out of the capillary, *C* and $\tilde{C}$ are blood O_2-binding capacities, respectively, directly related to hematocrit:

$$C = H_T C_{Hb}$$

$$\tilde{C} = H_D C_{Hb}$$

where H_T is tube (volume-weighted) hematocrit, H_D is discharge (flow-averaged) hematocrit, and C_{Hb} is the binding capacity of hemoglobin (Table 1) (Goldman and Popel 2001). P_b is the blood PO_2, and α_b and $\tilde{\alpha}_b$ are volume- and flow-weighted blood O_2 solubilities, respectively (Goldman and Popel, 2001), where,

$$\alpha_b = H_T\alpha_{cell} + (1- H_T)\ \alpha_{pl}$$

$$\tilde{\alpha}_b = H_D\alpha_{cell} + (1- H_D)\ \alpha_{pl}$$

where α_{cell} and α_{pl} are the O_2 solubilities inside the erythrocyte and in the plasma (Goldman and Popel 2001). The O_2 flux at the capillary-tissue interface was given by:

$$j = \kappa\left(P_b - P_w\right) \tag{3}$$

where κ is the mass transfer coefficient and P_w is the tissue PO_2 at the capillary surface. κ is a function of hematocrit as it describes the effect of RBC spacing on O_2 diffusion and exchange between capillary and tissue (Eggleton et al., 2000). At the capillary surface, the boundary condition was specified as:

$$-D\alpha\frac{\partial P_w}{\partial n} = j \tag{4}$$

where *n* is the unit vector normal to the capillary surface and *j* is given by equation (3). In the model presented here, zero O_2 flux conditions (no O_2 exchange across tissue boundary) were specified at the tissue boundaries, except where PO_2 was fixed on part or all of the bottom surface to represent the effect of the O_2 exchange chamber (see below). As in the model described by Goldman and Popel (1999), Michaelis-Menten consumption kinetics, $M=M_0\ P/(P+P_{cr})$, and the Hill equation for the oxyhemoglobin saturation curve, $S(P)=P^n/(P^n+P_{50}{}^n)$, were used along with the above O_2 transport equations to calculate the tissue O_2 transport.

Hemodynamic parameters (erythrocyte mean velocity, v_{rbc}, and hematocrit, H_T) were determined from *in vivo* experimental measurements in the EDL muscle of the rat. The

capillary network consisted of 72 parallel capillaries, each of which was discretized into 50 cylindrical segments, and the tissue domain surrounding the capillaries had dimensions of 216 x 532 x 500 μm and was discretized into 7,304,853 computational nodes using a grid spacing of approximately 2 μm (Figure 3.2A). Capillary entrance SO_2 (65%) and the tissue O_2 consumption rate (1.5×10^{-4} ml O_2/ml/s) were set based on previous experimental data (Fraser et al. 2012).

For simulations that included a terminal arteriole in the 3D network geometry, the arteriole (9 μm in diameter) was positioned approximately 30 μm from the bottom tissue surface and replaced 4 capillaries in the original parallel array capillary geometry (Figure 3.2B). Simulations including the arteriole were run at both 65% and 80% arteriolar entrance SO_2.

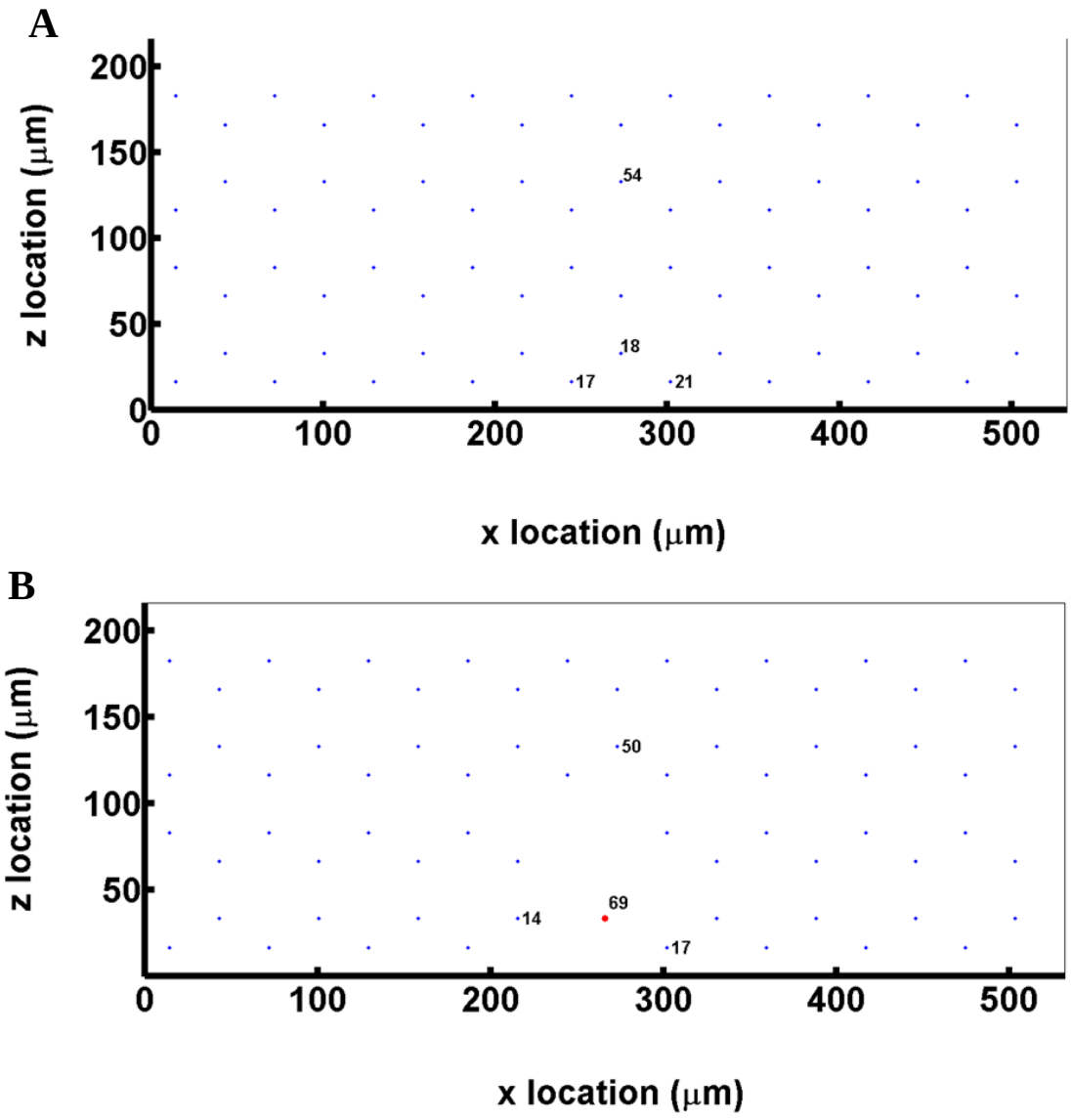

Figure 3.2 (A) A cross sectional view of the idealized capillary parallel-array geometry showing the positioning and numbering of the 72 hexagonally arranged capillaries in the modeled network **(B)** A cross sectional view of the idealized capillary parallel array geometry with a terminal arteriole (vessel 69, 9 μm in diameter) replacing 4 capillaries within 30 μm from bottom tissue surface.

3.2.2 ATP transport model

ATP transport in the idealized 3D capillary network was modeled as described by Goldman et al 2012, based on the O_2 transport mathematical model described earlier (Goldman and Popel 2000). Using a capillary entrance ATP concentration [ATP] of zero, plasma [ATP] was calculated by using a finite-difference method to solve the following continuum partial differential equation (Goldman et al 2012):

$$\begin{aligned}\left(1-H_T\right)\frac{\partial}{\partial t}\left[ATP\right] = -u\left(1-H_D\right)\frac{\partial}{\partial y}\left[ATP\right] \\ +H_T C_0\left(1-C_1 S\right)-\frac{2}{R}k_d\left[ATP\right]\end{aligned} \tag{5}$$

where u is the mean blood velocity at axial location y, H_D and H_T are the discharge and tube hematocrit, respectively, and R is the capillary radius. C_0 and C_1 (see Table 3) are constants used to linearly approximate the ATP release rate as a function of SO_2, while k_d provides an approximation of ATP degradation by the endothelium as previously described (Arciero et al., 2008).

To calculate the steady-state distributions of tissue PO_2 as well as capillary SO_2 and [ATP], time-dependent O_2 transport and ATP transport simulations were run, using zero initial conditions for all variables, until there were minimal changes in tissue O_2 consumption and PO_2, and capillary O_2 flux, SO_2 and [ATP] between consecutive time steps.

3.2.3 Tissue PO_2 boundary conditions used to model oxygen exchange chamber

For the idealized capillary geometry, 3D tissue PO_2 distribution and capillary [ATP] at steady state were calculated for O_2 delivery using a full gas exchange chamber, a circular micro-outlet (100 μm in diameter), a square micro-outlet (200 μm x 200 μm), or a rectangular micro-slit (1000 μm wide x 200 μm long). For each chamber type, simulations were run at 3 PO_2 boundary conditions either over full surface (with full gas exchange chamber) or only at the micro-slit opening: 15 mmHg, 40 mmHg and 150 mmHg. For the cases in which the PO_2 boundary condition is altered only at the micro-slit opening, the rest of the tissue surrounding the micro-slit is set to zero O_2 flux boundary condition. The results from all simulations were compared to a fourth control case in which full surface is set to zero O_2 flux boundary condition.

For the idealized capillary geometry that includes the terminal arteriole, O_2 diffusion was modeled for a full gas exchange chamber or a rectangular micro-slit (1000 μm wide x 200 μm long) at the four PO_2 boundary conditions discussed above. Each set of simulations was run with arteriolar entrance SO_2 of 65% or 80%. Table 2 lists the summary of simulations and boundary conditions used in this study.

Parameter	Description	Value
α	O_2 solubility	3.89×10^{-5} ml O_2 ml^{-1} $mmHg^{-1}$
D	O_2 diffusion coefficient	2.41×10^{-5} cm^2 s^{-1}
P_{cr}	Critical PO_2	0.5 mmHg
c_{Mb}	myoglobin concentration	1.02×10^{-2} ml O_2 ml^{-1}
D_{Mb}	myoglobin diffusion coefficient	3×10^{-7} cm^2 s^{-1}
P_{50}	Blood PO_2 at 50% hemoglobin SO_2	37 mmHg
n	Hill exponent	2.7
$P_{50,Mb}$	PO_2 at 50% myoglobin SO_2	5.3 mmHg
v_{rbc}	erythrocyte mean velocity	1.45×10^{-2} cm s^{-1}
C_{HB}	binding capacity of hemoglobin	0.52 ml O_2 ml^{-1}
H_T	Tube hematocrit	0.19
H_D	Discharge Hematocrit	0.2
C_0	Constant approximating linear ATP release rate as a function of SO_2	1.4×10^{-9} mol $s^{-1} \cdot cm^{-3}$
C_1	Constant approximating linear ATP release rate as a function of SO_2	0.891
k_d	ATP degradation rate	2.0×10^{-4} cm s^{-1}

Table 3.1 Parameter values used in oxygen and ATP transport simulations.

Network specifications	**Chamber type tested**	**Corresponding figure in manuscript**	**PO_2 condition at chamber outlet (in each chamber type tested)**
Capillary array	Full Chamber	3.3	• Zero O_2 flux (Control)
	Circle	3.4	• 40 mmHg
	Square	3.5	• 15 mmHg
	Rectangle	3.6	• 150 mmHg
Capillary array with arteriole (entrance SO_2=65%)	Full Chamber	3.8	• Zero O_2 flux (Control)
	Rectangle	3.10	• 40 mmHg
			• 15 mmHg
			• 150 mmHg
Capillary array with arteriole (entrance SO_2=80%)	Full Chamber	3.9	• Zero O_2 flux (Control)
	Rectangle	3.11	• 40 mmHg
			• 15 mmHg
			• 150 mmHg

Table 3.2 List of boundary conditions used in oxygen and ATP transport simulations (Summary of Transport Simulations, Chamber Types and Boundary Conditions)

3.3 Results

3.3.1 Mathematical modelling of SO_2-dependent ATP release in capillary networks in response to localized tissue PO_2 perturbations

In this study, the release of ATP in capillaries mediated by tissue hypoxia and the de-saturation of hemoglobin was modeled in a 3D idealized parallel capillary network. The dependence of the magnitude of total ATP release on the number of de-oxygenated capillaries was also examined. Based on our previously described experimental work (Ghonaim et al. 2011), we mathematically simulated O_2 delivery to and removal from selected capillaries on the surface of skeletal muscle tissue (rat EDL) using three designs of O_2 exchange micro-outlets used in our *in vivo* experiments (Figure 3.1B). In order to compare local O_2 perturbations using the micro-outlets to global perturbations using the full gas exchange chamber (Ellis et al., 2012, Ghonaim et al. 2011), O_2 delivery to and removal from the entire bottom tissue surface was also modeled. For each set of simulations, 3D tissue PO_2 distribution profiles and corresponding 3D capillary [ATP] maps were generated. Plots of calculated SO_2 and [ATP] along the length of selected capillaries (21, 18, 17, 54) at steady state were also created. All simulations were run using software written in Fortran, and the results were analyzed and the plots were produced using MATLAB.

3.3.1.1 Full surface gas exchange chamber

In this set of simulations, the 3D PO_2 distribution in the tissue and corresponding SO_2 and [ATP] distribution along capillary length were modeled for the control scenario in which the full bottom tissue surface is exposed to PO_2 perturbations. This would experimentally simulate using the full gas exchange chamber. As shown in Figure 3.3, at 40 mmHg, steady-state tissue PO_2 and capillary [ATP] distributions are comparable to the no-flux control condition. At the venular end of the capillaries, SO_2 values ranged from ~50% for surface capillaries (# 21, 18, and 17) to ~40% for capillaries deeper than 100 µm into the tissue (capillary 54), and the corresponding capillary [ATP] values were within 15% of those at zero O_2 flux boundary condition. However, under imposed tissue hypoxia (15 mmHg), the surface capillaries dropped their SO_2 by approximately 70% which corresponded to ~40% higher steady state capillary [ATP] relative to zero flux condition (Figure 3.3C). This was clearly depicted in the corresponding vessel map (Figure 3.3B). The deeper capillary (54) was less affected with ~30% lower hemoglobin SO_2 and ~12% increase in ATP release relative to zero flux. Exposing the full tissue surface to relatively high chamber PO_2 (150 mmHg) had the most significant impact on [ATP] in the capillary network. At 150 mmHg, hemoglobin SO_2 in both surface and deep tissue capillaries converged to ~100% with ~70% decrease in steady state [ATP] relative to no-flux (Figure 3.3C). The depth of the PO_2 perturbation into the tissue when using the full gas exchange chamber was ~ 100 µm as shown in the 3D PO_2 profiles (Figure 3.3A).

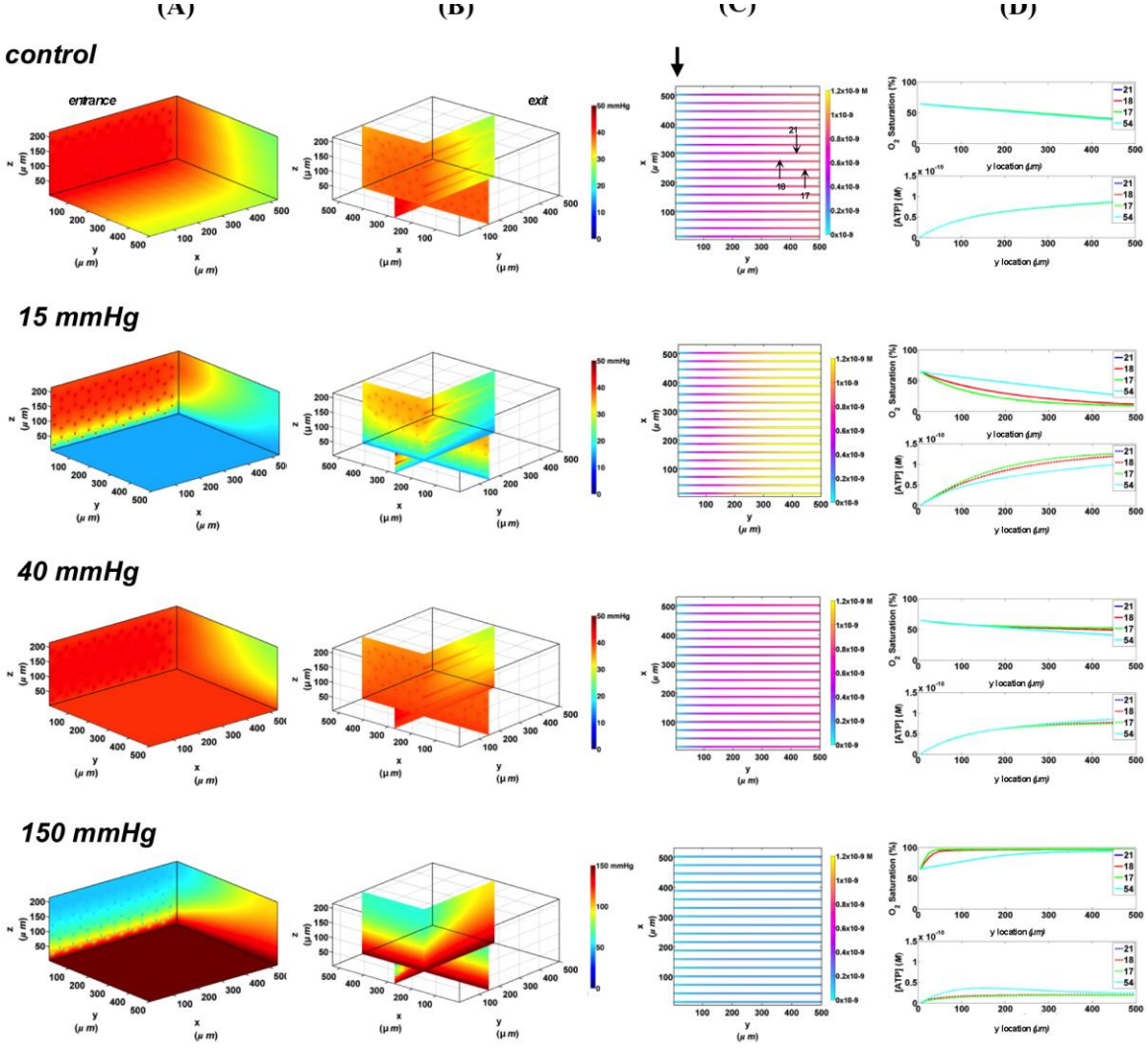

Figure 3.3 Simulations of 3D PO_2 and capillary [ATP] distribution in a tissue with idealized parallel capillary arrangement (72 hexagonally packed capillaries). In these simulations, we are modeling O_2 delivery to the bottom tissue surface using the full gas exchange chamber (Ellis et al., 2012; Ghonaim et al., 2011). Full bottom tissue surface is exposed to 15 mmHg, 40 mmHg, or 150 mmHg chamber PO_2 level relative to a zero flux

control boundary condition **(A)** Spatial 3D tissue PO_2 distribution (mmHg) at capillary entrance perspective **(B)** a capillary exit perspective showing combined X-Z plane slice at Y=150 µm and Y-Z plane slice at X= 277 µm (**C**) bottom perspective of a vessel map depicting distribution of [ATP] (mol/L=M) along the capillaries. Bolded arrow marks capillary entrance **(D)** Plots of SO_2 (%) and [ATP] changes along capillary length in selected capillaries (# 21, 18, 17, 54) marked by arrows on the vessel map. Capillaries 21 and 17 are 16 µm from the tissue surface, capillary 18 is 33 µm from tissue surface, and capillary 54 is deeper in the tissue, at 133 µm, and hence it is not shown in the current perspective of the vessel map. Note change in PO_2 scale from 0 to 50 mmHg in first three cases to 0 to 150 mmHg when surface is exposed to 150 mmHg.

3.3.1.2 Circular O_2 delivery micro-outlet

To investigate the effect of limiting the number of capillaries stimulated by local tissue PO_2 perturbations, we started by modeling capillary SO_2 and [ATP] changes when using a circular O_2 micro-outlet (100 µm in diameter, see Figure 3.1). Similar to previously discussed data (Ghonaim et al 2011), substantive changes in local tissue $PO_{2,}$ due to diffusion outwards from the circular outlet, is limited to less than ~50 µm, as shown in the 3D tissue PO_2 profiles (Figure 3.4A). Also, the hypoxic and hyperoxic stimuli were highly localized to only those capillaries directly over the micro-outlet (17, 18, 21) as shown in the vessel maps (Figure 3.4B). At 40 mmHg chamber PO_2 level, calculated

capillary SO_2 and [ATP] were in close agreement with the no-flux control for both surface and deep tissue capillaries with values being within ~1% and ~3%, respectively (Figure 3.4C). Under imposed hypoxia, the capillary SO_2 dropped as capillaries crossed the micro-outlet region reaching a minimum value ~40 μm downstream of the outlet after which SO_2 levels increased slightly due to re-oxygenation by surrounding capillaries. At the venular end, steady state SO_2 levels in surface capillaries were 15% lower relative to zero flux while capillary 54 experienced only a 6% drop in SO_2. This corresponded to only 10% increase in [ATP] in surface capillaries while [ATP] in capillary 54 remained unchanged relative to zero flux. At 150 mmHg, the increase in capillary SO_2 level is observed directly over the micro-outlet region reaching a maximum at the outlet exit. The capillary SO_2 levels dropped sharply downstream of the outlet due to O_2 diffusion into adjacent capillaries and tissue. Surface capillary SO_2 decreased to ~63% and deep tissue capillaries to 51% at ~200 μm downstream of the outlet. This corresponded to ~40% decrease in [ATP] in surface capillaries and ~20% decrease in [ATP] of deeper tissue capillaries relative to zero flux condition.

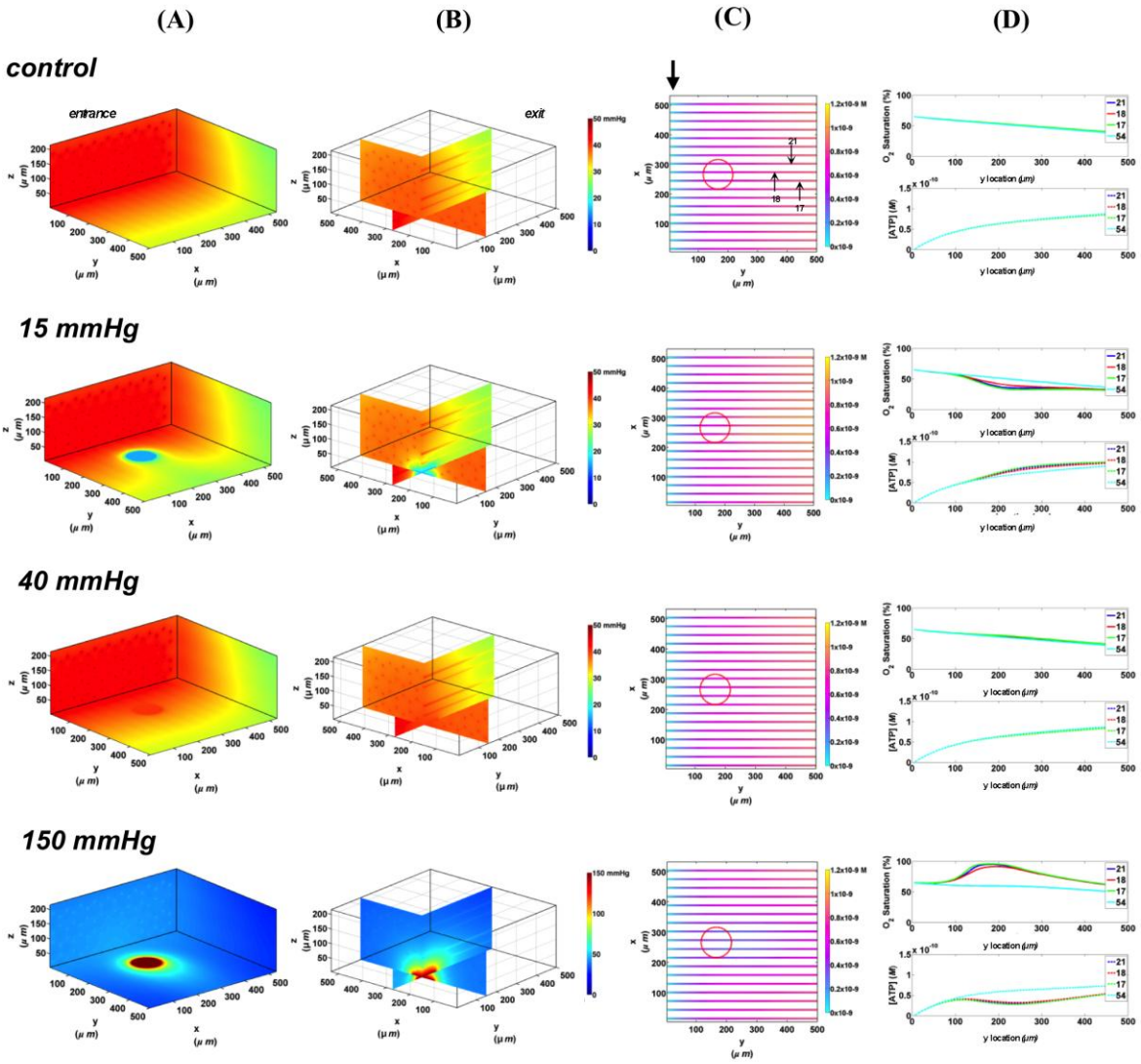

Figure 3.4 Simulations of 3D PO_2 and capillary [ATP] distribution in a tissue with idealized parallel capillary arrangement (72 hexagonally packed capillaries). In these simulations, we are modeling O_2 delivery through a circular oxygen micro-delivery outlet (100 μm in diameter) to bottom tissue surface using novel micro-delivery approach (see Figure 3.1). Tissue surface directly on top of the micro-delivery outlet is exposed to 15

mmHg, 40 mmHg, or 150 mmHg chamber PO_2 level relative to a zero flux control boundary condition (A) Spatial 3D tissue PO_2 distribution (mmHg) at capillary entrance perspective (B) a capillary exit perspective showing combined X-Z plane slice at Y=150 µm and Y-Z plane slice at X= 277 µm (C) bottom perspective of a vessel map depicting distribution of [ATP] (mol/L=M) along the capillaries. Bolded arrow marks capillary entrance (D) Plots of SO_2 (%) and [ATP] changes along capillary length in selected capillaries (21, 18, 17, 54) marked by arrows on the vessel map. Capillaries 21 and 17 are 16 µm from tissue surface, capillary 18 is 33 µm from tissue surface, and capillary 54 is deeper in the tissue, at 133 µm, and hence it is not shown in the current perspective of the vessel map.

3.3.1.3 Square O_2 delivery micro-outlet

Next, we simulated the effect of increasing the area of O_2 exchange, and hence perturbing a greater number of capillaries, by simulating an O_2 delivery micro-outlet 200 µm x 200 µm square. Similar to the circular micro-outlet design and as previously described (Ghonaim et al 2011), the change of local tissue PO_2 surrounding the square outlet is limited to less than ~50 µm, as shown in the 3D tissue PO_2 profiles (Figure 3.5A). In the case of the square micro-outlet, a larger number of surface capillaries experience the PO_2 perturbations, 7 of which were directly over the micro-outlet (Figure 3.5B). Also, capillaries at both sides of those directly over the outlet seemed to be slightly affected by the PO_2 perturbations. At 40 mmHg, calculated SO_2 and capillary [ATP] distributions were similar to the no-flux control with surface capillaries having 15% higher SO_2 and

10% lower [ATP] values relative to zero flux condition (Figure 3.5C). As observed with the circular micro-outlet, re-oxygenation of stimulated capillaries following imposed hypoxia (15 mmHg) was at ~40 µm downstream of the square micro-outlet (Figure 3.5C). At the capillary venular end, SO_2 level of surface capillaries dropped by ~51% while capillary 54 experienced only a 15% drop in SO_2 relative to zero flux. This corresponded to ~32% increase in [ATP] in surface capillaries while only 7% increase in [ATP] in capillary 54 relative to zero flux. At 150 mmHg, capillary SO_2 levels increased across the micro-delivery outlet reaching maximum values at the venular end of the outlet region. Similar to the results observed with the circular micro-outlet, SO_2 values sharply dropped downstream of the square micro-outlet bringing surface capillary SO_2 to ~83% and deeper capillaries to ~70% ~200 µm downstream of the outlet. This corresponded to ~66% decrease in [ATP] in surface capillaries and ~42% decrease in [ATP] of deeper tissue capillaries.

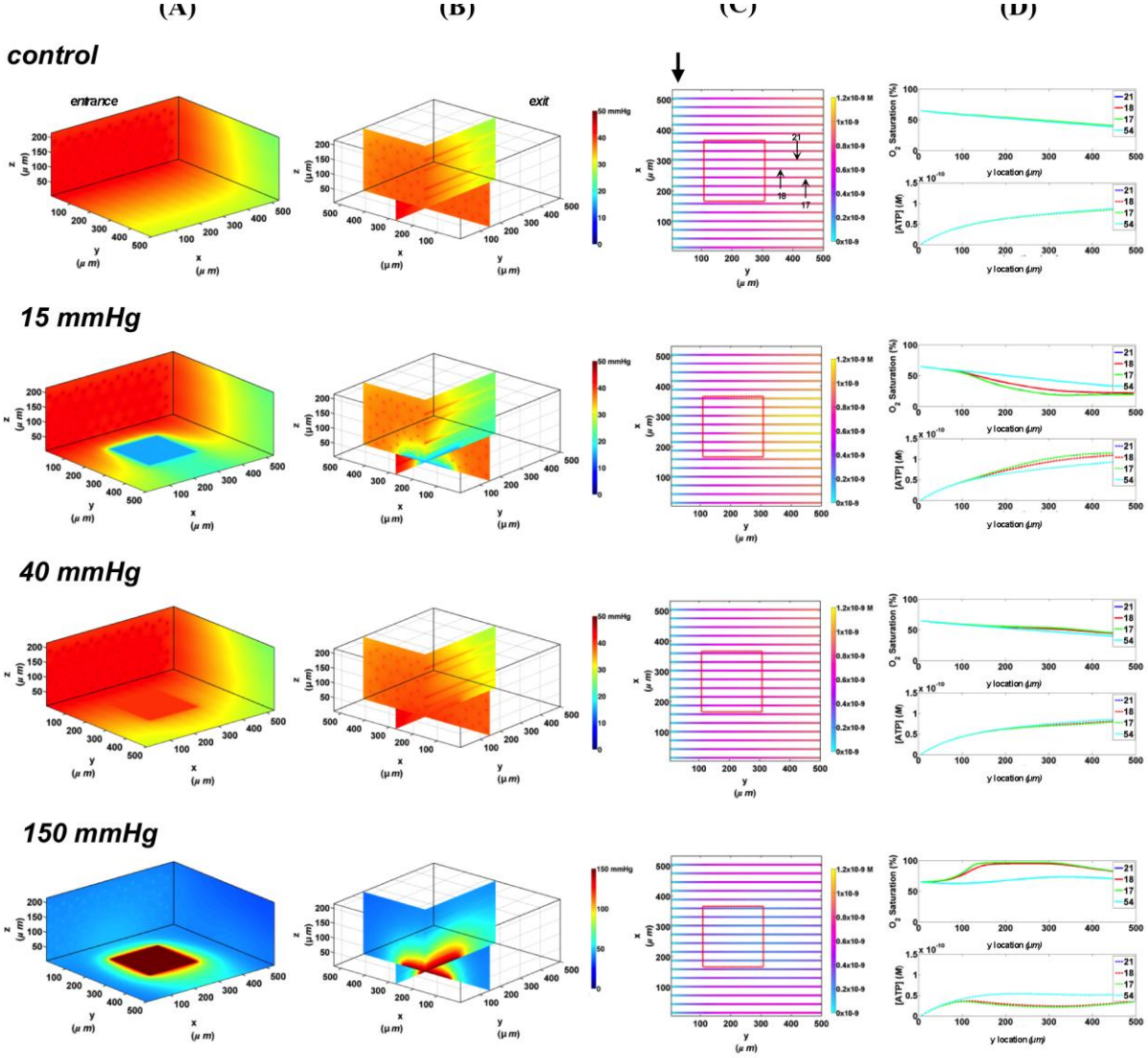

Figure 3.5 Simulations of 3D PO_2 and capillary [ATP] distribution in a tissue with idealized parallel capillary arrangement (72 hexagonally packed capillaries). In these simulations, we are modeling O_2 delivery through a square oxygen micro-delivery outlet (200 μm x 200 μm) to bottom tissue surface using our previously described novel micro-

delivery approach (see Figure 3.1). Tissue surface directly on top of the micro-delivery outlet is exposed to 15 mmHg, 40 mmHg, or 150 mmHg chamber PO_2 level relative to a zero flux control boundary condition (A) Spatial 3D tissue PO_2 distribution (mmHg) at capillary entrance perspective (B) a capillary exit perspective showing combined X-Z plane slice at Y=150 μm and Y-Z plane slice at X= 277 μm (C) bottom perspective of a vessel map depicting distribution of [ATP] (mol/L=M) along the capillaries. Bolded arrow marks capillary entrance (D) Plots of SO_2 (%) and [ATP] changes along capillary length in selected capillaries (21, 18, 17, 54) marked by arrows on the vessel map. Capillaries 21 and 17 are 16 μm from tissue surface, capillary 18 is 33 μm from tissue surface, and capillary 54 is deeper in the tissue, at 133 μm, and hence it is not shown in the current perspective of the vessel map.

3.3.1.4 Rectangular O_2 delivery micro-slit

The largest dimensions for an O_2 delivery micro-outlet currently being tested in our *in vivo* studies are for a rectangular micro-slit (1000 μm wide x 200 μm long). Since the 3D tissue dimensions in our computational model are less than the width of the experimental micro-slit, the effect of the slit extends to both edges of the tissue allowing us to visualize the depth of the PO_2 distribution into the tissue. As shown in the 3D PO_2 plots (Figure 3.6A), the PO_2 perturbations extended ~100 μm into the tissue with local tissue PO_2 changes similar to what was observed with other outlet designs. All surface capillaries

shown on the vessel map are affected by the PO_2 perturbation as the outlet covers the entire surface width (Figure 3.6B). At 40 mmHg, calculated SO_2 and capillary [ATP] distributions were similar to the no-flux control with surface capillaries having 17% higher SO_2 and 10.3% lower [ATP] values relative to zero flux O_2 boundary condition (Figure 3.6C). Under imposed hypoxia (15 mmHg), re-oxygenation of de-saturated surface capillaries was not observed within 200 µm downstream of the micro-slit. However, capillary SO_2 seemed to plateau approximately 100 µm downstream of the micro-slit. At the capillary venular end, SO_2 level of surface capillaries dropped by ~56% while capillary 54 experienced a ~20% drop in SO_2 relative to zero flux condition. This corresponded to ~ 35% increase in [ATP] in surface capillaries and only 8% increase in [ATP] in capillary 54 relative to zero flux. At 150 mmHg, capillary SO_2 levels increased across the micro-delivery outlet reaching maximum values at the venular end of the outlet region. Similar to the results observed with the previously discussed micro-outlet designs, SO_2 values instantly dropped downstream of the rectangular micro-slit bringing surface capillary SO_2 to ~90% and deep capillaries to ~80% ~200 µm downstream of the outlet. This corresponded to ~69% decrease in [ATP] in surface capillaries and ~55% decrease in [ATP] for deeper tissue capillaries.

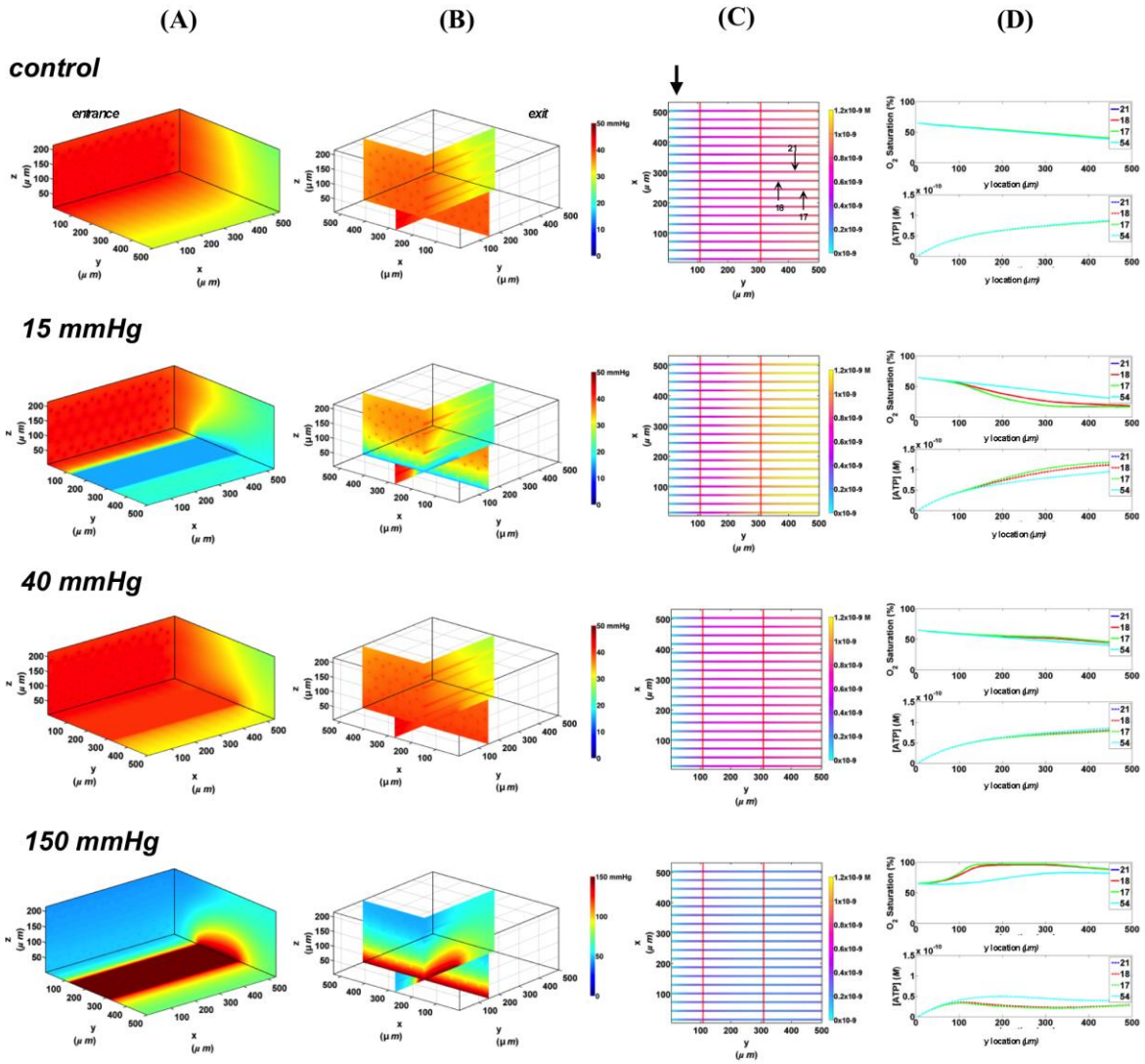

Figure 3.6 Simulations of 3D PO_2 and capillary [ATP] distribution in a tissue with idealized parallel capillary arrangement (72 hexagonally packed capillaries). In these simulations, we are modeling O_2 delivery through a rectangular oxygen micro-delivery outlet (1000 μm wide x 200 μm long) to the bottom tissue surface using our previously described novel micro-delivery approach (see Figure 3.1). The tissue surface directly on

top of the micro-delivery outlet is exposed to 15 mmHg, 40 mmHg, or 150 mmHg chamber PO_2 level relative to a zero flux control boundary condition (A) Spatial 3D tissue PO_2 distribution (mmHg) at capillary entrance perspective (B) a capillary exit perspective showing combined X-Z plane slice at Y=150 µm and Y-Z plane slice at X= 277 µm (C) bottom perspective of a vessel map depicting distribution of [ATP] (mol/L=M) along the capillaries. Bolded arrow marks capillary entrance (D) Plots of SO_2 (%) and [ATP] changes along capillary length in selected capillaries (21, 18, 17, 54) marked by arrows on the vessel map. Capillaries 21 and 17 are 16 µm from tissue surface, capillary 18 is 33 µm from tissue surface, and capillary 54 is deeper in the tissue, at 133 µm, and hence it is not shown in the current perspective of the vessel map.

3.3.1.5 Comparing change in relative ATP magnitude in response to varying the area of imposed tissue hypoxia

The change in the total magnitude of ATP (ATPtot) in the modeled network when imposing a hypoxic challenge (15 mmHg boundary condition) was calculated as percent increase above ATPtot at zero flux (Figure 3.7). Percent increase in ATP magnitude in the network was compared when exposing all of the bottom tissue surface to hypoxia (full chamber) or locally using the three micro-outlet designs discussed above. As shown in Figure 3.7, the total ATP magnitude increased with increases in micro-outlet dimensions and essentially the number of capillaries experiencing the PO_2 drop. The

percent increase in ATPtot was more than doubled when locally perturbing tissue PO_2 using the rectangular micro-slit compared to the other micro-outlet designs. The total ATP magnitude calculated when limiting the area of tissue hypoxia using the rectangular micro-slit was only 38% lower relative to a full exposed surface (Figure 3.7). The increase in the total ATP magnitude in a network exposed to local hypoxia was minimal (~2%) as modeled when using the circular micro-outlet and only 6% above that at zero flux when using the square micro-outlet.

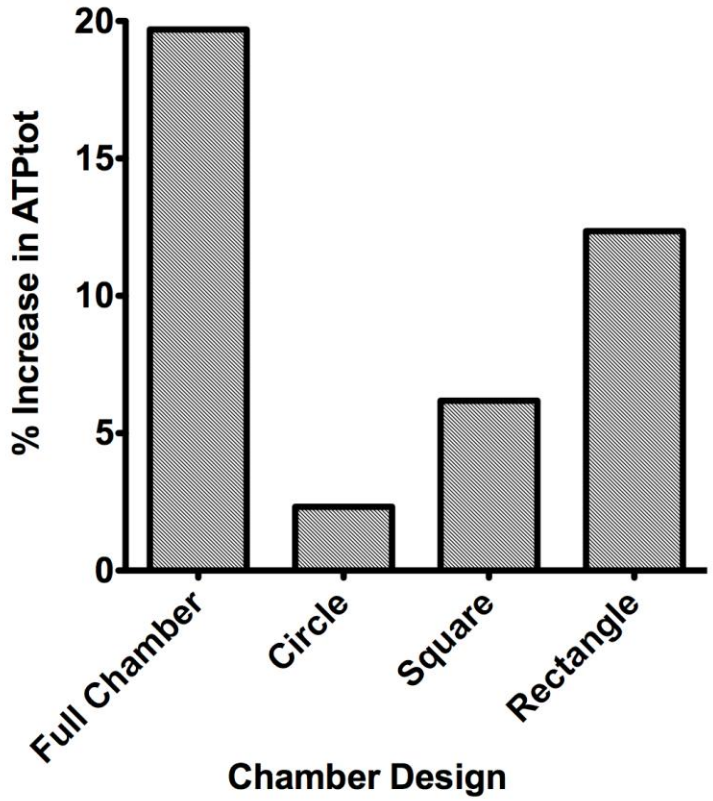

Figure 3.7 Percent increase in the total magnitude of ATP (ATPtot) relative to zero flux control boundary condition calculated for idealized parallel capillary network with no

arteriole at 15 mmHg chamber PO_2 level. Percent increase in ATP magnitude in the network were calculated when the entire bottom tissue surface is exposed to the PO_2 perturbation using a full gas exchange chamber or locally using a circular (100 µm in diameter), square (200 µm x 200 µm) or rectangular O_2 delivery micro-slit (1000 µm wide x 200 µm long).

3.3.2 Mathematical modelling of arteriolar SO_2 and ATP concentration in response to localized tissue PO_2 perturbations

In order to investigate the role terminal arterioles play in regulating SO_2-mediated ATP signaling in capillary networks, particularly in the EDL muscle where larger arterioles are located much deeper in the tissue, the 3D idealized capillary geometry was modified to include a terminal arteriole, 9 µm in diameter, positioned 30 µm away from bottom tissue surface. The 3D tissue PO_2 distribution, as well as SO_2 and [ATP] in the arteriole (vessel 69) and in the surrounding surface (capillaries 14 and 17) and deep tissue capillaries (represented by capillary 50), were modeled. Simulations were run for the case in which the full tissue surface is exposed to PO_2 perturbations (original gas exchange chamber) and for the case of spatially limited O_2 delivery using the rectangular O_2 delivery micro-slit. Also, the effect of varying arteriolar entrance SO_2 on the overall magnitude of ATP in response to altered tissue PO_2 was examined.

3.3.2.1 Full surface gas exchange chamber at 65% and 80% arteriolar entrance SO_2

In the 3D tissue PO_2 profiles and [ATP] vessel maps generated for these simulations, the PO_2 perturbations were shown to affect the terminal arteriole to a much lesser extent than the surface capillaries (Figure 3.8A,B and 3.9A,B). Also, these simulations showed the influence of the arteriole as an O_2 source on the SO_2 levels of nearby surface capillaries. For instance, the steady state SO_2 level in capillary 14, positioned right next to the arteriole, was ~25% higher than the zero flux control condition when exposed to 40 mmHg chamber PO_2 and identical to the SO_2 level of the terminal arteriole (Figure 3.8 and 3.9). However, the SO_2 level of the deeper tissue capillary (50), which was located at the same depth as capillary 54, was unchanged relative to zero flux. In general, the different arteriolar entrance SO_2 has no effect on the surface or deep tissue capillaries and had minimal influence on the arteriolar SO_2 at steady state. At 15 mmHg, the SO_2 level of the terminal arteriole entering at 65% dropped by 60% relative to zero flux condition corresponding to 44% increases in [ATP]. A smaller drop in SO_2 was calculated (52% decrease) for the arteriole entering at 80% corresponding to 40% increase in [ATP]. The SO_2 level in the surrounding surface capillaries, as well as deeper tissue capillaries, dropped by ~70% and 35%, respectively, corresponding to ~45% and 16% higher steady state capillary [ATP] relative to zero flux (Figure 3.8C and 3.9C). At 150 mmHg, hemoglobin SO_2 levels in surface and deep tissue capillaries as well as in the arteriole converged to ~100% with ~77% decrease in steady state [ATP] in the capillaries and

75% decrease in [ATP] in the arteriole relative to zero flux control (Figure 3.8C and 3.9C).

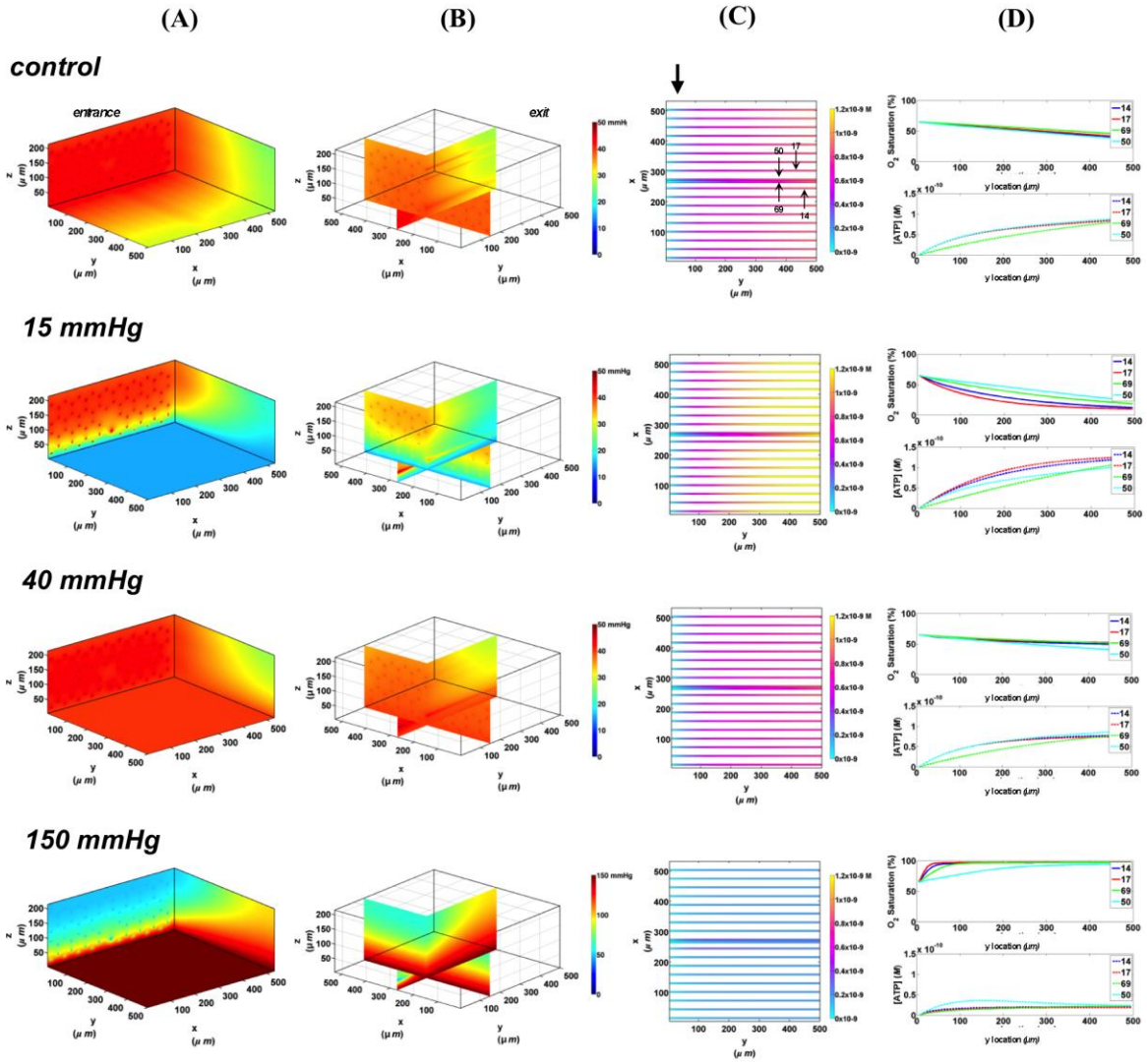

Figure 3.8 Simulations of 3D PO_2 and capillary [ATP] distribution in a tissue with idealized parallel capillary arrangement (68 hexagonally packed capillaries), plus a traversing terminal arteriole (vessel 69) at an entrance SO_2 of 65%. In these simulations,

we are modeling O_2 delivery to the bottom tissue surface using the full gas exchange chamber (Ellis et al., 2012; Ghonaim et al., 2011). Full bottom tissue surface is exposed to 15 mmHg, 40 mmHg, or 150 mmHg chamber PO_2 level relative to a zero flux control boundary condition (A) Spatial 3D tissue PO_2 distribution (mmHg) at capillary entrance perspective (B) a capillary exit perspective showing combined X-Z plane slice at Y=150 µm and Y-Z plane slice at X= 266 µm (C) bottom perspective of a vessel map depicting distribution of [ATP] (mol/L=M) along the arteriole and surrounding capillaries. Bolded arrow marks arteriolar and capillary entrance (D) Plots of SO_2 (%) and [ATP] changes along vessel length in selected vessels (14, 17, 69-arteriole, 50) marked by arrows on the vessel map. Capillary 17 is 16 µm from tissue surface, the arteriole and capillary 14 are 33 µm from tissue surface, and capillary 50 is deeper in the tissue, at 133 µm, yet is shown adjacent to the arteriole in the current perspective of the vessel map.

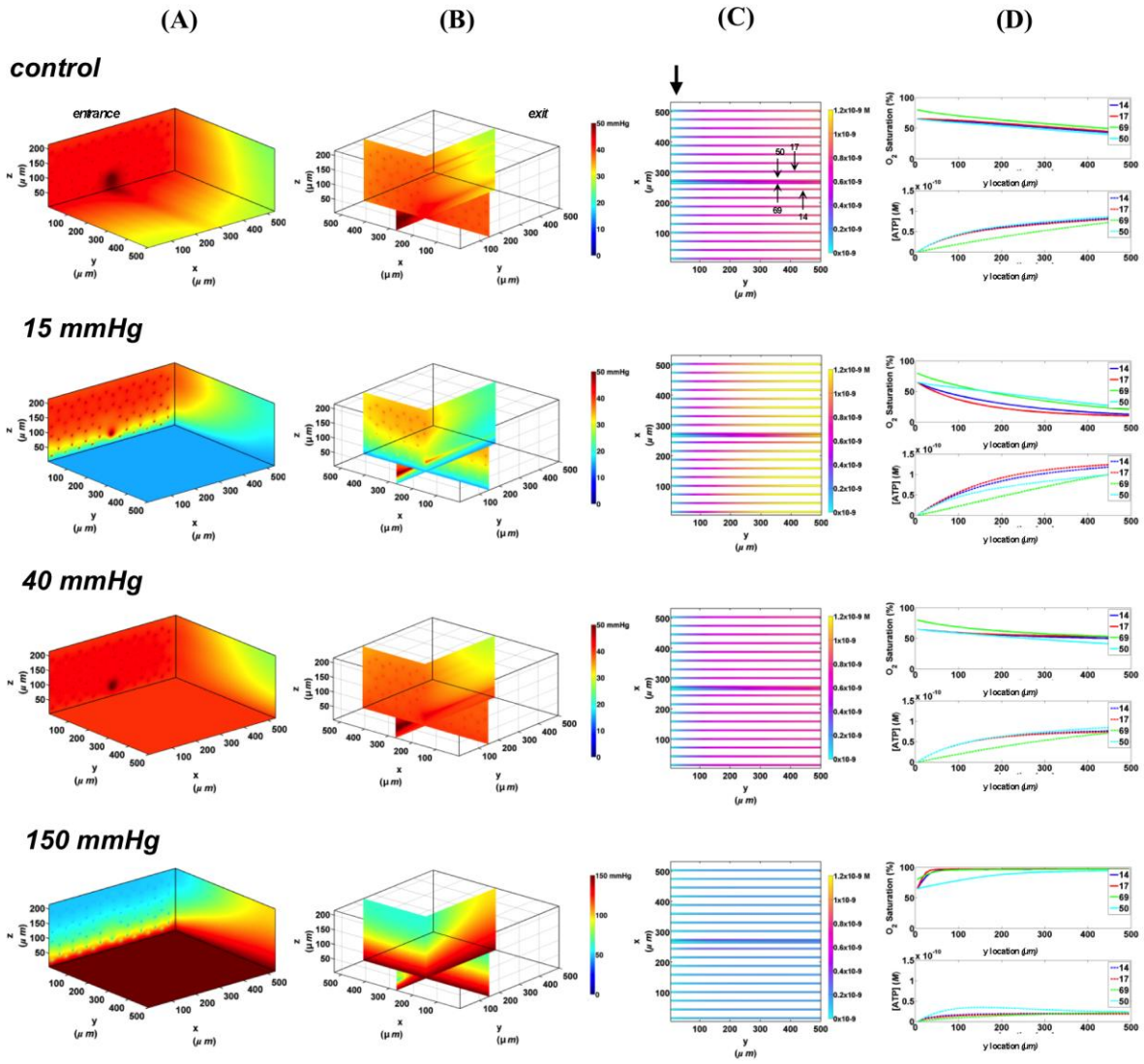

Figure 3.9 Simulations of 3D PO_2 and capillary [ATP] distribution in a tissue with idealized parallel capillary arrangement (68 hexagonally packed capillaries), which includes a traversing terminal arteriole (vessel 69) at an entrance SO_2 of 80%. In these simulations, we are modeling O_2 delivery to bottom tissue surface using the full gas exchange chamber (Ellis et al., 2012; Ghonaim et al., 2011). Full bottom tissue surface is

exposed to 15 mmHg, 40 mmHg, or 150 mmHg chamber PO_2 level relative to a zero flux control boundary condition (A) Spatial 3D tissue PO_2 distribution (mmHg) at capillary entrance perspective (B) a capillary exit perspective showing combined X-Z plane slice at Y=150 μm and Y-Z plane slice at X= 266 μm (C) bottom perspective of a vessel map depicting distribution of [ATP] (mol/L=M) along the arteriole and surrounding capillaries. Bolded arrow marks arteriolar and capillary entrance (D) Plots of SO_2 (%) and [ATP] changes along vessel length in selected vessels (14, 17, 69-arteriole, 50) marked by arrows on the vessel map. Capillary 17 is 16 μm from tissue surface, the arteriole and capillary 14 are 33 μm from tissue surface, and capillary 50 is deeper in the tissue, at 133 μm, yet is shown adjacent to the arteriole in the current perspective of the vessel map.

3.3.2.2 Rectangular oxygen delivery micro-slit at 65% and 80% arteriolar entrance SO_2

In these simulations, the capillary array that includes the terminal arteriole is exposed to local perturbations in tissue PO_2 through the rectangular micro-slit. At 40 mmHg chamber PO_2, the calculated steady state SO_2 and [ATP] levels at the venular end of surface and deep tissue capillaries as well as in the arteriole are within 5% of those at zero flux condition and uninfluenced by the arteriolar entrance SO_2 (Figure 3.10 and 3.11). Under imposed hypoxia (15 mmHg), the calculated arteriolar SO_2 values at steady state were 50% higher than the case in which the full surface is exposed to the PO_2

perturbations and identical to those of deeper tissue capillaries. Hence, a minimal drop in SO_2 (38% decrease) was calculated in the arteriole relative to zero flux. These arteriolar steady state SO_2 values were uninfluenced by the different arteriolar entrance SO_2. The influence of the arteriole as an O_2 source to nearby capillaries downstream of the micro-slit can be clearly observed in the 3D PO_2 profiles at 15 mmHg (Figure 3.10A and 3.11A). However, the surface capillaries (14, 17) experienced a sharper drop in SO_2 in response to the imposed hypoxia with 53% drop in SO_2 and a corresponding 39% increase in [ATP]. As observed when locally stimulating surface capillaries in the absence of the arteriole, capillaries were re-oxygenated ~40 μm downstream of the hypoxic micro-slit region. At 150 mmHg, the steady state SO_2 levels in surface capillaries and in the arteriole converged to ~88% while the SO_2 level of capillary 50 was slightly lower at 83% which corresponded to 65% and 57% decrease in [ATP], respectively, relative to zero flux (Figure 3.10C and 3.11C).

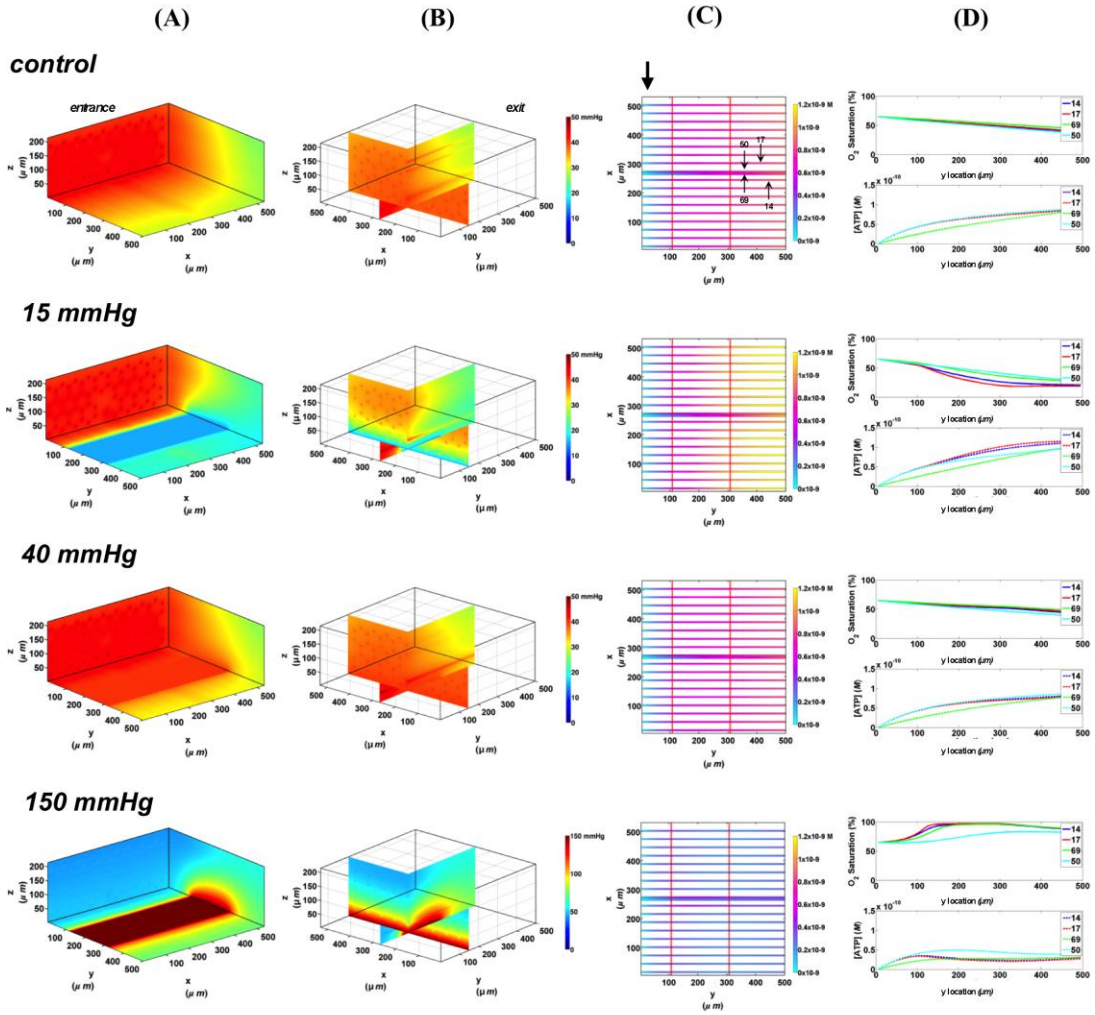

Figure 3.10 Simulations of 3D PO_2 and capillary [ATP] distribution in a tissue with idealized parallel capillary arrangement (68 hexagonally packed capillaries), which includes a traversing terminal arteriole (vessel 69) at an entrance SO_2 of 65%. In these simulations, we are modeling O_2 delivery through a rectangular oxygen micro-delivery outlet (1000 μm wide x 200 μm long) to bottom tissue surface using our previously described novel micro-delivery approach (see Figure 3.1). Tissue surface directly on top

of the micro-delivery outlet is exposed to 15 mmHg, 40 mmHg, or 150 mmHg chamber PO_2 level relative to a zero flux control boundary condition (A) Spatial 3D tissue PO_2 distribution (mmHg) at capillary entrance perspective (B) a capillary exit perspective showing combined X-Z plane slice at Y=150 μm and Y-Z plane slice at X= 266 μm (C) bottom perspective of a vessel map depicting distribution of [ATP] (mol/L=M) along the arteriole and surrounding capillaries. Bolded arrow marks arteriolar and capillary entrance (D) Plots of SO_2 (%) and [ATP] changes along vessel length in selected vessels (14, 17, 69-arteriole, 50) marked by arrows on the vessel map. Capillary 17 is 16 μm from tissue surface, the arteriole and capillary 14 are 33 μm from tissue surface, and capillary 50 is deeper in the tissue, at 133 μm, yet is shown adjacent to the arteriole in the current perspective of the vessel map.

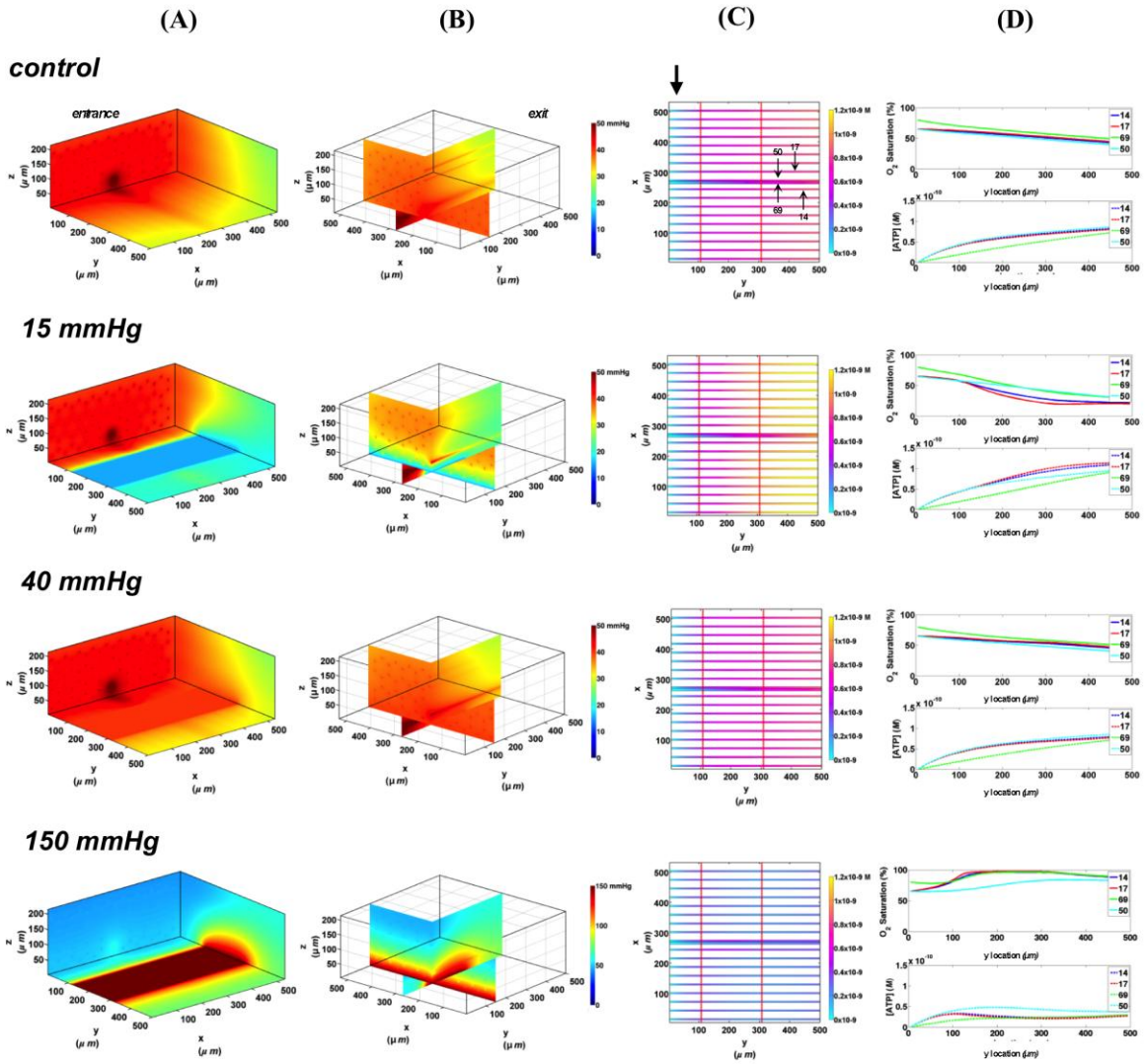

Figure 3.11 Simulations of 3D PO_2 and capillary [ATP] distribution in a tissue with idealized parallel capillary arrangement (68 hexagonally packed capillaries), which includes a traversing terminal arteriole (vessel 69) at an entrance SO_2 of 80%. In these simulations, we are modeling O_2 delivery through a rectangular oxygen micro-delivery outlet (1000 μm wide x 200 μm long) to bottom tissue surface using our previously described novel micro-delivery approach (see Figure 3.1). Tissue surface directly on top

of the micro-delivery outlet is exposed to 15 mmHg, 40 mmHg, or 150 mmHg chamber PO_2 level relative to a zero flux control boundary condition (A) Spatial 3D tissue PO_2 distribution (mmHg) at capillary entrance perspective (B) a capillary exit perspective showing combined X-Z plane slice at Y=150 µm and Y-Z plane slice at X= 266 µm (C) bottom perspective of a vessel map depicting distribution of [ATP] (mol/L=M) along the arteriole and surrounding capillaries. Bolded arrow marks arteriolar and capillary entrance (D) Plots of SO_2 (%) and [ATP] changes along vessel length in selected vessels (14, 17, 69-arteriole, 50) marked by arrows on the vessel map. Capillary 17 is 16 µm from tissue surface, the arteriole and capillary 14 are 33 µm from tissue surface, and capillary 50 is deeper in the tissue, at 133 µm, yet is shown adjacent to the arteriole in the current perspective of the vessel map.

3.3.2.3 Estimating relative arteriolar ATP magnitude in response to tissue PO_2 perturbations

In order to estimate the contribution of the terminal arteriole to ATP mediated signaling in capillary networks, the steady state magnitude of ATP in the arteriole (ATPart) at various tissue PO_2 conditions was calculated and normalized against total ATP magnitude in the network (ATPtot) under zero flux condition (Figure 3.12). The relative arteriolar ATP magnitudes were calculated when the full tissue surface was exposed to the PO_2 perturbations (full gas exchange chamber) or to local perturbations using the rectangular O_2 delivery micro-slit. As shown in Figure 3.12, the arteriolar ATP

magnitude decreased with increase in chamber PO_2 level. However, the model suggested that under hypoxic conditions (15 mmHg), the terminal arteriole would contribute less than 3% of the total ATP signal originating from a capillary network. Also, although the percent decrease in ATP magnitude in the arteriole is similar to that calculated for the total network when increasing chamber PO_2 from 15 mmHg to 150 mmHg, the absolute change in ATP magnitude (moles) in the arteriole is ~95% less. Finally, it should be noted that [ATP] in the arteriole is ~20% lower when limiting area of PO_2 perturbations using the rectangular micro-slit.

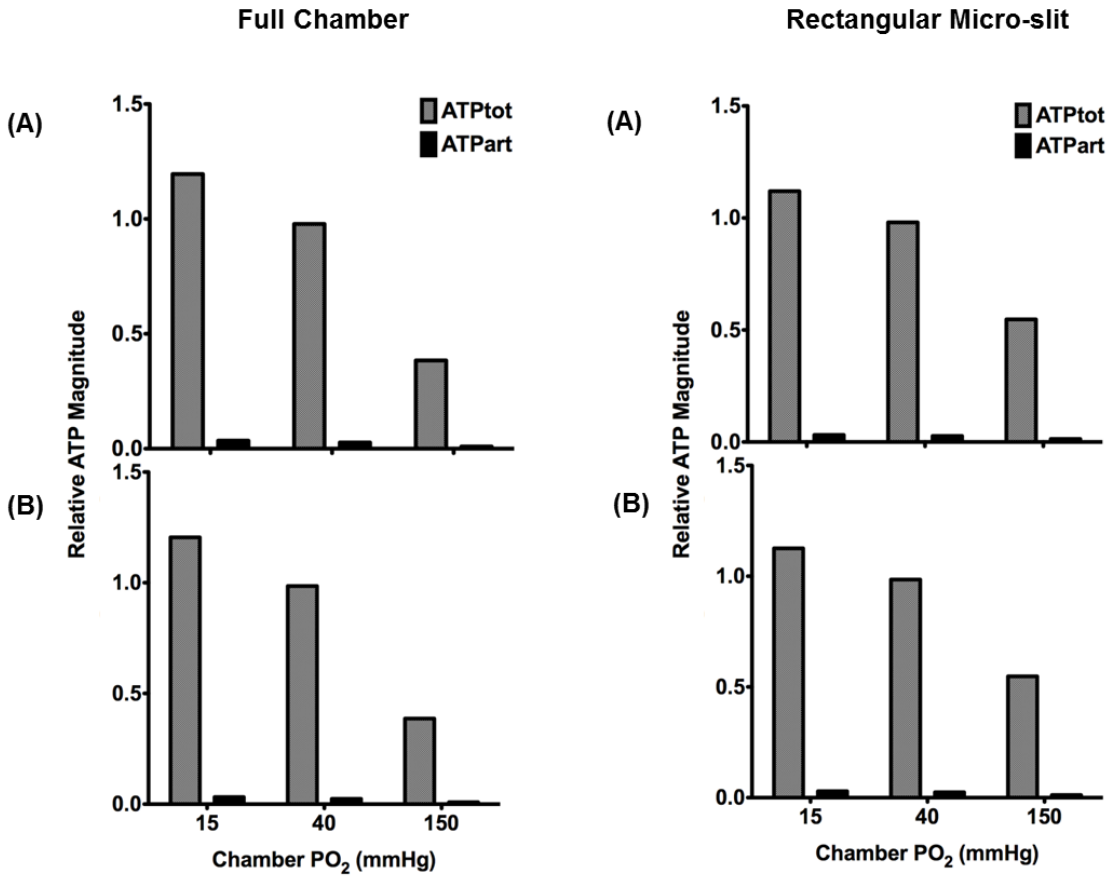

Figure 3.12 Total ATP magnitude (moles) at steady state calculated for entire network (ATPtot from all 68 capillaries) or in the terminal arteriole only (ATPart) normalized against ATPtot calculated at no-flux condition. Relative ATP magnitudes are calculated for an idealized 3D parallel capillary array network with a terminal arteriole (9 μm in diameter) positioned 30 μm from tissue surface. Simulations were run with entire bottom tissue surface being exposed to PO_2 perturbations using full gas exchange chamber or locally using a rectangular O_2 delivery micro-slit (1000 μm wide x 200 μm long). For both conditions, relative ATP magnitudes are calculated for the case in which the terminal arteriole has an entrance SO_2 of (A) 65% or (B) 80%.

3.4 Discussion

In the microcirculation, ATP is released from the erythrocytes in an SO_2 dependent manner. Released ATP would bind to purinergic receptors on the vascular endothelium which activates a signaling pathway leading to the opening of Ca^{2+} gated K^+ channels and the hyperpolarization of the endothelial cell (Ellsworth et al., 2008, Tran et al., 2012). The hyperpolarization signal is then conducted upstream through gap junctions. At the arteriolar wall, the incoming hyperpolarization signal is conducted to the SMC layer through myo-endothelial gap junctions resulting in vaso-relaxation and increase in erythrocyte supply rate (Ellsworth et al., 2008, Tran et al., 2012). The magnitude of the hyperpolarization signal would depend on the number of endothelial cells activated along the capillary and on the total number of capillaries stimulated within a network under hypoxic conditions. This understanding of how erythrocyte-released ATP controls micro-vascular O_2 delivery is consistent with the modeling results presented in this paper. The net increase in total ATP magnitude in the network with increase in the area exposed to hypoxia is the summative contribution of additional stimulated capillaries (Figures 3.3-3.7). Also, these results help explain our observations of no associated vascular response to changes in capillary SO_2 when experimentally testing the effect of O_2 delivery through a circular micro-outlet (100 µm in diameter) *in vivo* (Ghonaim et al., 2011). Although this design maybe optimal for locally altering SO_2 in single capillaries, the stimulus would probably not be sufficient to elicit a micro-vascular response. Increasing the dimensions

of the micro-outlet would be necessary to stimulate a large enough number of capillaries, thus amplifying total magnitude of ATP release and signal.

Also, as our modeling data suggest, increasing the micro-outlet dimensions minimizes the effect of stimulated capillary re-oxygenation downstream of the micro-outlet. This is because the capillaries of interest would be surrounded by capillaries experiencing the same drop in PO_2. This is more representative of the situation *in vivo* as the outlet physiologically simulates an arteriole crossing the capillary bed acting as an O_2 source or a venule withdrawing O_2, which would affect multiple capillaries. In terms of the signaling response, delayed re-oxygenation following hypoxic stimulation ensures the ATP signal persists longer distances downstream thus stimulating a larger number of endothelial cells. Since each endothelial cell in skeletal muscle is ~100 μm long, using the rectangular slit is estimated to activate at least 3.5 endothelial cells in each stimulated capillary. In comparison with the square micro-outlet, which has the same length (200 μm) as the rectangular micro-slit, approximately one more endothelial cell is activated per capillary with the latter design. It should be noted that in the modeled geometry, which lacks realistic capillary branching and has an idealized, uniform capillary density, we are examining relative changes in the total magnitude of ATP when using various outlet designs. During *in vivo* experiments, a maximum of two micro-vascular units (~10 capillaries) may be positioned along the entire width of the rectangular micro-slit, while only one or two capillaries with a branching point could be positioned over the circular micro-outlet (Ghonaim et al., 2011). Hence a 1000 μm wide x 200 μm long outlet might

cover the threshold number of capillaries needed to elicit a micro-vascular response. This indicates the rectangular micro-slit would be optimal for affecting a sufficient number of capillaries by local O_2 perturbations to generate a sufficient ATP signal for eliciting a conducted micro vascular response.

The limited amount of change in tissue PO_2 due to diffusion (~50 μm), as measured from the 3D tissue PO_2 profiles, beyond the edge of the micro-outlets (Figures 3.4-3.6A,B) was consistent with our previous observations (Ghonaim et al., 2011). The simulations indicated that the PO_2 perturbations are highly localized to only those capillaries directly over the micro-outlet region. Experimentally, the results suggest that the micro-outlet should be positioned at least 50 μm downstream of the terminal feeding arteriole to ensure that micro-vascular responses are only elicited from the capillaries positioned directly over the outlet. The extent of axial O_2 diffusion in the tissue when using the rectangular micro-slit was 50% deeper than that previously modeled for the circular micro-outlet (Figure 6B, 10B, 11B) (Ghonaim et al., 2011) and similar to that of the full surface model (Ellis et al., 2012, Ghonaim et al., 2011). Due to the shape of the PO_2 profile, the maximal axial diffusion distance was estimated from the center of the outlet. The increase in the axial diffusion distance might be a compromise when using larger O_2 micro-outlets. With our current microscopic techniques we are unable to resolve vessels deeper than 60 μm.

Since in our experiments, we examine micro-vascular signaling from selected capillaries, it was critical that we assess the possible contribution of arterioles beyond our ability to

focus. Since arterioles have relatively higher erythrocyte velocities than in the capillaries, they are anticipated to experience a much lesser change in SO_2 in response to PO_2 perturbations. This was supported by our simulation data (Figure 3.8-3.11). The main effect of a nearby terminal arteriole on a capillary within 50 μm is that it would act as an O_2 source. As shown in our modeling data (Figure 3.8-3.11D), higher measured SO_2 in a capillary relative to other capillaries with comparable flow rates in the same preparation might imply the presence of a nearby arteriole. Since arterioles in the EDL muscle preparation are deeper in the tissue, their contribution to the total magnitude of ATP in a locally stimulated capillary network is probably negligible. The contribution of a terminal arteriole positioned directly over the micro-slit ~30 μm from the bottom surface was calculated to be less than 3% of the total magnitude of the ATP (Figure 3.12). Hence, when locally stimulating capillaries, even in the presence of an underlying arteriole, the observed micro-vascular responses mediated by intra-luminal ATP would be primarily due to ATP released in the stimulated capillaries.

In conclusion, we have modeled SO_2-dependent changes in [ATP] at steady state in 3D idealized parallel capillary networks in response to local PO_2 perturbations. As the number of affected capillaries increases, the total magnitude of ATP in the network increases. The results indicated that O_2 delivery or removal to overlaying tissue through a rectangular micro-slit (1000 μm wide x 200 μm long) would be optimal relative to other micro-outlet designs of smaller dimensions or a full surface classical exchange type chamber. Using the rectangular micro-slit it is anticipated that a sufficient number of

capillaries will be stimulated to produce sufficient ATP to elicit micro-vascular responses. This would be accomplished while maintaining the stimulus localized to the selected capillaries. The results also indicated that terminal arterioles have minimal influence on the total magnitude of ATP in the network under hypoxic condition. Hence, when locally stimulating the capillary bed, the majority of the signal elicited by ATP release would originate in the capillaries. The computational model presented provides valuable insights into how to study the ATP release mechanism and signaling in capillary networks in vivo. The modeling data help guide us in the design of an optimal tool for studying SO_2-dependent ATP release in capillaries *in vivo*. In the future, we aim to model time-dependent ATP release to local PO_2 perturbations in a realistic capillary network geometry reconstructed from experimental data. Combining our *in vivo* experimental observations with computational modeling of the dynamics of SO_2-dependent ATP release will help provide a more comprehensive understanding of O_2 mediated blood flow regulation in micro-vascular networks.

3.5 References

Arciero J. C., Carlson B. E., Secomb T. W. (2008). Theoretical model of metabolic blood flow regulation: roles of ATP release by red blood cells and conducted responses. *Am. J. Physiol. Heart Circ. Physiol.* **295**: H1562–H1571

Bagher P., Segal S.S. (2011) Regulation of blood flow in the microcirculation: role of conducted vasodilation. *Acta. Physiol. (Oxf).* **202**:271-84

Bergfeld G.R., Forrester T. (1992) Release of ATP from human erythrocytes in response to a brief period of hypoxia and hypercapnia. *Cardiovasc. Res.* **26**:40–47

Collins D.M., McCullough W.T., Ellsworth M.L. (1998) Conducted vascular responses: communication across the capillary bed. *Microvasc. Res.* **56:** 43–53

Dietrich H.H. (1989) Effect of locally applied epinephrine and norepinephrine on blood flow and diameter in capillaries of rat mesentery. *Microvasc. Res.* **38**: 125-135

Dietrich H.H., Tyml K. (1992a) Microvascular flow response to localized application of norepinephrine on capillaries in rat and frog skeletal muscle. *Microvasc. Res.* **43**: 73-86

Dietrich H.H., Tyml K. (1992b) Capillary as a communicating medium in the microvasculature. *Microvasc. Res.* **43**: 87-99

Duling B.R. (1974) Oxygen sensitivity of vascular smooth muscle.11. In vivo studies. *Am. J. Physiol*. **227:** 42-49

Duling B.R., Berne R.M. (1970) Longitudinal gradients in periarteriolar oxygen tension: a possible mechanism for the participation of oxygen in local regulation of blood flow. *Circ. Res.* **27**: 669-678

Eggleton C.D., Vadapalli A., Roy T.K., Popel A.S. (2000). Calculations of intracapillary oxygen tension distributions in muscle. *Math.Biosci.* **167:** 123–143.

Ellis C.G., Ellsworth M.L., Pittman R.N. (1990) Determination of red blood cell oxygenation *in vivo* by dual video densitometric image analysis. *Am. J. Physiol. Heart. Circ. Physiol.* **258**: H1216–H1223

Ellis C.G., Ellsworth M.L., Pittman R.N., Burgess W.L. (1992) Application of image analysis for evaluation of red blood cell dynamics in capillaries. *Microvasc. Res.* **44**: 214–225

Ellis C.G., Milkovich S.L., Goldman D. (2012) What is the efficiency of ATP signaling from erythrocytes to regulate distribution of O_2 supply within the microvasculature? *Microcirculation*. **5**: 440-450

Ellsworth M.L., Ellis C.G., Goldman D., Stephenson A.H., Dietrich H.H., Sprague R.S. (2008) Erythrocytes: oxygen sensors and modulators modulators of vascular tone. *Physiology.* **24**: 107–116

Ellsworth M.L., Forrester T., Ellis C.G., Dietrich H.H. (1995) The erythrocyte as a regulator of vascular tone. *Am. J. Physiol*. **269**:H2155-H2161

Fraser G.M., Goldman D., Ellis C.G. (2012) Microvascular flow modeling using in vivo hemodynamic measurements in reconstructed 3D capillary networks. *Microcirculation.* **19**:510-20

Ghonaim N.W., Lau L.W., Goldman D., Ellis C.G., Yang J. (2011) A micro-delivery approach for studying microvascular responses to localized oxygen delivery. *Microcirculation.* **18**:646–654

Goldman D., Fraser G.M., Ellis C.G., Sprague R.S., Ellsworth M.L., Stephenson A. (2012) Toward a multiscale description of microvascular flow regulation: O_2 dependent release of ATP from human erythrocytes and the distribution of ATP in capillary networks. *Front. Physiol.* **3**:1-11

Goldman D., Popel A. S. (1999). Computational modeling of oxygen transport from complex capillary networks. Relation to the microcirculation physiome. *Adv. Exp. Med. Biol*. **471**: 555–563

Goldman, D., Popel A.S. (2000). A computational study of the effect of capillary network anastomoses and tortuosity on oxygen transport. *J. Theor.Biol.* **206**: 181–194

Goldman, D., Popel A.S.(2001). A computational study of the effect of vasomotion on oxygen transport from capillary networks. *J. Theor.Biol.* **209**:189-99

González-Alonso J., Olsen D.B., Saltin B. (2002) Erythrocyte and the regulation of human skeletal muscle blood flow and oxygen delivery: role of circulating ATP. *Circ. Res.* **91**:1046–1055

Jackson W.F. (1987) Arteriolar oxygen reactivity: where is the sensor? *Am. J. Physiol. Heart. Circ. Physiol.* **253:** H1120-H1126

Jagger J.E., Bateman R.M., Ellsworth M.L., Ellis C.G. (2001) Role of erythrocyte in regulating local O2 delivery mediated by hemoglobin oxygenation. *Am. J. Physiol. Heart. Circ. Physiol.* **280**: H2833–H2839

Japee S.A., Ellis C.G., Pittman R.N. (2004) Flow visualization tools for image analysis of capillary networks. *Microcirculation.* **11**:39–54. doi: 10.1080/10739680490266171

Japee S.A., Pittman R.N., Ellis C.G. (2005) Automated method for tracking individual red blood cells within capillaries to compute velocity and oxygen saturation. *Microcirculation.* **12**:507–515. doi: 10.1080/10739680591003341

Japee S.A., Pittman R.N., Ellis C.G. (2005) A new video image analysis system to study red blood cell dynamics and oxygenation in capillary networks. *Microcirculation.* **12**:489–506

Miseta A., Bogner P., Berenyi E., Kellermayer M., Galambos C., Wheatley D., Cameron I. (1993) Relationship between cellular ATP, potassium, sodium and magnesium concentrations in mammalian and avian erythrocytes. *Biochim. Biophys. Acta.* **1175**: 133–139

Song H., Tyml K. (1993) Evidence for sensing and integration of biological signals by the capillary network. *Am. J. Physiol.* **265**: H1235-H1242

Stein J.C., Ellsworth M.L. (1993) Capillary oxygen transport during severe hypoxia: role of hemoglobin oxygen affinity. *J. Appl. Physiol.* **75**: 1601–1607

Tran C.H.T., Taylor M.S., Plane F., Nagaraja S., Tsoukias N.M., Solodushko V., Vigmond E.J., Furstenhaupt T., Brigdan M., Welsh D.G. (2012) Endothelial Ca^{2+} wavelets and the induction of myoendothelial feedback. *Am. J. Physiol. Cell. Physiol.* **302:**C1226-C1242

Chapter 4

4 Conducted microvascular response to localized oxygen exchange using a novel micro-delivery approach[1]

[1] In preparation for submission to Circulation Research (2013).

4.1 Introduction

For a long time, micro-vascular responses to changes in the oxygen (O_2) environment have been observed as changes in vascular tone (Duling and Berne 1970, Jackson and Duling 1983, Jackson 1987). This observation has been exploited in experiments involving the use of suffusion solutions as a standard procedure for testing the viability of the tissue preparation (Jackson et al. 2010). In a healthy tissue, increasing O_2 levels of the suffusion solution would result in arteriolar vasoconstriction and consequent flow reduction. Equilibrating the suffusion solution back at near zero O_2 levels would result in an observed increase in flow that would recover normal perfusion. The finding that O_2 content (proportional to hemoglobin O_2 saturation; SO_2) is more important than O_2 partial pressure (PO_2) in generating a micro-vascular response (Stein et al. 1993) suggested the erythrocyte maybe actively involved in mediating the observed O_2-dependent flow responses. The ability of the erythrocyte to release signaling molecules that act to modulate blood flow in response to drop in internal hemoglobin SO_2 (Stein et al. 1993, Ellsworth et al. 1995) further confirmed the erythrocyte's proposed role as a mobile vascular O_2 sensor and effector. Of special interest is the potent vasodilator adenosine

triphosphate (ATP), which was found to be released by erythrocytes under low SO_2 conditions (Ellsworth et al. 1995). Jagger et al. (2001) demonstrated that the relationship between ATP release from the erythrocyte and hemoglobin SO_2 is linear. The mechanisms that underlay SO_2-dependent ATP release by the erythrocyte are not fully elucidated, but are suggested to involve conformational changes in the hemoglobin molecule as it desaturates (Jagger et al. 2001, Wan et al. 2008; Sridharan et al. 2010b; Forsyth et al. 2011) which activates signalling pathways similar to those involved in shear stress dependent ATP release (Sprague et al. 1998; 2001; 2008). Once ATP is released, it binds to purinergic receptors (P_{2y}) on the vascular endothelium (You et al. 1999, Horiuchi et al. 2001) leading to conducted hyperpolarization between adjacent endothelial cells through gap junctions and to smooth muscle cells (SMCs) through myoendotheial cell junctions (Campbell et al. 1996, Dietrich et al. 2008, Fukao et al. 2001).

Activation of SMCs leads to local and conducted vasodilation up the arteriolar tree which translates to increase in perfusion (Segal et al. 1989, Segal and Duling 1989). It has been suggested that other vasodilators such as SNOs and nitric oxide (NO) may be released from the erythrocyte under low SO_2 (Jia et al. 1996, Stamler et al. 1997, Patel et al. 1999, Cosby et al. 2003, Gladwin et al. 2004). However, the physiological role of SNOs *in vivo* is still to be identified (Ellsworth et al. 2009). Also, the suggested mechanisms lack the temporal resolution required to rapidly control O_2 distribution and although implicated in

local vasodilation, these mechanism have not been shown to result in conducted micro-vascular signaling (Ellsworth et al. 2009).

There is a lot of debate as to the site of ATP release and action in the microvasculature. It has been suggested that ATP would primarily be released in terminal arterioles such that it would directly activate SMCs resulting in prompt responses (Duling and Berne, 1970, Duling, 1974, Jackson, 1987). However, the spatial resolution of the microvascular signal in the arterioles would be highly compromised by the relatively short erythrocyte transit times (Ellis et al. 2012). Also, the parabolic flow profile implies that only cells nearest the wall will experience the drop in SO_2 and thus contribute in the release of ATP. Cells flowing in the center line would experience the SO_2 drop to a much lesser extent and any released ATP would need to diffuse a long distance prior to acting on the endothelium (Ellis et al. 2012).

Studies have shown that ATP injected into the vascular lumen of venules would result in a signal conducted to the upstream arterioles (Collins et al. 1998). The high level of hematocrit collected in the venules, combined with low SO_2 levels, results in large amounts of released ATP (Ellis et al. 2012). Hence venules would be the site for strong vasodilatory signals (Arciero et al. 2008). However, since venules collect erythrocytes with a wide range of SO_2 values from upstream capillaries, signals originating from the venules would contribute to regional blood flow regulation rather than to control the distribution of blood supply to specific capillary beds (Ellis et al. 2012).

In order for the O_2 regulatory system to maintain a homogenous O_2 supply across the capillary bed, the O_2 regulatory signal has to originate within the capillary itself to ensure proper distribution of O_2 supply to match the dynamic changes in capillary SO_2 (Ellis et al 2012). The relatively longer erythrocyte transit times in the capillaries and the small diffusion distance of ATP to the endothelium from every passing erythrocyte imply that the capillary bed could be the site for effective SO_2-dependent ATP signaling (Ellis et al 2012). Since capillaries are composed of endothelial cells which are electrically coupled (Dietrich, 1989, Dietrich and Tyml, 1992a,b, Song and Tyml, 1993, Collins et al., 1998, Bagher and Segal, 2011), signal can be conducted to the upstream arteriole in the same way that it was conducted from the downstream venule (Collins et al. 1998). Signals integrated from capillaries in nearby yet independent microvascular units would lead to more tightly controlled responses.

One of the factors that contribute to the heterogeneity in capillary SO_2 is the observed cross talk between microvessels within the complex microvascular geometry (Swain and Pittman 1989, Ellsworth and Pittman 1990, Stein et al. 1993, Ellsworth et al. 1994, Tsai et al. 2003). An arteriole crossing over a group of capillaries will act as a diffusion shunt increasing O_2 content in the affected capillaries. On the other hand, a crossing venule would act to remove O_2 from the capillaries thus decreasing their erythrocyte SO_2 level (Ellis et al. 2012). This implies that under normal physiological conditions, and in the absence of changes in metabolic demand, there is heterogeneity in capillary SO_2 levels partially attributed to variations in the surrounding microvascular geometry and

environment. The heterogeneity in capillary SO_2 could also be due to the uneven erythrocyte distribution at upstream arteriolar branch points. In the arterioles, cells nearest the wall will have lower SO_2 than in the centerline (Ellsworth and Pittman 1986, Carvalho and Pittman 2008). Plasma skimming will result in downstream capillaries receiving different populations of erythrocytes at different SO_2 levels (Tyml et al. 1981, Ellis et al. 1994, Pries et al. 1996).

In order to investigate micro-vascular response to local tissue PO_2 perturbations, we have developed a micro-delivery system which allows for altering the erythrocyte SO_2 in selected capillaries in response to local tissue PO_2 changes (Ghonaim et al. 2011) (Figure 4.1). In this setup, O_2 from a gas mixture flowing through the micro-delivery system is exchanged with tissue (rat Extensor Digitorum Longus) positioned directly above an O_2 micro-outlet microfabricated in ultrathin glass/plastic. The micro-delivery system is used in conjunction with *in vivo* video microscopy (IVVM) system which allows for recording blood flow responses while simultaneously controlling erythrocyte SO_2 in selected capillaries (Ellis et al. 2010; 2012). Theoretical modeling and *in vivo* testing with a circular micro-outlet (100 μm in diameter) confirmed that erythrocyte SO_2 can be altered and measured in single capillaries flowing over a micro-outlet with the above dimensions (Ghonaim et al. 2011) and that the effect is restricted to the immediate area of the micro-outlet. Further modelling work (Ghonaim et al. 2013) indicated that the total magnitude of ATP in the network is proportional to the number of affected capillaries. The results suggested that with a rectangular micro-slit design (1000 μm wide x 200 μm long) a

sufficient number of capillaries are stimulated to produce sufficient ATP signal while limiting the area of perturbation to the immediate vicinity of the micro-slit.

In this study, we aimed to investigate conducted SO_2-dependent microvascular responses in the capillary bed using the O_2 micro-delivery system. We hypothesize that capillaries are able to signal upstream arterioles for changes in erythrocyte supply rate in response to changes in capillary SO_2 via SO_2-depndent erythrocyte signaling. The rectangular micro-slit design previously modeled for O_2 exchange was tested *in vivo* (Figure 4.2B). Our results indicated that capillaries are able to regulate the distribution of arteriolar blood flow in response to changes in their erythrocyte SO_2. Also, in support with our modeling data (Ghonaim et al. 2013), there appeares to be a threshold for the minimum number of capillaries that need to be stimulated by altered SO_2 in order to induce a conducted microvascular response. Although erythrocyte SO_2 can be measured in single capillaries flowing over an O_2 micro-outlet window down to 100 μm in diameter, at least 3-4 capillaries need to be stimulated within a branching capillary network in order to induce a microvascular response. The variability in the minimum number of capillaries that need to be stimulated is likely dependent on the number of capillaries supplied by a specific branch of the arteriolar tree. Microvascular responses originate from a capillary network positioned directly over the outlet with the terminal end of the feeding arteriolar end positioned >50 μm upstream from the micro-outlet, which suggests the signal was conducted upstream from the site of stimulation. These results support the hypothesis that capillaries can sense and integrate biological responses.

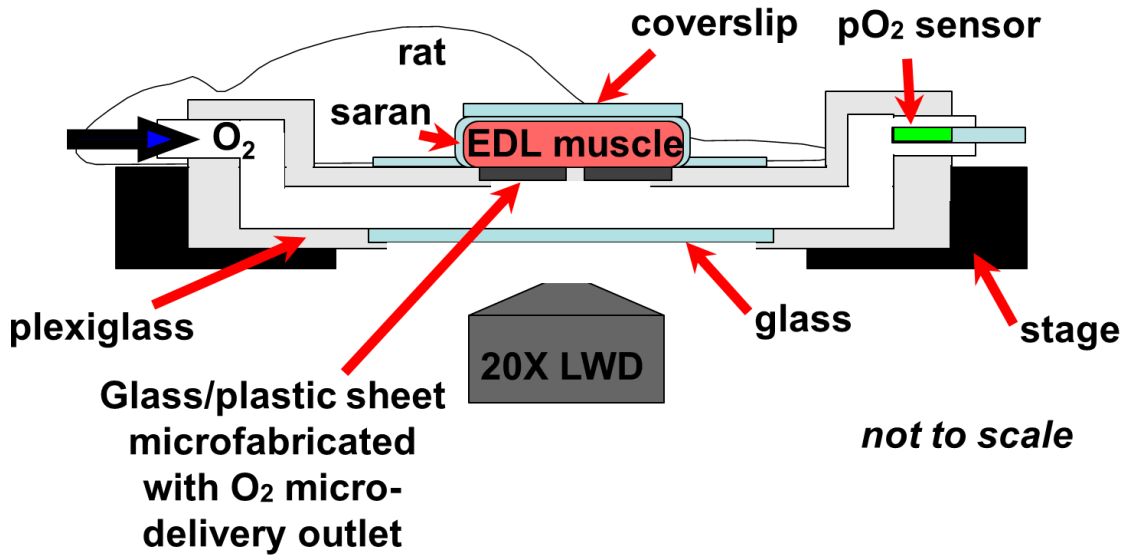

Figure 4.1 The O_2 micro-delivery system. Extensor Digitorum Longus (EDL) rat muscle is surgically exposed and positioned on the viewing platform of an inverted microscope. O_2 is delivered to the surface of the muscle through a micro-delivery outlet patterned in ultrathin glass/plastic sheet. O_2 levels in the gas exchange chamber near the muscle surface are oscillated using computer controlled flow meters. Real-time videos of the illuminated tissue are monitored and recorded using a digital camera (Ellis et al. 2010, Ghonaim et al. 2011).

4.2 Materials and Methods

4.2.1 Microfabrication

Ultrathin glass/plastic sheets were patterned with the O_2 delivery micro-outlets using state-of-the art microfabrication techniques. The O_2 delivery micro-outlet is positioned directly beneath selected capillaries in the microvascular bed at the surface of the EDL muscle with the aid of an inverted microscope. The micro-outlets are covered with a Polydimethylsiloxane **(***PDMS***)** O_2 permeable layer to prevent fluid leakage into the device and direct exposure of the tissue to gas in the exchange chamber. The area of the microvascular bed, and hence the number of capillaries, that is stimulated is proportional to the area of the O_2 delivery micro-outlet. O_2 levels in the gas exchange chamber near the muscle surface are oscillated using computer-controlled flow meters, and O_2 is delivered to the tissue through the patterned outlets (Figure 4.1). Real-time videos of the illuminated tissue are monitored and recorded using a digital camera.

4.2.1.1 Patterning ultrathin glass

The O_2 exchange circular micro-outlet (100 µm in diameter) was patterned in 30 µm thick D263C borosilicate glass substrate (SCHOTT North America, Inc., Elmsford, NY, USA), respectively, by photolithography and subsequent wet etching in hydrogen fluoride (Figure 4.2A). The photolithography and wet etching steps were carried out similar to previously described procedures (Ilie et al. 2003, Srivastava et al. 2005). Since the etching is isotropic, there is a certain degree of undercutting beneath the masking

layers (Ilie et al. 2003). This results in the pattern to be larger on the glass relative to the photomask. All pattern dimensions were optically measured at the top glass surface (glass surface directly beneath the masking layers) using QCapture ProTM 6.0 software (QImaging®, Surrey, BC, Canada).

4.2.1.2 Patterning poly-methyl methacrylate (PMMA) sheet

The O_2 exchange micro-slit (1000 μm wide x 200 μm long) was patterned in 130 μm thick poly-methyl methacrylate (PMMA) substrate (Astra Products, Inc., Baldwin, NY, USA) by laser micromachining (Figure 4.2B).

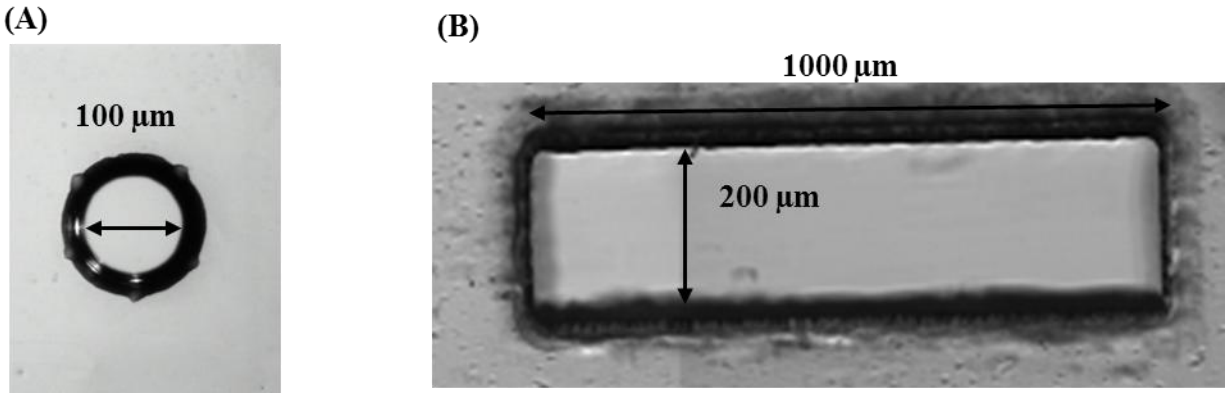

Figure 4.2 The O_2 delivery micro-outlets (A) A circular O_2 delivery micro-outlet 100 μm in diameter patterned in D263Tborosilicate ultrathin glass substrate (SCHOTT North America, Inc., Elmsford, NY, USA) as it appears under an upright light microscope at 10x objective. (B) A 200 μm long x 1000 μm wide rectangular O_2 delivery micro-slit patterned in poly-methyl methacrylate (PMMA) substrate (Astra Products, Inc., Baldwin, NY, USA) by laser micromachining as it appears under an inverted light microscope at 5x objective.

4.2.2 *In Vivo* Video Microscopy

Erythrocyte SO_2 and supply rates were measured in response to O_2 exchange through the micro-outlets/micro-slits using IVVM techniques. Microvascular conducted responses result in changes in the erythrocyte supply rate due to changes in resistance in the upstream arteriolar tree. By varying the area of O_2 exchange and hence the number of capillaries stimulated on the microvascular bed, the relationship between the onset of conducted microvascular response to low PO_2 and the number of capillaries stimulated could be investigated.

Experiments using the 100 μm diameter circular outlet were performed on a Nikon inverted microscope. Experiments using the 200 μm long x 1000 μm wide rectangular O_2 delivery micro-slit were performed on a newer Olympus inverted microscope system with digital video cameras.

4.2.2.1 Animal preparation

All procedures described are approved from the University of Western Ontario's Animal Care and Use Committee. Five male Sprague-Dawley rats (Charles River Laboratories, Wilmington, MA***, USA***) (150-200 g) were anesthetized with pentobarbital sodium (6.5 mg/100 g body wt IP) and were subjected to a preparatory surgery as described (Ellis et al. 2002; 2010). The animals were mechanically ventilated at 30% O_2 (70% Nitrogen), and the inspired O_2 level (Oxychek) and blood pressure (MicroMed) were constantly monitored and recorded (Ellis et al. 2010). The Extensor Digitorum Longus (EDL)

muscle of the hind limb was identified and prepared for in vivo video microscopy as described by Tyml and Budreau (1991). The distal end of the EDL muscle was tied with a suture and the distal tendon cut. The muscle was extended along the viewing platform of either a Nikon inverted microscope equipped with long-working distance 10X and 20X objectives and a beam splitter for dual video cameras (DAGE-MTI CCD cameras**,** DAGE-MTI, Michigan City, IN, USA) or an Olympus IX-81 inverted microscope with 10 X and long working distance 20X objectives and DualCam beamsplitter with dual 12bit digital video cameras (Rolera XR cooled CCD). A suture attached to the distal end of the muscle was taped to the platform such that the muscle was stretched to its *in vivo* length. The muscle was covered with Saran Wrap (Dow Corning, Midland, MI, USA) and a cover slip to isolate it from room air and to preserve moisture. The tissue was trans-illuminated with either a 100-W xenon lamp on the Nikon microscope or a 75-W xenon lamp on the Olympus and viewed using the dual video camera system as described (Ellis et al. 2010).

4.2.2.2 Dual wavelength intravital video microscopy system **DλIVVM**

Real-time video recordings (Nikon system: 640 x 480, 30 frames/second, 8 bit gray scale; Olympus: 696 x 520, 20.7 frames/second, 12 bit gray scale) of red blood cell (RBC) flow through capillaries were simultaneously obtained at two wavelengths, 431/442 nm, an O_2 sensitive wavelength for hemoglobin, and 420/454 nm, an isosbestic or O_2 insensitive wavelength (Ellsworth et al. 1987) using the dual video camera IVVM system (Ellis et al.

2010). Live video sequences from the DAGE-MTI CCD cameras on the Nikon were digitized using a DT frame grab board and stored as uncompressed 8 bit AVI movie files using custom acquisition software from Neovision (Ellis et al. 2010) for post-processing. Live digital video sequences were streamed from the Rolera XR cameras on the Olympus to the computer and stored as 16 bit uncompressed PNG files. Geometric, spatiotemporal, and photometric off-line analyses of the video sequences were conducted as described by Ellis et al. (Ellis et al. 1990; 1992) and Japee et al. (Japee et al. 2004; 2005) using algorithms written in MATLAB (Mathworks, Natick, MA) to generate functional mages of the capillary network and to quantify changes in capillary hemodynamic parameters and erythrocyte SO_2.

In this study, either variance or sum of the absolute differences (SAD) functional images were used to illustrate the capillaries selected for analysis and surrounding geometry in an area of interest. In the variance image, areas with high temporal variation in light intensity (e.g. due to frequent passage of RBCs and plasma) will appear brighter, making capillaries more visible (Japee et al. 2004). In the SAD images, the sign of the variance is ignored, making the capillaries appear even brighter. Frame-by-frame measurements of hemodynamic parameters including RBC velocity (μm/sec), supply rate (RBC/sec), hematocrit (%), and RBC SO_2 (%) were conducted (30 frames/sec on the Nikon, 20.7 frames/sec on the Olympus) (Ellis et al. 1990; 1992, Japee et al. 2004; 2005) (Also see Figure 4.3). In all subsequent figures presented in this study, the data points were plotted as 10 sec averages for increased clarity.

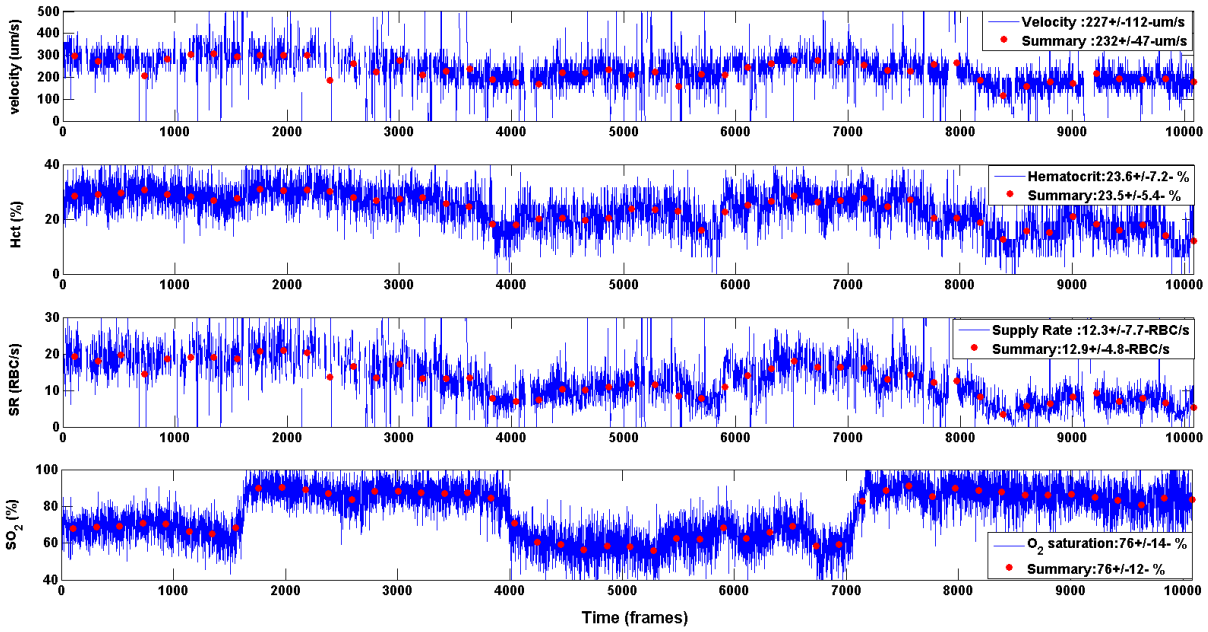

Figure 4.3 Frame-by-frame change in RBC velocity (μm/sec), RBC hematocrit (% Hct), RBC supply rate (SR), and RBC SO_2 (%). An eight minute (10,080 frames x 2) video sequence was captured using a dual wavelength video microscopy system, and post-processed for changes in various hemodynamic parameters using algorithms written in MATLAB (Mathworks, Natick, MA) as described by Ellis et al. (Ellis et al. 1990; 1992) and Japee et al. (Japee et al. 2004; 2005)

4.3 Results

4.3.1 Examining the dependence of microvascular response on the number of capillaries stimulated

The aim of this set of experiments was to investigate the relationship between the onset of conducted microvascular response to low PO_2 and the number of capillaries stimulated. O_2 was exchanged through an O_2 micro-outlet patterned in ultrathin glass/plastic sheet to live tissue in direct interface. Selected capillaries were positioned over the O_2 micro-outlet with the aid of an inverted light microscope. O_2 levels were oscillated at tissue surface and the erythrocyte SO_2 and supply rate changes were measured and recorded. Unless otherwise stated, each capillary network analyzed in this manuscript has been captured from an independent EDL muscle preparation (total of 5 animals).

4.3.1.1 O_2 exchange through a circular micro-outlet (100 µm in diameter)

A selected capillary, designated as Cap1, on the surface of the EDL muscle was positioned on top of a circular micro-outlet 100 µm in diameter (Figure 4.4A). The size of the circular micro-outlet allows for 1-2 capillaries to be affected by the local PO_2 perturbations (Ghonaim et al. 2011, 2012). The O_2 level in the chamber was decreased from 20% (152 mmHg) to 2% (15 mmHg) for a 120-second low O_2 challenge and back to 20%. A video sequence was recorded over a six minute period beginning two minutes

before the low O_2 challenge. The video was postprocessed for changes in capillary hemodynamic parameters and erythrocyte SO_2. Cap1 was divided into three sections designated as Cap1a, Cap 1b and Cap 1c, according to their position relative to the micro-outlet (Figure 4.4A). Each section was analyzed separately. The SO_2 profile for erythrocytes flowing in Cap1a, that is prior to entering the micro-outlet, seems to be unaffected by the low O_2 with an SO_2 level of ~ 68.6±10.1% (SD, N=287) (Figure 4.4B). However, the SO_2 profile for erythrocytes flowing directly over the micro-outlet in Cap1b was strongly associated with the chamber O_2 level with a lag time of ~ 7 sec (Figure 4.4B). The time delay in SO_2 changes relative to the chamber O_2 level was similar to previously reported values (Ghonaim et al. 2011). At 20% chamber O_2, the SO_2 level in Cap1b was ~80.4±4.7% (N=91). The SO_2 level then decreased to ~34.9±13.5% (N=114) in response to lowering chamber O_2 (2%) followed by an increase to ~73.1±11.2% (N=59) during recovery back to 20% O_2. For Cap1c, the SO_2 profile also resembled the chamber O_2 level, yet it showed the erythrocytes were sensing higher tissue PO_2 relative to Cap 1b (Figure 4.4B). At 20% chamber O_2, the SO_2 level in Cap1b was ~74.08±5.1% (N=91). The SO_2 level then decreased to ~46.9±11.9% (N=113) in response to lowering chamber O_2 (2%) followed by an increase to ~72.63±14.3% (N=49) during recovery back to 20% O_2. Although Cap1 clearly experienced changes in erythrocyte SO_2 in response to the local O_2 perturbation, no corresponding changes in capillary erythrocyte supply rate were measured (Figure 4.4C).

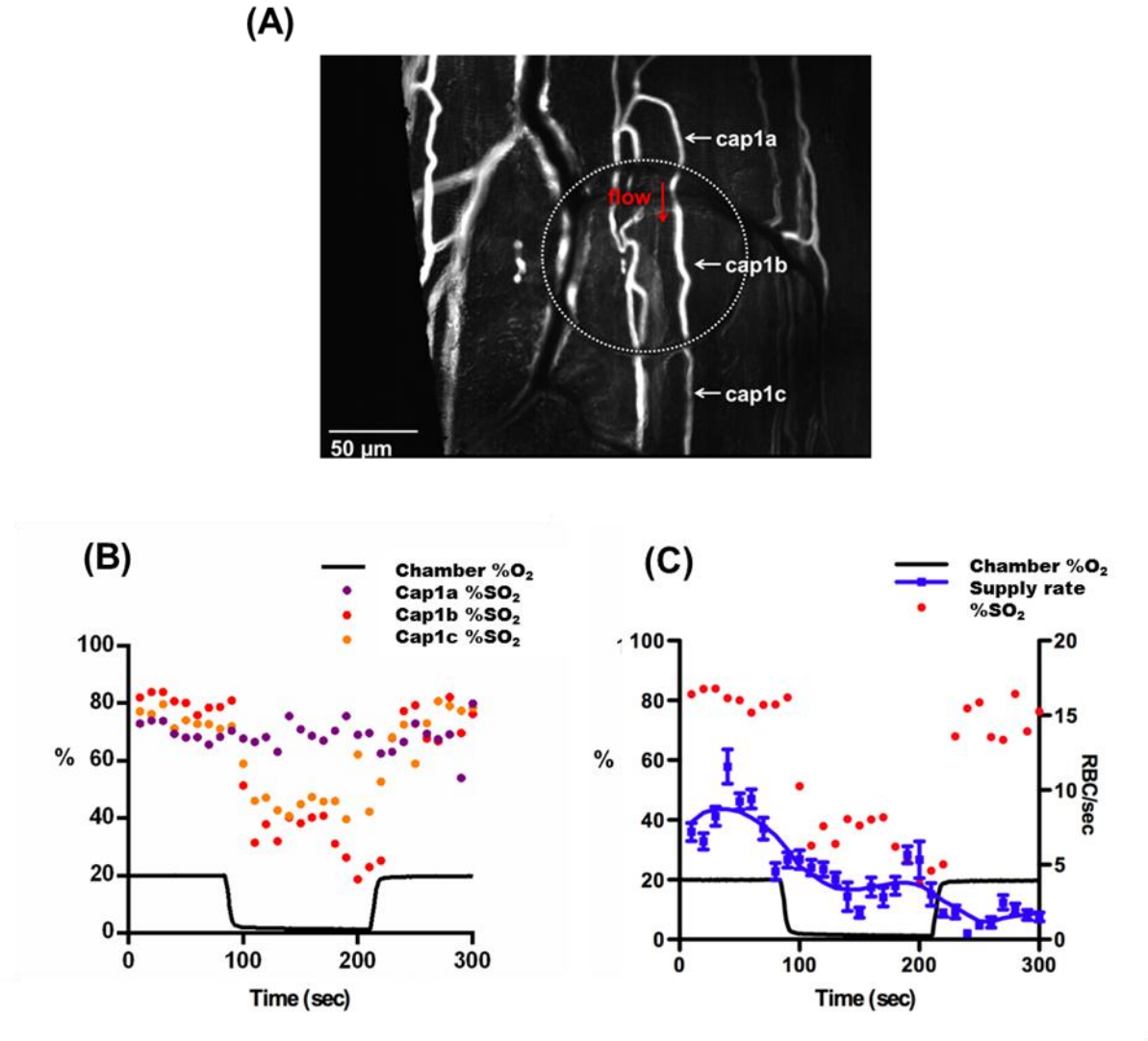

Figure 4.4 EDL muscle preparation with transparent 100 µm diameter micro-outlet positioned under the muscle. (A) A Variance image showing the microvascular network (20X) with flowing erythrocytes (white lines) and the location of the micro-outlet outlined by the white dashed line. A long capillary, in focus over its entire length, was

selected and positioned directly over the micro-outlet. This capillary, designated as Cap1, was sampled in three separate segments: Cap1a upstream of the micro-outlet, Cap1b directly over the outlet and Cap1c downstream of the outlet. O_2 levels in the chamber were oscillated in a square wave: 5% O_2 (PO_2 = 38 mmHg) for 30 seconds, 20% O_2 (PO_2 = ~150 mmHg) for 120 seconds, 2% O_2 (PO_2 = ~15 mmHg) for 120 seconds and back to 20% O_2. A six minute video sequence was captured beginning as chamber O_2 was increased from 5% to 20%.. (B) All three segments were analysed for changes in erythrocyte %SO_2 and supply rate. The erythrocyte %SO_2 level in Cap 1a experienced minimal changes in response to the PO_2 perturbations while the SO_2 profiles of Cap 1b and Cap 1c were more closely associated with chamber O_2 (C) however, the supply rate changes measured in Cap1b segment showed no correspondence with measured SO_2 changes. Measured supply rate data (10 sec mean) were plotted along with a fitted smoothing curve (blue solid line; Prism v 5.0, 2nd order smoothing polynomial function, number of neighbors to average = 6 neighbors on each size).

4.3.1.2 O_2 exchange through the rectangular micro-slit (200 µm long x 1000 µm wide)

In order to examine the effect of influencing a larger number of capillaries, a rectangular micro-slit (200 µm long x 1000 µm wide) was used and a small capillary branching network near the surface of the EDL muscle was positioned directly over the micro-slit (3-4 capillaries within the network) (Figure 4.5A,B). The tissue was equilibrated at 5% (38 mmHg PO_2) O_2 level for 30 seconds. The O_2 level in the chamber was increased to 20% (152 mmHg) then decreased to 2% (15 mmHg) for a 120-second low O_2 challenge

and back to 20%. A video sequence was recorded over a six minute period beginning as chamber O_2 was increased from 5% to 20%. One capillary in the network (Cap2) was kept in sharp focus during the sample interval and the video was postprocessed for changes in hemodynamic parameters and erythrocyte SO_2 in a segment of this capillary. Similar to the previous observations, the PO_2 perturbations resulted in corresponding changes in the SO_2 profile in Cap2 with a delay time of ~7 sec (Figure 4.5C). At baseline chamber O_2 (5%), the SO_2 level in Cap2 was ~51.0±5.7% (N=55). Increasing chamber O_2 to 20% (at 50 sec) resulted in a corresponding increase in SO_2 to ~ 67.6±4.7% (N=79). The SO_2 level then decreased to ~21.1±12.0% (N=110) in response to lowering chamber O_2 (2%) (at 130) followed by an increase to ~61.3±9.6% (N=74) during recovery back to 20% O_2 (at 250sec). Stimulating the branching capillary network by altering capillary SO_2 resulted in associated changes in capillary erythrocyte supply rate as measured in Cap2 (Figure 4.5C). Increasing the chamber O_2 level from baseline of 5% up to 20% resulted in ~70% decrease in mean erythrocyte supply rate relative to baseline (minimum at ~1.3 RBC/sec at 190 sec) (Figure 4.5C). After reaching minimum value at ~190 sec, the supply level was observed to increase reaching a maximum of ~4.5 RBC/sec at ~ 250 sec (Figure 4.5). The increase in supply is associated with the decrease in SO_2 (at ~137 sec) in response to low chamber O_2 (at 130 sec). This indicates there is ~50 sec delay in supply rate response to low SO_2 measured from the time point at which SO_2 level decreases in response to low chamber O_2 to the time point at which supply rates increase above minimum value. Increasing chamber O_2 back to 20% (at 250 sec) resulted in sharp and near instantaneous decrease in supply rate to a minimum of ~1.3 RBC/sec.

Since the branching capillary network was positioned with the feeding arteriolar tree and terminal arteriolar end being upstream of the O_2 micro-slit (Figure 4.5A,B), the measured microvascular responses were probably conducted upstream from the capillary bed into the supplying arteriolar network.

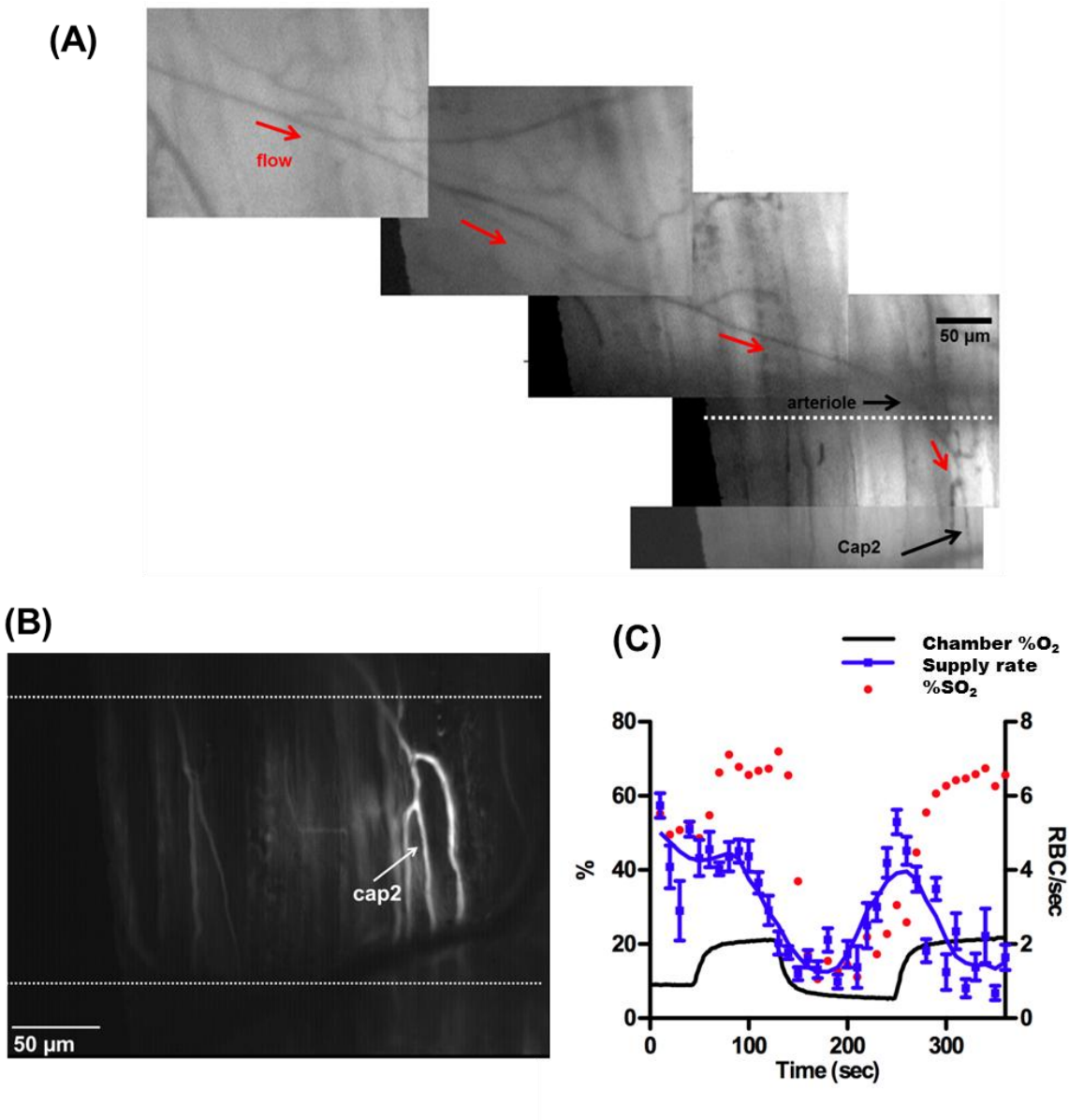

Figure 4.5 (A, B) A selected capillary, Cap2, in a branching capillary network, was positioned directly over a rectangular micro-slit (1000 µm wide x 200 µm long) outlined by white dashed line with the arteriolar tree upstream of the micro-slit. Cap2 was analysed for changes in erythrocyte $\%SO_2$ and supply rate (RBC/sec) as O_2 levels in the

chamber are oscillated in a square wave. The tissue was equilibrated at 5% O_2 (38 mmHg PO_2) level for 30 seconds. The O_2 level in the chamber was increased to 20% (~152 mmHg) then decreased to 2% (~15.2 mmHg) for a 120 second low O_2 challenge and back to 20%. A six minute video sequence was captured beginning 2 min prior to the low O_2 challenge. (C) The erythrocyte SO_2 profile for Cap 2 resembles that of chamber O_2. Stimulating the branching capillary network results in measured changes in erythrocyte supply rate. Measured supply rate data (10 sec mean) were plotted along with a fitted smoothing curve (blue solid line; Prism v 5.0, 2nd order smoothing polynomial function, number of neighbors to average = 6 neighbors on each size).

4.3.2 Examining the reproducibility of the microvascular response to the SO_2 changes in selected capillaries

4.3.2.1 Measuring reproducibility over consecutive capture sequences

In order to test the reproducibility of the supply rate responses to capillary SO_2 changes, the low O_2 perturbation was repeated over two video sequences, with a 20 min time gap on a selected capillary branching network (5-6 capillaries within the network) positioned directly over the rectangular micro-slit (Figure 4.6A,B). The tissue was equilibrated at 5% O_2 (38 mmHg PO_2 level) for 60 seconds. The O_2 level in the chamber was increased to 20% (152 mmHg) then decreased to 2% (15 mmHg) for a 160-second low O_2 challenge and back to 20%. A video sequence was recorded over an eight minute period

beginning one minute before the increase in chamber O_2 from 5 to 20%. The tissue was then allowed to equilibrate with chamber O_2 of 5% for 20 min after which the same O_2 perturbation was repeated. A selected capillary in the network designated Cap3 was analyzed for changes in erythrocyte SO_2 and hemodynamic parameters. In both consecutive sequences, the erythrocyte SO_2 profile for Cap3 was closely associated with the chamber O_2 a delay time of ~7 sec as previously measured (Figure 4.6C,D). In the first captured sequence (Figure 4.6C), the SO_2 level in Cap3 at baseline chamber O_2 (5%) was ~67.4±2.2% (N=8). Increasing chamber O_2 to 20% (at 70 sec) resulted in a corresponding increase in SO_2 to ~ 87.0±2.0% (N=11). The SO_2 level then decreased to ~61.7±4.6% (N=15) in response to lowering chamber O_2 (2% at 190 sec) followed by an increase to ~85.8±3.0% (N=15) during recovery back to 20% O_2 (at 340 sec). In general, the measured SO_2 changes in the second captured sequence (20 min later) due to the PO_2 perturbation (Figure 4.6D) were comparable to those measured in the first sequence (Figure 4.6C). At baseline chamber O_2 (5%), the SO_2 level in Cap3 was ~70.4±3.3% (N=12). Increasing chamber O_2 to 20% (at 120 sec) resulted in a corresponding increase in SO_2 to ~ 87.6±6.3% (N=14). The SO_2 level then decreased to ~57.2±4.5% (N=13) in response to lowering chamber O_2 (2% at 250 sec) followed by an increase to ~87.1±1.2% (N=10) during recovery back to 20% O_2 (at 400 sec). During the first PO_2 perturbation (Figure 4.6C), increasing chamber O_2 level from baseline to 20% resulted in 50% decrease in supply rate relative to baseline (minimum of ~10 RBC/sec at 210 sec). After reaching minimum value, supply levels increased in response to low SO_2 (at 200 sec) reaching a maximum of ~16 RBC/sec at 340 sec, which was slightly below that at

baseline (~18.3±1.7 RBC/sec, N=8). The delay time in supply rate response to decrease in SO_2 level was ~10 sec. The increase in the supply rate was associated with a re-oxygenation effect as observed in the SO_2 profile at ~250 seconds (Figure 4.6C). Increasing chamber O_2 back to 20% (at 340 sec) resulted in sharp and near instantaneous decrease in supply rate to a minimum of ~7 RBC/sec. Repeating the same PO_2 perturbation on the selected field of view 20 minutes later resulted in similar supply rate responses (Figure 4.6D). In the second sequence, the baseline supply rate level for Cap3 was slightly lower (~14.6±1.2 RBC/sec, N=13) and the overall supply rate profile was slightly shifted to lower values. Increasing chamber O_2 level from baseline to 20% resulted in 80% decrease in supply rate relative to baseline (minimum at ~2.9 RBC/sec at 270 sec). After reaching minimum value, supply levels increased in response to low SO_2 (at 260 sec) bringing the supply rate level up to slightly below that at baseline with a maximum of ~12 RBC/sec. The measured delay time in supply rate response to decrease in SO_2 level was similar to that measured during the first perturbation ~10 sec. Increasing chamber O_2 back to 20% (at 400 sec) resulted in sharp and instantaneous decrease in supply rate to a minimum of ~7.3 RBC/sec. A similar flow response was observed in the other capillaries in the field of view. Since the feeding arteriolar end was positioned upstream of the O_2 micro-slit (Figure 4.6A,B), the measured microvascular responses are anticipated to be conducted from the capillary bed to the supplying arterioles.

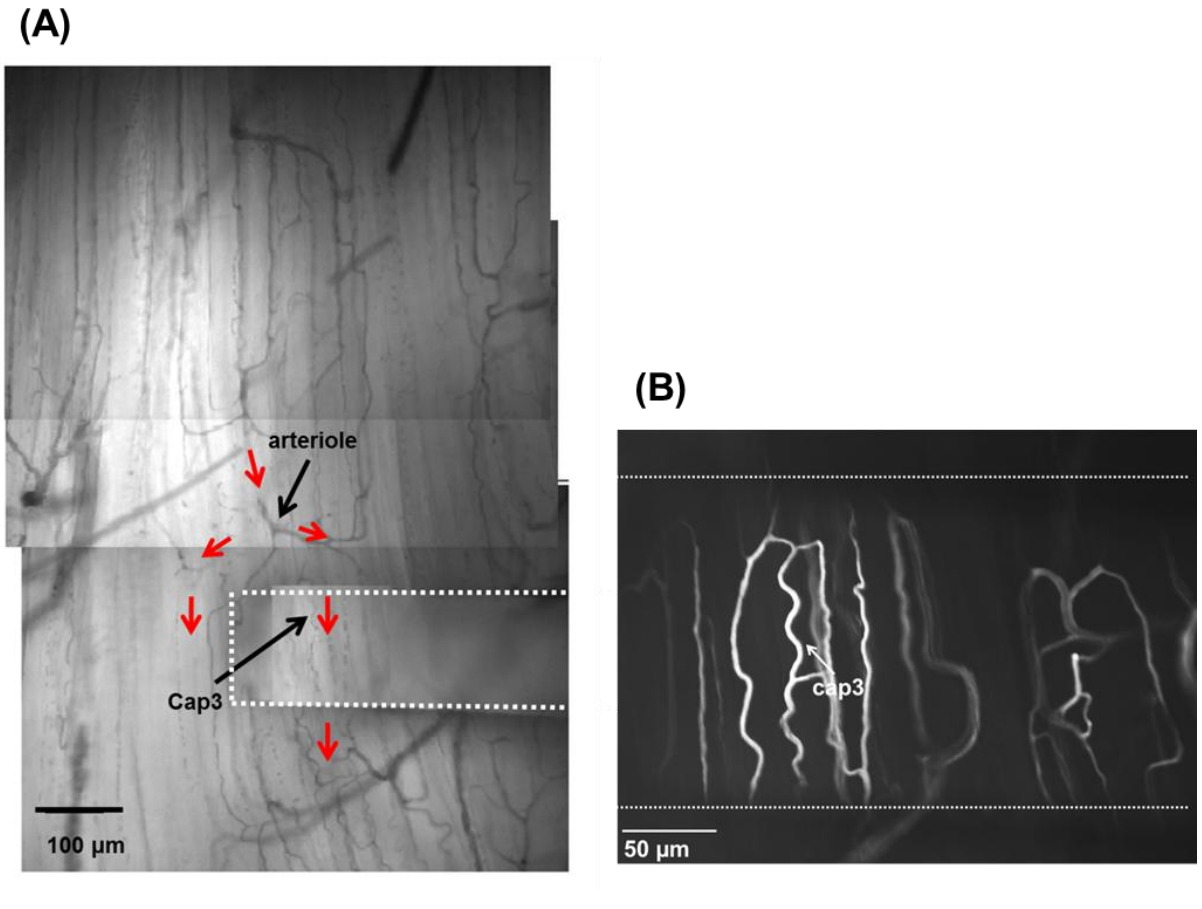
(A)
arteriole
Cap3
100 µm
(B)
cap3
50 µm
20 min later
(C)
Chamber %O2
Supply rate
%SO2
%
RBC/sec
Time (sec)
(D)
Chamber %O2
Supply rate
%SO2
%
RBC/sec
Time (sec)

Figure 4.6 (A, B) A selected capillary, Cap3, in a branching capillary network, is positioned directly over a rectangular micro-slit (1000 μm wide x 200 μm long) outlined by white dashed line with the arteriolar tree upstream of the micro-slit. Cap3 was analysed for changes in erythrocyte $\%SO_2$ and supply rate as O_2 levels in the chamber are oscillated in a square wave. The tissue is equilibrated at 5% O_2 (38 mmHg PO_2) level for 60 seconds. The O_2 level in the chamber is increased to 20% (~152 mmHg) then decreased to 2% (~15.2 mmHg) for a 160 second low O_2 challenge and back to 20%. An eight minute video sequence is captured beginning 3 min prior to the low O_2 challenge. (C) The SO_2 profile for Cap3 is closely associated with chamber O_2 and SO_2 changes result in corresponding changes in supply rate. (D) Similar SO_2 and supply rate responses are measured after repeating the PO_2 oscillation approximately 20 min following the perturbation shown in (C). Measured supply rate data were plotted along with a smoothing curve (blue solid line; Prism v 5.0, 2^{nd} order smoothing polynomial function, number of neighbors to average = 6 neighbors on each size).

4.3.2.2 Measuring reproducibility over consecutive PO_2 perturbations in a single sequence

The reproducibility of the supply rate responses to capillary SO_2 changes were also tested by repeating the PO_2 perturbation in the same sequence. Erythrocyte SO_2 and supply rate changes were measured in a selected capillary (Cap4) positioned upstream of the micro-slit with capillary venular end positioned over the micro-slit (Figure 4.7A,B). Cap4 is one of ~6-8 capillaries draining directly over the micro-slit originating from same upstream

arteriole. The tissue was initially equilibrated at 5% (38 mmHg PO_2) O_2 level for 30 seconds. O_2 levels in the chamber were the oscillated in two consecutive square waves (period ~ 400 seconds). The O_2 level in the chamber was increased to 20% (152 mmHg) then decreased to 2% (15 mmHg) for a 190 second low O_2 challenge and back to 20%. The chamber O_2 levels were then decreased back to baseline level (5%). A video sequence was recorded over a thirteen minute period (16,146 frames x 2) beginning as the chamber O_2 was increased from 5 to 20%. The measured erythrocyte SO_2 profile for Cap4 was closely associated with the chamber O_2 a delay time of ~ 20-30 sec, which is 2-3 times higher than previously measured (Figure 4.7C). The measured baseline SO_2 level was ~46.4±2.1% (N=6). In the first increase in chamber O_2 to 20% (at 50 sec), the SO_2 level in Cap4 increased to ~ 67.1±6.1% (N=19). The SO_2 level then decreased to ~41.1±6.0% (N=17) in response to lowering chamber O_2 (2% at 220 sec). The following increase in chamber O_2 back to 20% (at 410 sec) resulted in a corresponding increase in SO_2 to ~75.7±14.1% (N=18) followed by a decrease to ~48.8±6.5 (N=19) at baseline O_2 (5% at 570 sec). The results showed strong and reproducible supply rate response to altered erythrocyte SO_2. For both perturbation cycles, the supply rate was shut down completely in response to 20% chamber O_2 (Figure 4.7C). On the other hand, decreasing chamber O_2 resulted in supply rate increase from zero flow to ~30% above baseline (9.0±2.0 RBC/sec, N=6) in both cycles (Figure 4.7C). Zero time delay in supply rate response to low SO_2 was measured at both perturbation cycles. Also, although the selected section in Cap4 was within 50 μm upstream of the micro-slit, the feeding arteriolar end was more than 200 μm upstream. This suggested the responses observed in

Cap4 are probably conducted several hundred µm upstream into the arteriolar tree to alter supply rate.

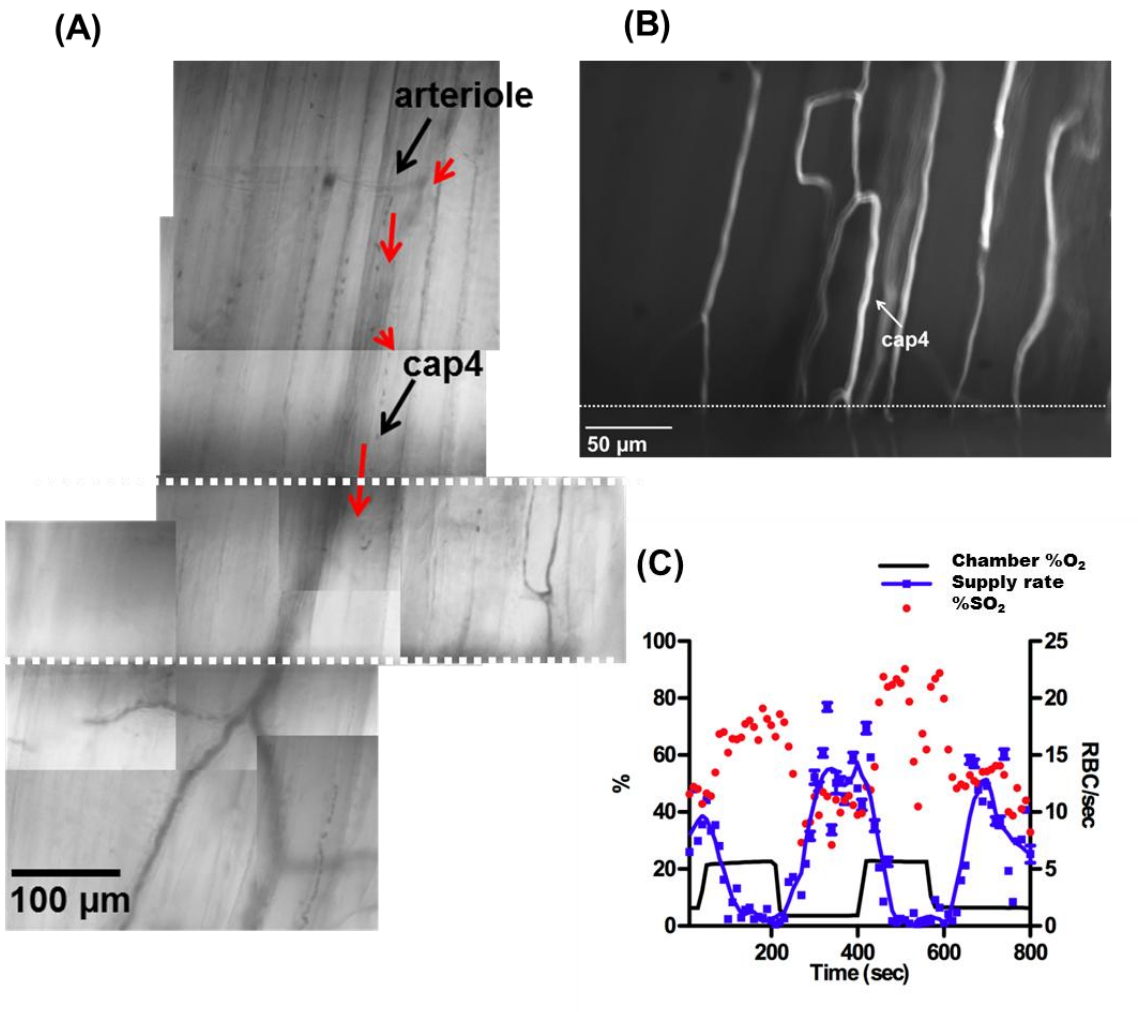

Figure 4.7 (A, B) A selected capillary, Cap4, in a branching capillary network, is positioned upstream of a rectangular micro-slit (1000 µm wide x 200 µm long) outlined by white dashed with the venular end of the capillary positioned directly over the micro-

slit. The feeding arteriolar end upstream of the selected capillary and flow direction are indicated (A). Cap4 was analysed for changes in erythrocyte %SO_2 and supply rate as O_2 levels in the chamber are oscillated in two consecutive square waves (period ~ 400 seconds). The tissue is equilibrated at 5% (38 mmHg PO_2) O_2 level for 30 seconds. The O_2 level in the chamber is increased to 20% (~152 mmHg) then decreased to 2% (~15.2 mmHg) for a 190 second low O_2 challenge and back to 20%. The chamber O_2 levels were then decreased back to baseline level (5%). A thirteen minute video sequence is captured beginning 2 min prior to decreasing chamber O_2. (C) The SO_2 profile for Cap4 is closely associated with chamber O_2 profile. Altering erythrocyte SO_2 in the selected capillary result in strong reproducible supply rate responses. Measured supply rate data were plotted along with a smoothing curve (blue solid line; Prism v 5.0, 2^{nd} order smoothing polynomial function, number of neighbors to average = 6 neighbors on each size).

4.3.3 Examining the influence of the PO_2 perturbations on capillaries positioned near the micro-slit

In order to examine the effect of the O_2 exchange micro-slit on surrounding capillaries *in vivo*, erythrocyte SO_2 and supply rate changes were measured in a selected capillary (Cap 5) positioned within 50 μm from the side edge of micro-slit (Figure 4.8A,B). The arteriole feeding Cap5 branches off the same arterial tree feeding Cap3 network (see above). The tissue was initially equilibrated at 5% (38 mmHg PO_2) level for 60 seconds. The O_2 level in the chamber was increased to 20% (152 mmHg) then decreased to 2% (15 mmHg) for a 130 second low O_2 challenge and back to 20%. A video sequence was

recorded over an eight minute period beginning 3 minutes prior to the low O_2 challenge. Cap5 was divided into three sections Cap5a, Cap5b, and Cap5c (Figure 4.8B) and each section was individually analyzed. The results indicated that Cap5a, which is located furthest upstream from the micro-slit and directly downstream from the feeding arteriole, experienced least changes in erythrocyte SO_2 relative to Cap5b and Cap 5c (Figure 4.9B). At baseline chamber O_2 (5%), the mean SO_2 level in Cap5a was ~63.4±2.6% (N=6). Increasing chamber O_2 to 20% (at 70 sec) resulted in a corresponding increase in mean SO_2 to ~83.2±5.6% (N=11). The mean SO_2 level then decreased to ~74.8±3.8% (N=12) in response to lowering chamber O_2 (2% at 170 sec) followed by an increase to ~84.8±4.7% (N=8) during recovery back to 20% O_2 at 300 sec. Downstream from Cap5a, the sensed SO_2 changes were larger and the measured three dimensional SO_2 profiles along the capillary length were more closely associated with chamber O_2 (Figure 4.9A). In Cap5b, baseline mean SO_2 level was ~47.6±2.7% (N=6). Increasing chamber O_2 to 20% resulted in a corresponding increase in mean SO_2 to ~73.6±5.6% (N=11). The mean SO_2 level then decreased to ~49.2±3.7% (N=12) in response to lowering chamber O_2 (2%) followed by an increase to ~75.4±4.3% (N=8) during recovery back to 20% O_2. The greatest SO2 changes in measured in Cap5c. At baseline, the mean SO_2 level in Cap5c was ~36.8±1.3% (N=6). The increase in chamber O_2 resulted in a corresponding increase in mean SO_2 to ~68.4±7.4% (N=11). Decreasing chamber O_2 (2%) resulted in decreasing mean SO_2 level to ~38.5±5.1% (N=12) followed by an increase to ~70.5±4.3% (N=8) during recovery back to 20% O_2. Despite the relatively smaller changes in SO_2 in Cap5a, supply rate responses were measured in with ~40 sec delay time in response to low SO_2 at

180 sec (Figure 4.9B). The measured supply rate profile was almost identical in all three sections of Cap5. However, the association between supply rate responses and SO_2 changes was stronger in Cap5b and Cap5c relative to Cap5a (Figure 4.9B). The baseline supply rates in Cap5a, 5b, and 5c were ~6.1±1.0 RBC/sec N=6, ~5.9±1.0 RBC/sec N=6, and ~5.5±1.0 RBC/sec N=6, respectively. Increasing chamber O_2 to 20% resulted in ~60% decrease in supply rate relative to baseline (minimum of ~3 RBC/sec at 220 sec). The supply rate increased ~40 sec following decrease in SO_2 (at ~180 seconds) to a maximum of ~5.5 RBC/sec at 280 sec to match baseline level (Figure 4.9B). Increasing chamber O_2 back to 20% resulted in sharp and instantaneous decrease in supply rate to a minimum of ~1.5 RBC/sec. The increase in supply rate in reponse to low SO_2 resulted in slight re-oxygenation observed at ~230 seconds which seemed to compensate for the decrease in erythrocyte SO_2. This effect was most pronounced in Cap5a and decreased downstream. The results indicated that the effect of the micro-slit might be extending slightly beyond 50 μm, which was the radial diffusion distance proposed in our previously described theoretical model (Ghonaim et al. 2013)

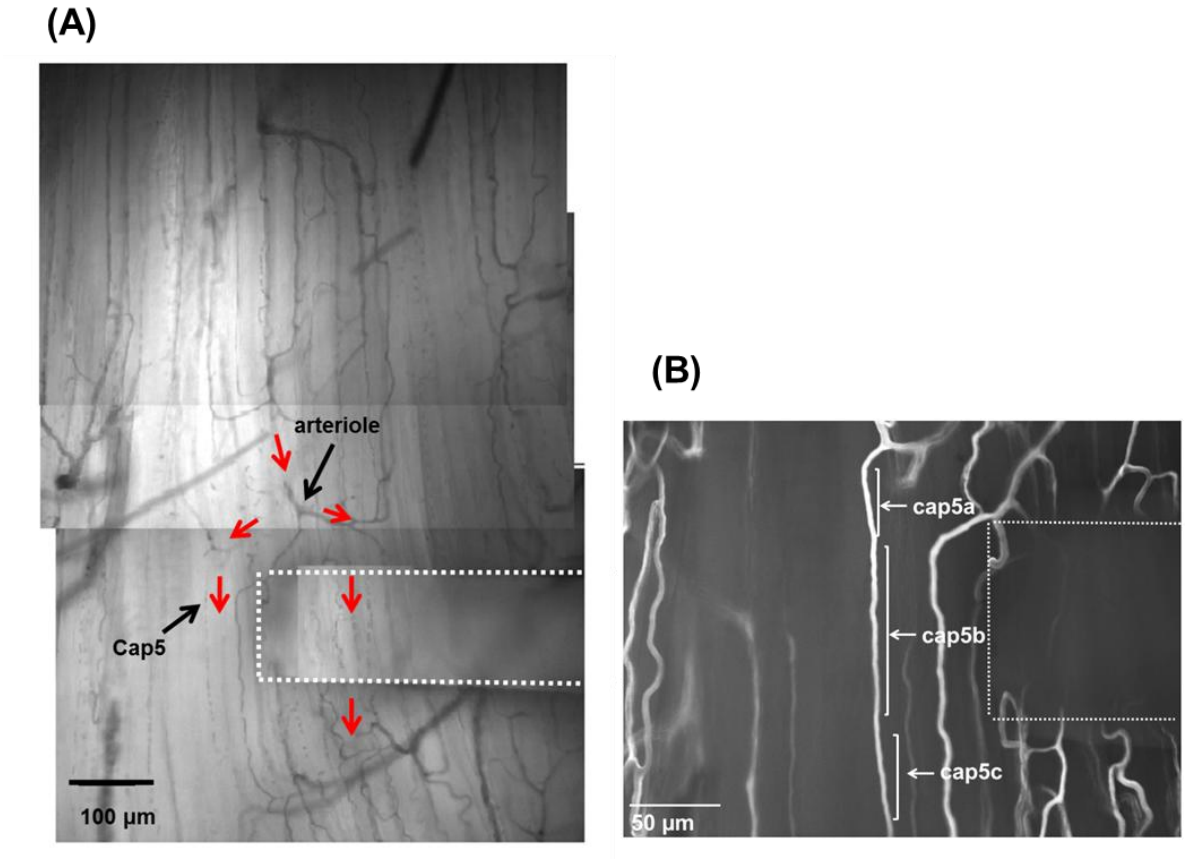

Figure 4.8 (A, B) A selected capillary, Cap5, is positioned outside adjacent to the edge of the rectangular micro-slit (1000 µm wide x 200 µm long) outlined by white dashed line. (A) The feeding arteriolar end upstream of the selected capillary and flow direction are indicated. (B) Cap5 was divided into three sections, Cap 5a, Cap 5b, and Cap 5c and each section was analysed individually for changes in erythrocyte SO_2 and supply rate.

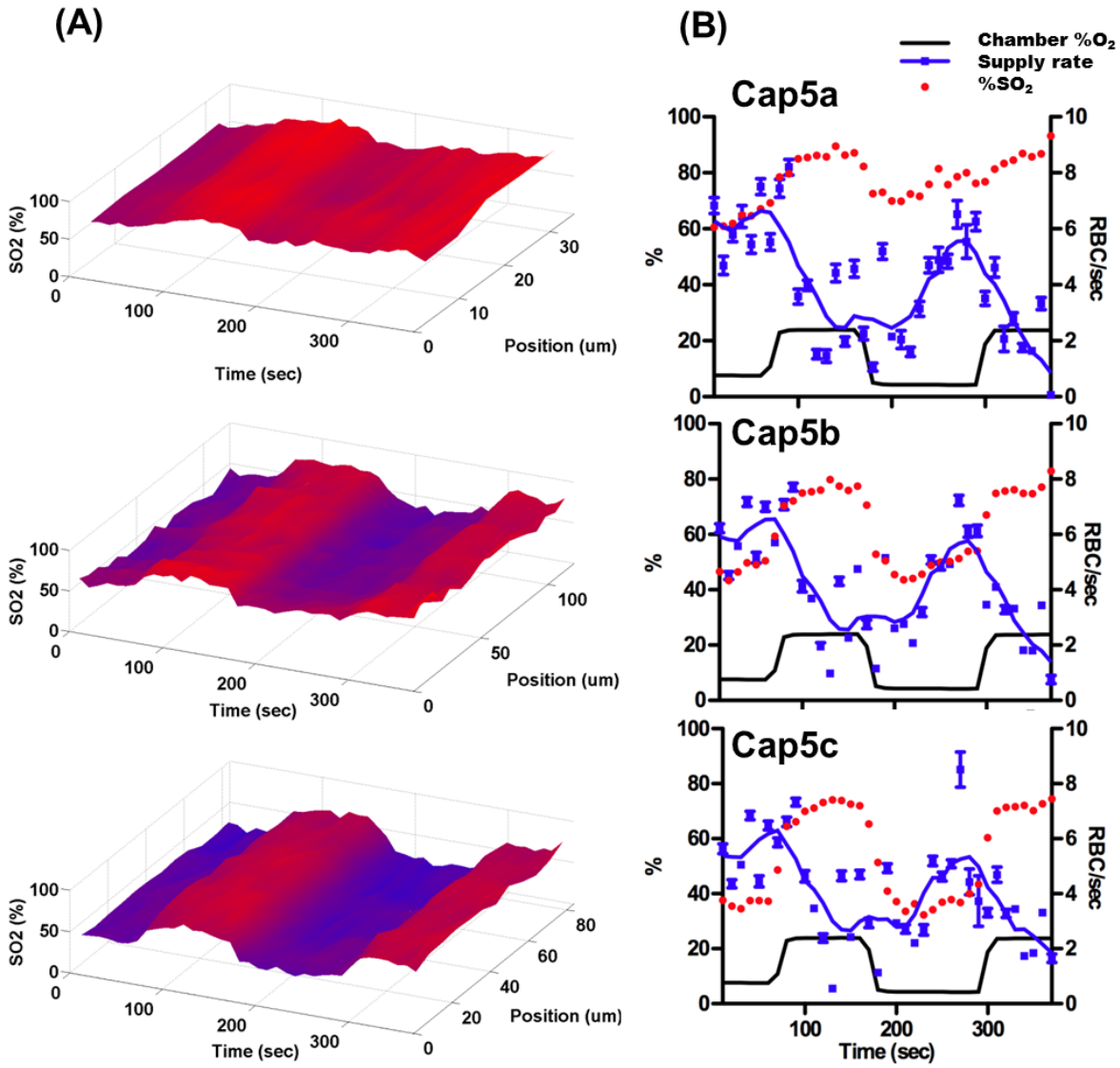

Figure 4.9 Cap5 (see Figure 4.8) was analysed for changes in erythrocyte $\%SO_2$ and supply rate as O_2 levels in the chamber are oscillated in a square wave. The tissue is equilibrated at 5% (38 mmHg PO_2) O_2 level for 60 seconds. The O_2 level in the chamber is increased to 20% (~152 mmHg) then decreased to 2% (~15.2 mmHg) for a 130 second low O_2 challenge and back to 20%. An eight minute video sequence was captured

beginning 3 min prior to the low O_2 challenge. (A) The three dimensional (3D) SO_2 plots displaying SO_2 values across capillary section length with time (B) The SO_2 profiles for Cap5 sections further downstream (closer to micro-slit) are more closely associated with chamber O_2. The SO_2 changes in Cap5 result in corresponding changes in supply rate. Measured supply rate data were plotted along with a smoothing curve (blue solid line; Prism v 5.0, 2nd order smoothing polynomial function, number of neighbors to average = 6 neighbors on each size).

4.3.4 Measuring relative changes in supply rate in response to local PO_2 perturbations

In this experiment, relative changes in supply rate in response to altering SO_2 level in selected capillaries *in vivo* were estimated. Supply rate changes were measured and normalized against baseline mean supply rate in three selected capillaries. The capillaries originate from two branching capillary network fed by the same upstream arterial tree in the same field of view (total of 8-9 capillaries). The three capillaries designated Cap6, Cap7, and Cap8 (Figure 4.10A,B) were positioned directly over the rectangular micro-slit (Figure 4.10A,B). The tissue was initially equilibrated at 5% (38 mmHg PO_2) O_2 level for 30 seconds. The O_2 level in the chamber was increased to 20% (at 50 sec) (152 mmHg) then decreased to 2% (at 130 sec) (15 mmHg) for low O_2 challenge and back to 20% (at 250 sec). A video sequence was recorded over an eight minute period beginning 2 minutes prior to the low O_2 challenge. The measured SO_2 profiles for all three capillaries were closely associated with the chamber O_2 level (Figure 4.10C). In Cap6, baseline

mean SO_2 level was ~72.7±0.2% (N=4). Increasing chamber O_2 to 20% resulted in a corresponding increase in mean SO_2 to ~85.0±2.0% (N=7). The mean SO_2 level then decreased to ~65.3±2.6% (N=11) in response to lowering chamber O_2 (2%) followed by an increase to ~84.0±4.4% (N=9) during recovery back to 20% O_2. In Cap7, baseline mean SO_2 level was ~64.7±0.6% (N=4). Increasing chamber O_2 to 20% resulted in a corresponding increase in mean SO_2 to ~74.9±8.7% (N=10). The mean SO_2 level then decreased to ~39.1±5.7% (N=10) in response to lowering chamber O_2 (2%) followed by an increase to ~73.5±9.8% (N=13) during recovery back to 20%. In Cap8, baseline mean SO_2 level was ~72.3±0.6% (N=4). Increasing chamber O_2 to 20% resulted in a corresponding increase in mean SO_2 to ~80.7±9.4% (N=6). The mean SO_2 level then decreased to ~48.7±3.2% (N=10) in response to lowering chamber O_2 (2%) followed by an increase to ~86.1±6.4% (N=8) during recovery back to 20%. Despite the variability in the mean SO_2 levels at baseline and during the perturbations in the three selected capillaries, the relative changes in supply rate in response to the SO_2 changes were consistent (Figure 4.10D). Supply rate increased by ~50% above baseline in response to low O_2 and was almost shut down in response to the 20% chamber O_2 level (Figure 4.10D). Zero delay time was measured between the time point at which SO_2 level decreases in response to low chamber O_2 and the time point at which supply rate increases (Figure 4.10D).

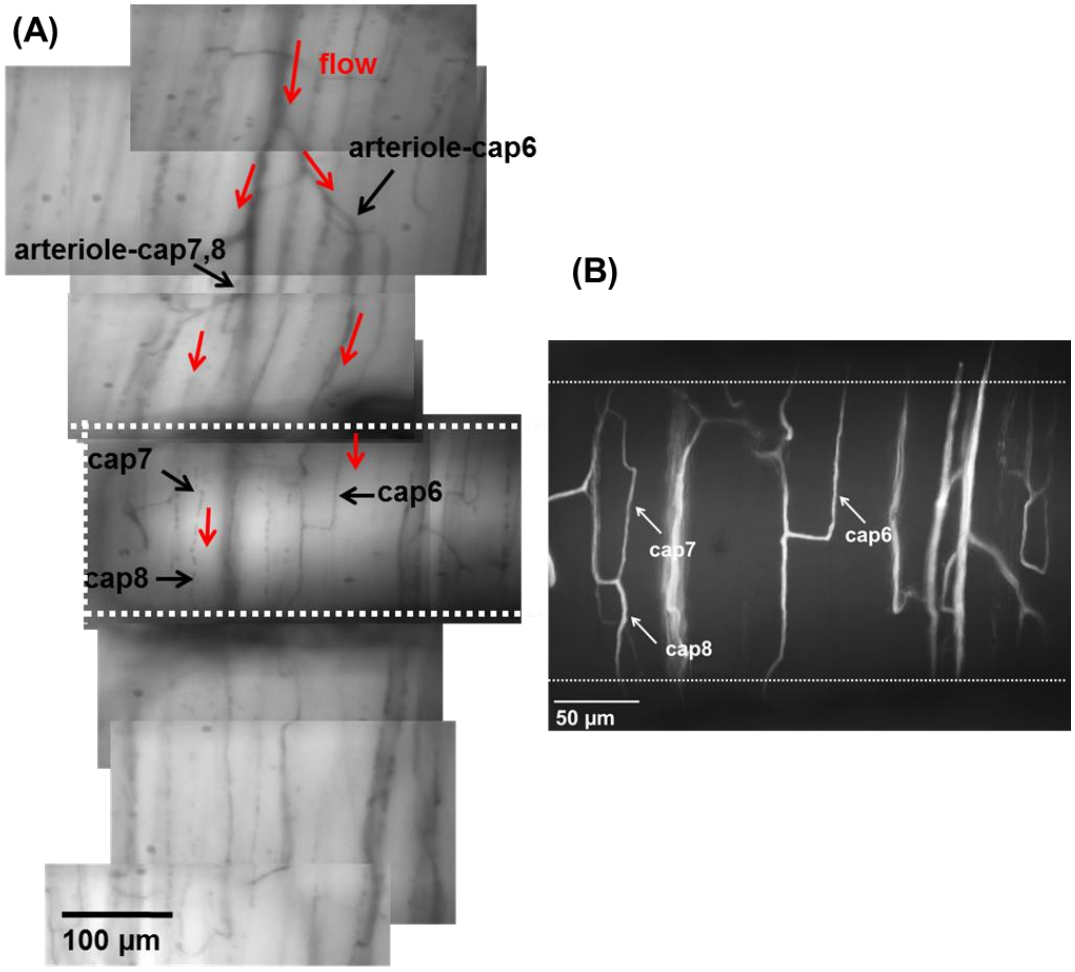
(A)
flow
arteriole-cap6
arteriole-cap7,8
cap7
cap6
cap8
100 µm
(B)
cap7
cap6
cap8
50 µm

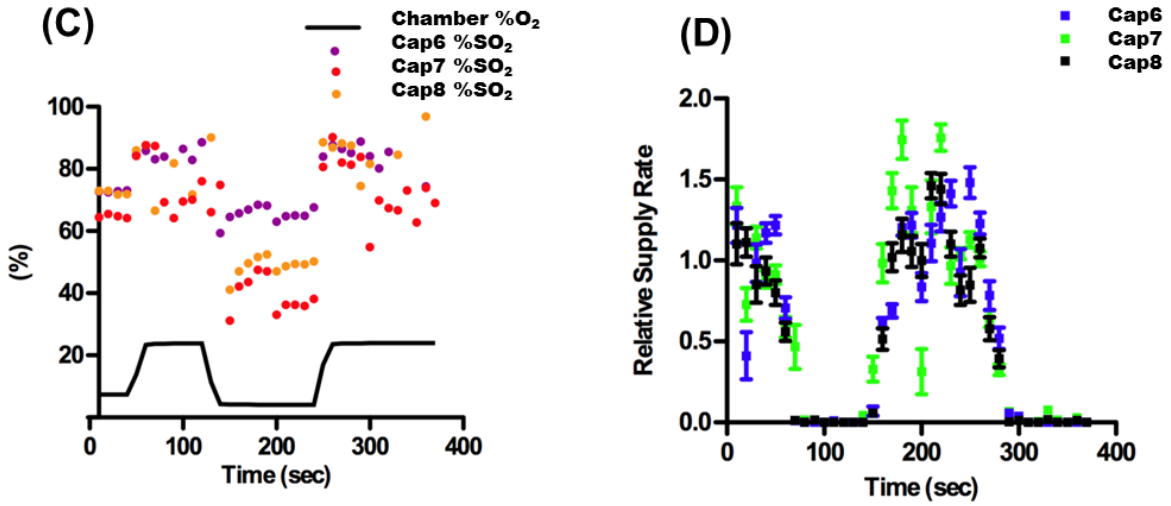
(C)
Chamber %O2
Cap6 %SO2
Cap7 %SO2
Cap8 %SO2
(%)
100
80
60
40
20
0
100
200
300
400
Time (sec)
(D)
Cap6
Cap7
Cap8
Relative Supply Rate
2.0
1.5
1.0
0.5
0.0
0
100
200
300
400
Time (sec)

Figure 4.10 (A, B) Selected capillary, Cap6, Cap7, and Cap8, are positioned directly over the rectangular micro-slit (1000 μm wide x 200 μm long) outlined by white dashed line. (A) The feeding arteriolar end upstream of the selected capillary and flow direction are indicated. Cap6 is supplied by one terminal branch of the arteriolar tree; Cap7 & Cap8 are supplied by another branch. Both terminal arterioles branch from the same parent arteriole. (B) Cap6, 7, 8 as visualised at 20X were analysed for changes in erythrocyte SO_2 and supply rate. Capillaries were analysed for changes in erythrocyte $\%SO_2$ and supply rate as O_2 levels in the chamber are oscillated in a square wave. The tissue is equilibrated at 5% (38 mmHg PO_2) O_2 level for 30 seconds. The O_2 level in the chamber is increased to 20% (~152 mmHg) then decreased to 2% (~15.2 mmHg) for a 120 second low O_2 challenge and back to 20%. An eight minute video sequence is captured beginning 2 min prior to the low O_2 challenge. (C) The erythrocyte SO_2 profiles in Cap 6, 7, and 8 are closely associated with chamber O_2. (D) Supply rates in the three selected capillaries were normalized against mean baseline supply rate to display relative changes. Change in capillary SO_2 result in very similar normalized supply rate responses in all three capillary segments.

4.3.5 Measuring changes in erythrocyte velocity and capillary hematocrit in response to local PO_2 perturbations and their contribution to observed supply rate changes

Next, we tested whether observed supply rate responses to altered erythrocyte SO_2 are due to changes in erythrocyte velocity or changes in capillary hematocrit. Changes in

erythrocyte SO_2, supply rate, erythrocyte velocity (μm/sec), and capillary hematocrit (%) in response to the local PO_2 perturbation were measured in three selected capillaries in a branching network (total of ~5 capillaries in a network). The three capillaries designated Cap9, Cap10, and Cap11 (Figure 4.11A, B) were positioned with their venular ends directly over the rectangular micro-slit and the feeding arteriole positioned upstream of the micro-slit (Figure 4.11B). The chamber O_2 levels were oscillated in two consecutive square waves (period ~400 seconds). The tissue was initially equilibrated at 5% (38 mmHg PO_2) O_2 level for 30 seconds. For each PO_2 oscillation, The O_2 level in the chamber was increased to 20% (at 50 sec) (152 mmHg) then decreased to 2% (15 mmHg) for a 100 second low O_2 challenge and back to 20%. A video sequence was recorded over an eight minute period beginning 2 minutes prior to the low O_2 challenge. The measured SO_2 profiles for all three capillaries were almost identical and were closely associated with the chamber O_2 level (Figure 4.11C). In Cap9, baseline mean SO_2 level was ~43.5±3.7% (N=4). The first increase in chamber O_2 to 20% resulted in a corresponding increase in mean SO_2 to ~81.8±10.5% (N=20). The mean SO_2 level then decreased to ~67.6±5.6% (N=20) in response to lowering chamber O_2 (2%) followed by an increase to ~93.7±8.6% (N=17) during recovery back to 20% O_2. The chamber O_2 levels were then decreased back to baseline (5%) bringing mean SO_2 level to ~63.0±8.1% (N=19). In Cap10, baseline mean SO_2 level was ~62.7±1.9% (N=4). The first increase in chamber O_2 to 20% resulted in a corresponding increase in mean SO_2 to ~81.6±6.7% (N=20). The mean SO_2 level then decreased to ~54.5±4.3% (N=20) in response to lowering chamber O_2 (2%) followed by an increase to ~87.9±4.0% (N=17) during recovery back to 20% O_2.

The chamber O_2 levels were then decreased back to baseline (5%) bringing mean SO_2 level to ~69.4±2.3% (N=19). In Cap11, baseline mean SO_2 level was ~58.7±3.5% (N=4). The first increase in chamber O_2 to 20% resulted in a corresponding increase in mean SO_2 to ~84.8±6.0% (N=20). The mean SO_2 level then decreased to ~47.7±9.5% (N=20) in response to lowering chamber O_2 (2%) followed by an increase to ~89.6±7.7% (N=17) during recovery back to 20% O_2. The chamber O_2 levels were then decreased back to baseline (5%) bringing mean SO_2 level to ~60.8±3.7% (N=19). Supply rate changes in response to altered SO_2 levels were observed in all three capillaries (Figure 4.11D) and were closely associated with changes in capillary hematocrit (Figure 4.11F) rather than erythrocyte velocity (Figure 4.11E). In Cap9, the baseline supply rate, velocity, and hematocrit were measured at ~7.0±0.2 RBC/sec, N=4, ~261.1±18.6 μm/sec, N=4, and ~9.5±1.2 %, N=4, respectively. Increasing chamber O_2 to 20% resulted in ~50% decrease in supply rate and a 17% decrease in hematocrit relative to baseline. A delay time of ~50 sec was measured for supply rate increase in response to decrease in SO_2 (at ~220 seconds). The supply rate level increased to slightly above baseline with a maximum of ~9.8 RBC/sec (at 420 sec) which was also associated with increase in hematocrit to a maximum of ~ 14.5% (Figure 4.11D,F). Increasing chamber O_2 back to 20% resulted in sharp and instantaneous decrease in supply rate to a minimum of ~1.5 RBC/sec (at 650 sec) and in hematocrit to a minimum of ~4%. Decreasing chamber O_2 level back to baseline resulted in supply rate increase to a maximum of ~11 RBC/sec and in hematocrit to ~10.3%. No changes in erythrocyte velocity were observed throughout the perturbation (Figure 4.11E). In Cap10, the baseline supply rate, velocity, and hematocrit were

measured at ~4.3±0.9 RBC/sec, N=4, ~158.4±2.0 μm/sec, N=4, and ~15.3±0.3 %, N=4, respectively. Increasing chamber O_2 to 20% resulted in ~25% decrease in supply rate and 11% decrease in hematocrit relative to baseline. The supply rate increased ~50 following decrease in SO_2 (at ~220 sec) to slightly above baseline with a maximum of ~8.3 RBC/sec which was also associated with increase in hematocrit to a maximum of ~18% (Figure 4.11D,F). Increasing chamber O_2 back to 20% resulted in sharp and instantaneous decrease in supply rate to a minimum of ~0.8 RBC/sec and in hematocrit to a minimum of ~10%. Decreasing chamber O_2 level back to baseline resulted in supply rate increase to a maximum of ~3.5 RBC/sec and in hematocrit to ~18%. The erythrocyte velocity increased by 25% in response to low O_2 in Cap10 but did not seem to change in response to high O_2 (Figure 4.11E). In Cap11, the baseline supply rate, velocity, and hematocrit were measured at ~6.2±0.6 RBC/sec, N=4, ~166.3±10.3 μm/sec, N=4, and ~12.8±0.6 %, N=4, respectively. Increasing chamber O_2 to 20% resulted in ~40% decrease in supply rate and 32% decrease in hematocrit relative to baseline. The supply rate increased ~50 sec following decrease in SO_2 (at ~220 seconds) to a maximum of ~6.8 RBC/sec which was also associated with increase in hematocrit to a maximum of ~16.2% (Figure 4.11D,F). Increasing chamber O_2 back to 20% resulted in sharp and instantaneous decrease in supply rate to a minimum of ~3.5 RBC/sec and in hematocrit to a minimum of ~10%. Decreasing chamber O_2 level back to baseline resulted in supply rate increase to a maximum of ~6.2 RBC/sec, matching that at first baseline, and increase in hematocrit to ~17.4%. No changes in erythrocyte velocity measured in Cap11 (Figure 4.11E).

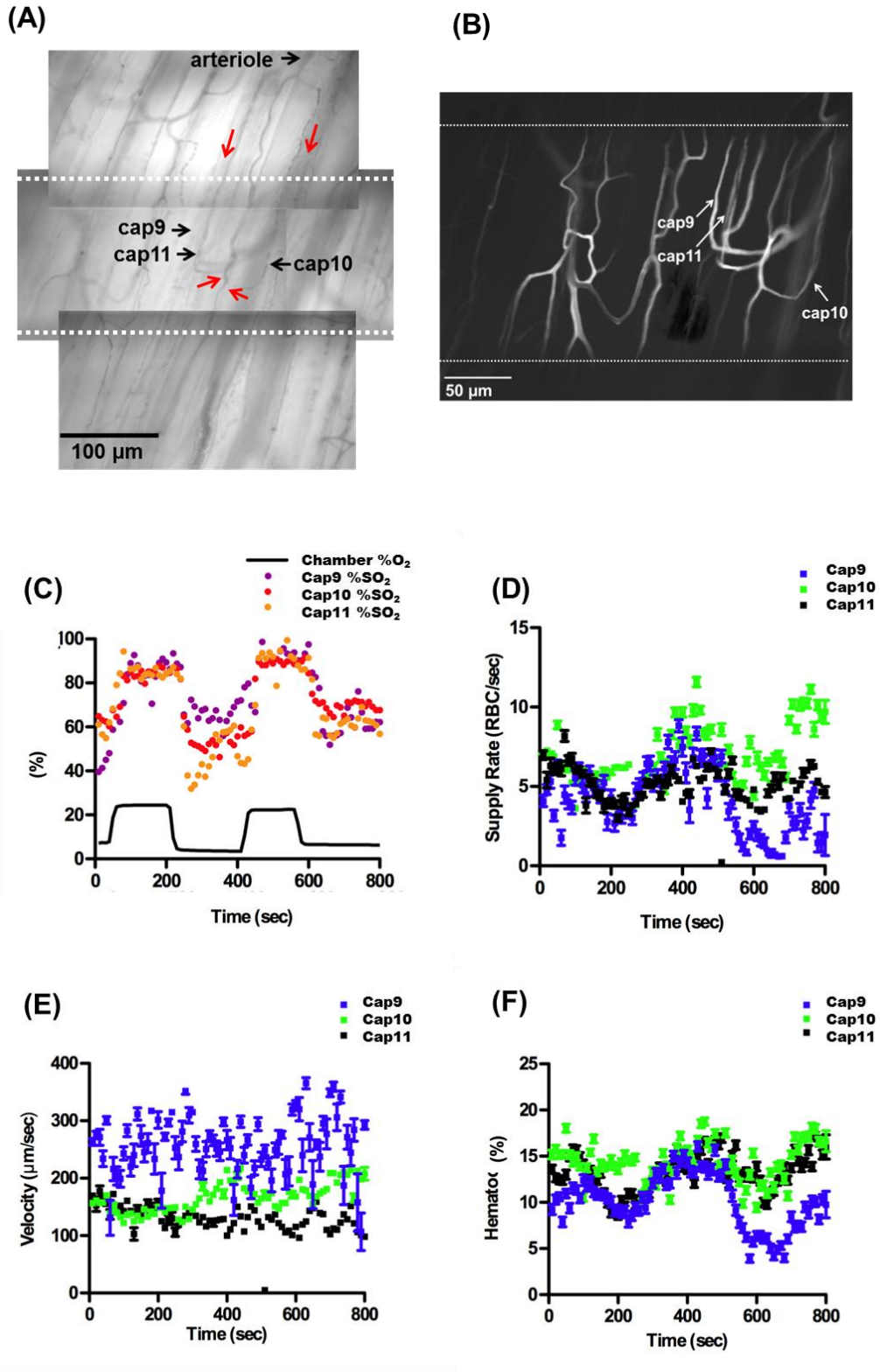
(A)
arteriole
cap9
cap11
cap10
100 µm
(B)
cap9
cap11
cap10
50 µm
(C)
Chamber %O2
Cap9 %SO2
Cap10 %SO2
Cap11 %SO2
(%)
Time (sec)
(D)
Cap9
Cap10
Cap11
Supply Rate (RBC/sec)
Time (sec)
(E)
Cap9
Cap10
Cap11
Velocity (µm/sec)
Time (sec)
(F)
Cap9
Cap10
Cap11
Hematoc (%)
Time (sec)

Figure 4.11 Selected capillaries (Cap 9, 10, and 11) are positioned directly over the rectangular micro-slit (1000 μm wide x 200 μm long) outlined by white dashed line. (A) The feeding arteriolar end upstream of the selected capillary and flow direction are indicated. The three selected capillaries all drain into a venule positioned deeper in the tissue (B) Cap9, 10, 11 as visualised at 20X were analysed for changes in erythrocyte SO_2 and supply rate. Capillaries were analysed for changes in erythrocyte SO_2 (%), supply rate (RBC/sec), mean erythrocyte velocity (μm/sec), and mean hematocrit (%) as O_2 levels in the chamber are oscillated in two consecutive square waves (period ~ 400 seconds). The tissue is equilibrated at 5% (38 mmHg PO_2) O_2 level for 30 seconds. The O_2 level in the chamber is increased to 20% (~152 mmHg) then decreased to 2% (~15.2 mmHg) for a 200 second then increased back to 20%. The chamber O_2 level is then lowered back to baseline level (5%). An eight minute video sequence is captured beginning 2 min prior to the low O_2 challenge. (C) The erythrocyte SO_2 profiles in Cap 1, 2, and 3 are closely associated with chamber O_2. (D) Change in capillary SO_2 result in supply rate responses. Supply rate changes seem to be more related to changes in (E) hematocrit rather than in (F) RBC velocity.

In order to determine if changes in capillary SO_2 and supply rate in response to the PO_2 perturbations are significant, the mean SO_2 and supply rate (± standard error of the mean SEM) in all capillaries analyzed in this study were calculated and plotted against condition in chamber. The mean SO_2 or supply rate levels at the various chamber O_2 conditions were compared using a 2way analysis of variance test (ANOVA) with $P<0.05$ (Figure 4.12). The results indicated the mean capillary erythrocyte SO_2 level during the low O_2 challenge is not significantly different relative to baseline ($P=0.1062$) yet significantly different relative to the high O_2 condition ($P<0.0001$). The corresponding mean supply rate level at low O_2 is significantly different relative to both baseline and high O_2 ($P<0.0001$). At high chamber O_2 condition, both the mean capillary erythrocyte SO_2 and supply rate levels are significantly different relative to baseline ($P<0.0001$) (Figure 4.12).

Finally, the correlation between mean capillary supply rate and erythrocyte SO_2 in capillaries affected by the PO_2 perturbations using the rectangular micro-slit design was tested. The mean supply rate levels calculated from all capillaries presented in this paper were plotted against corresponding mean SO_2 levels. The mean data points (± SEM) were fitted using a linear regression function in Prism v 5.0 and the goodness of fit was assessed using the R^2 value (Figure 4.13A). Also, the mean supply rate from individual representative capillaries analyzed in this study was plotted against corresponding SO_2 and correlation was assessed (Figure 4.13B-F). In general, there seems to be a linear relationship between mean supply rate and erythrocyte SO_2 level. Also, the slope of the

line of best fit seems to be related to the baseline supply rate level in the individual capillaries (Figure 4.13). There is a greater change in supply rate with change in SO_2 in capillaries with higher baseline supply rate level. This suggests the strength of the conducted signal is related to the erythrocyte supply rate.

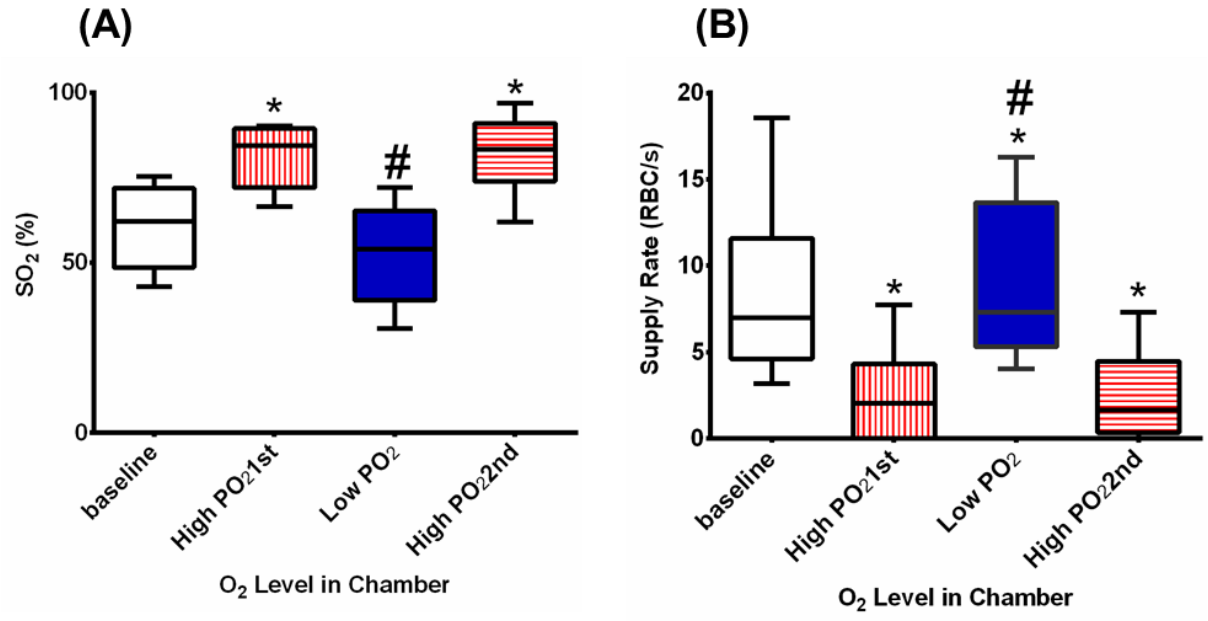

Figure 4.12 (A) mean capillary SO_2 ± SEM and (B) mean supply rate ± SEM at different O_2 conditions in chamber in a single PO_2 perturbation: baseline O_2 level (5%, 38 mmHg), first increase in O_2 level (20%, 152 mmHg), low O_2 level (2%, 15.2), second increase in O_2 level (20%) (Recovery). At each O_2 condition, the mean erythrocyte SO_2 or supply rate values at the last 10 second time point in all capillaries presented in this study were used to calculate the overall SO_2 or supply rate means. The means were compared using a 2way analysis of variance (ANOVA) ($P<0.05$) in Prism v 5.0. The symbol (*) represents

means significantly different relative to baseline mean. The symbol (#) represents the case in which the mean at low O_2 condition is significantly different from the means at the high O_2 conditions. Mean capillary SO_2 ± SEM is significantly altered relative to baseline in response to high O_2 yet not to low O_2. Corresponding mean capillary supply rates ± SEM levels at high and low O_2 are significantly different relative to baseline. The mean supply rate level at low O_2 is significantly different that at high O_2.

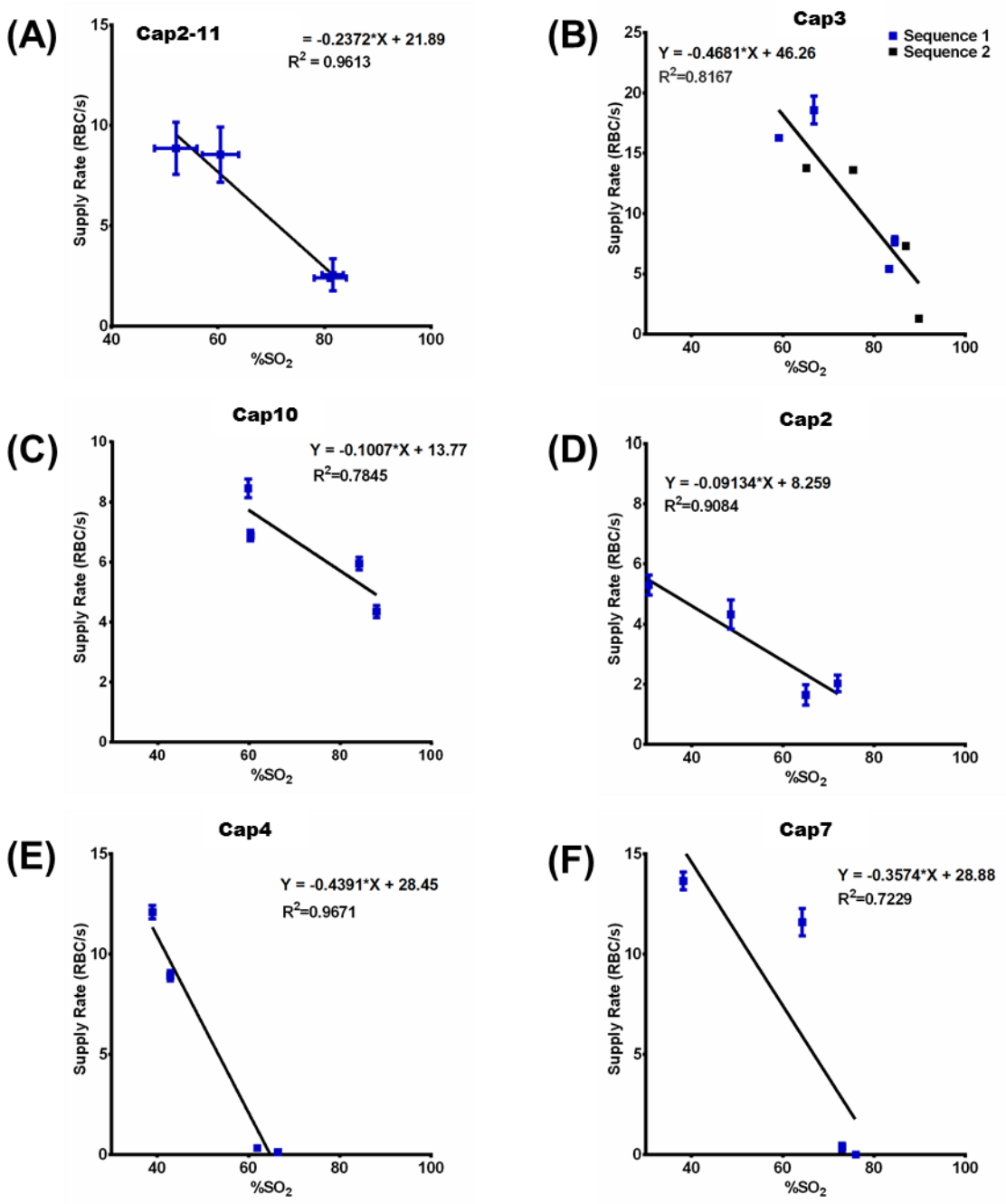

Figure 4.13 The correlation between mean capillary supply rate ± SEM and mean SO_2 measured from (A) all capillaries affected by the rectangular micro-slit in this study (Cap2-11) or (B-F) individual representative capillaries from each animal used in this

study (Cap2, 3, 4, 7, 10). The mean supply rate data points were fitted using a linear regression function in Prism v 5.0 and goodness of fit was assessed using an R^2 value. There seems to be a linear relationship between measured mean supply rate and erythrocyte SO_2.

4.4 Discussion

The finding that erythrocytes have the ability to release signaling molecules in response to alterations in the micro-vascular O_2 environment has transformed our perspective of the physiological role erythrocytes play (Ellsworth et al. 1995, Jia et al. 1996). Of special interest is the potent vasodilator, ATP, shown to be released from the erythrocyte in an SO_2 dependent manner (Jagger et al. 2001) as well as in response to other stimuli (Bergfeld and Forrester 1992, Sprague et al 2006). ATP release from the erythrocyte under low SO_2 conditions is proposed to trigger a conducted vasodilation (Ellsworth et al. 2009, Sprague and Ellsworth 2012). The micro-vascular response would be initiated by binding of ATP to P_{2y} receptors on the vascular endothelium resulting in conducted hyperpolarization in the endothelium and eventually in smooth muscle cells (You et al. 1999, Horiuchi et al. 2001, Sprague 2008, Ellsworth et al. 2009, Sprague and Ellsworth 2012, Ellis et al. 2012).

Multiple studies have examined the onset of conducted micro-vascular responses in the arterioles as well in the venules (Collins et al. 1998, Dulling and Berne, 1970, Duling, 1974, Jackson, 1987). Results have shown the capillary bed acts as a communication

medium through which the hyperpolarization signal would be conducted from the venules to upstream arterioles (Dietrich, 1989, Dietrich and Tyml, 1992a,b, Song and Tyml, 1993, Collins et al., 1998, Bagher and Segal, 2011). Since the largest SO_2 drop takes place in the capillary bed, it has been suggested as a major site for SO_2-dependent ATP release by the erythrocytes (Ellis et al 2012). The relatively long erythrocyte transit time in the capillary and the short ATP diffusion distance from every erythrocyte passing through the capillary bed to the endothelium would ensure temporal and spatial localization of the signal (Ellis et al 2012).

In order to examine SO_2-dependent signaling in the capillary bed, we have developed a novel technique, an O_2 micro-delivery system that allows for altering erythrocyte SO_2 in a limited number of selected capillaries *in vivo* (Figure 4.1) (Ghonaim et al. 2011). Combining this technique with existing DλIVVM technology allows for visualizing and measuring changes in blood flow parameters while simultaneously altering erythrocyte SO_2. Also, the extent of the PO_2 perturbation in the tissue and its effect on total magnitude of ATP in a capillary network have been modeled using O_2 exchange micro-outlets of various dimensions (Ghonaim et al. 2013). Our modelling data suggested there is a direct relationship between the number of capillaries affected by the PO_2 perturbation and the total magnitude of capillary ATP (Ghonaim et al. 2013). This is probably related to the number of activated endothelial cells in the affected capillaries within a network (Ellis et al. 2012). The model shows that the circular micro-outlet (100 μm in diameter) only affects one or two capillaries positioned directly above the micro-outlet and that the

change in capillary SO_2 is quickly dissipated downstream from the micro-outlet. Since the length of the endothelial cell in skeletal muscle is ~104 μm, a small number of endothelial cells would be affected by changes in erythrocyte SO_2 when using the circular micro-outlet. However, in the rectangular micro-slit (200 μm long x1000 μm wide), a larger number of capillaries are positioned above the micro-slit. Also, the PO_2 perturbation is carried much further downstream and the re-oxygenation effect is less rapid since the impact of the outlet affects a broader area. Therefore, based on the modeling results, a rectangular micro-slit was proposed to allow for stimulating a larger number of endothelial cells which would result in a larger hyperpolarization signal that can be conducted upstream. This micro-slit design was also proposed to ensure capillaries surrounding the network of interest will experience the same PO_2 drop when decreasing chamber O_2, which would minimize re-oxygenation and emphasize the response.

The PO_2 perturbation regime used in this study to alter capillary erythrocyte SO_2 involved a step change in chamber O_2 from 5% baseline condition (38 mmHg PO_2) to 20% (152 mmHg). The chamber O_2 level is then decreased for a low O_2 challenge from 20% to 2% (15 mmHg) followed by recovery back to 20%. Physiologically, at higher chamber O_2 level, the micro-slit would simulate a crossing arteriole acting as an O_2 source to underlying capillaries, while at lower chamber O_2 level, it would simulate a crossing venule acting to withdraw O_2. At the low O_2 level, the PO_2 (15 mmHg) is higher than the P_{50} (*k*) values reported by Golub and Pittman (2012) (10.5±0.8 mmHg) and Wilson et al. (2012) (~12 mmHg), hence, it is unlikely the tissue metabolism is altered

with the tested range of chamber O_2 values. Also, during the low O_2 challenge (15 mmHg), the narrow depth of the perturbation (Ghonaim et al. 2011, 2013) implies only the surface of muscle fibers at the tissue surface would be affected. This is supported by our statistical data, which indicate that erythrocytes do not sense significant changes in tissue PO_2 at low O_2 relative to baseline since measured SO_2 levels at the two respective conditions were not significantly different ($P<0.05$) (Figure 4.12). This allows us to examine the micro-vascular regulation mechanisms to altered PO_2 environments surrounding the capillaries without lowering PO_2 enough to disturb metabolic function. Finally, although alterations in tissue metabolism may result in the release of signaling molecules, no mechanism is yet elucidated that explains communication between muscle fibers and arterioles feeding a specific network of interest.

In this study, micro-vascular responses to altering SO_2 in multiple capillaries were examined *in vivo* using the rectangular O_2 micro-slit. The results were compared to the case in which a single capillary is positioned over a circular micro-outlet 100 µm in diameter (Figure 4.4). Although erythrocyte SO_2 could be altered in single capillaries crossing the circular micro-outlet, no corresponding supply rate responses were measured (Figure 4.4). This has been consistently observed when testing with the circular micro-outlet *in vivo* (data not shown). The observed time delay between chamber O_2 perturbations and capillary SO_2 changes would involve O_2 delivery time from the chamber O_2 inlet to tissue surface followed by the diffusion time into the capillary lumen and finally into the erythrocyte to bind hemoglobin. In capillaries upstream of slit, such

as the case with Cap4, the constant influx of erythrocytes with SO_2 unaffected by the micro-slit would require a larger change in the surrounding tissue PO_2 to show a marked effect on SO_2. This might explain the longer time delay measured for altering Cap4 SO_2 levels from the slit (Figure 4.7). The results indicate that in order to trigger supply rate changes in response to altered capillary SO_2, at least 3-4 capillaries in a branching network had to be affected by the PO_2 perturbation using our larger micro-slit design (200 µm long x 1000 µm wide rectangular slit) (Figure 4.5-4.11). The results confirmed our modeling data (Ghonaim et al. 2013), indicating there is a threshold for the minimum number of capillaries that need to be stimulated by low O_2 to elicit a micro-vascular response.

The results indicated there is a variable time delay from 10 to ~50-60 seconds in the supply rate response to low PO_2, while much shorter time delays were observed in the response to increased SO_2 (Figure 4.5, 4.6, 4.9 and 4.11). *In vitro* measurements of ATP release rates provide estimates in the order of 150-500 msec (Dietrich et al. 2000, Wan et al. 2008), hence the dynamics of ATP release alone would not account for the long time delay observed. The response time to low O_2 in the capillary would be dependent on other factors such as the time it takes to activate sufficient number of endothelial cells as well as on the geometry of the upstream arteriolar tree. At relatively higher supply rates, a single ATP releasing erythrocyte would activate a larger number of endothelial cells within a relatively shorter time (Ellis et al. 2012). On the other hand, slow moving erythrocytes will take longer to reach downstream endothelial cells (Ellis et al. 2012).

Our results show a dependence of the magnitude of the supply rate response on baseline supply rate in the capillary (prior to perturbation) (Figure 4.13). The calculated slope for the linear relationship between supply rate and SO_2 was smaller in capillaries with lower baseline supply rate (Cap2,10) (Figure 4.13). Also, the signal for increased supply rate is not solely originating within the single capillary being analyzed; rather the entire network affected by the micro-outlet is contributing to the strength of the signal. Depending on the geometry of the arteriolar tree upstream of the capillary of interest as well as the distance to the feeding arteriole, a minimum threshold number of capillary endothelial cells may need to be activated to elicit effective vasodilation. Finally, depending on the branching of the upstream arteriolar tree, there would be some time delay in adjusting the erythrocyte distribution at bifurcations during vasodilation and for this altered hematocrit travel downstream to ensure capillary units with various O_2 environments are receiving appropriate O_2 supply.

All capillaries selected for analysis in this study were positioned such that the feeding arteriole is further than 50 μm upstream of the micro-slit, which was modeled as the extent of radial O_2 diffusion from the micro-slit (Ghonaim et al. 2011, 2013). Therefore, since in our experiments only capillaries are affected by the PO_2 perturbations, the observed supply rate responses must be conducted to the upstream arterioles. This supports the hypothesis that micro-vascular signals are initiated and conducted from the capillary bed (Ellis et al. 2012). This is further strengthened by the observed reproducibility of the supply rate responses to altered capillary SO_2 (Figure 4.6 and 4.7).

Also, there seems to be variation in the magnitude of the supply rate response between different affected capillary networks. This might be related to the number of affected capillaries draining from the same upstream arteriole. An arteriole with a larger number of downstream branching capillary networks positioned over the micro-slit is anticipated to experience a larger hyperpolarization signal (Figure 4.7 and 4.10). Two factors that contribute to supply rate responses would include increase in erythrocyte velocity due to vasodilation of upstream arterioles and the increase in hematocrit due to preferential erythrocyte distribution at upstream bifurcations. Our results indicate that the observed supply rate responses in the capillaries are more related to changes in hematocrit rather than velocity (Figure 4.11). This supports the preferential erythrocyte distribution as an important mechanism of O_2 regulation in the microvasculature.

The results clearly demonstrate that at low PO_2, the O_2 regulation system is able to locally sense the decrease in erythrocyte SO_2 and to compensate for this altered O_2 environment by increasing the supply rate. According to our observations, the increase in supply rate results in a re-oxygenation effect by bringing larger number of O_2 carrying erythrocytes. Since the measured supply rate profiles are strongly associated with capillary erythrocyte SO_2 changes, we anticipate the response pathway involves the release of erythrocyte derived signaling molecules, most likely ATP. However, not only erythrocytes but also other cell types could be affected by the PO_2 perturbations in the selected capillary networks. It is unlikely that observed responses involve nerve stimulation since pentobarbital, which was used as the anesthetic throughout our

experiments, is known to severely suppress sympathetic nerve activity (Best et al. 1984). Further studies must be conducted to measure SO_2-dependent ATP release and more accurately assess its role in mediating observed micro-vascular responses.

One of the limitations in this study is the inability to resolve deeper tissue capillaries and hence measure their SO_2 and supply rate changes to assess their possible contribution to the overall signal *in vivo.* Another limitation is that in our computational model of radial O_2 diffusion from the micro-slit we do not take into account diffusion through the PDMS layer, which may increase the extent of radial diffusion. This might explain observing SO_2 changes in Cap5 (Figure 4.9) situated outside of the micro-slit. The complexities of the SO_2 mediated micro-vascular response demand analysis of SO_2 and hemodynamics locally in a capillary of interest as well as globally in the surrounding micro-vascular geometry.

In conclusion, SO_2-dependent signalling in selected capillaries has been tested *in vivo* using the O_2 micro-delivery system. The results indicated that capillaries are able to signal upstream arterioles for changes in supply rate in response to low SO_2. Also, there seems to be a threshold for the minimum number of capillaries that need to be stimulated by altered SO_2 in order to elicit the conducted supply rate responses. The dependency of supply rate responses on changes in hematocrit supports preferential erythrocyte distribution at upstream bifurcations in O_2 regulations. These findings provide valuable insight into O_2 transport and its regulation both in health and disease. The increased diffusion distance of O_2 in sepsis and the compromised vascular reactivity in Type-II

diabetes eventually lead to tissue hypoxia and organ failure (Goldman et al. 2004, Sprague et al. 2006; 2010). Understanding the fundamental mechanisms that govern O_2 regulation leads to the understanding of the pathophysiology underlying microvascular diseases. Further *in vitro* and *in vivo* work is needed to look at the dynamics of ATP release and its role in SO_2-dependent signalling and regulation.

4.5 References

Arciero J.C., Carlson B.E., Secomb T.W. (2008) Theoretical model of metabolic blood flow regulation: roles of ATP release by red blood cells and conducted responses. *Am. J. Physiol. Heart Circ. Physiol.* **295**: H1562–H1571

Bagher P., Segal S.S. (2011) Regulation of blood flow in the microcirculation: role of conducted vasodilation. *Acta. Physiol. (Oxf).* **202**:271-84

Bergfeld G.R., Forrester T. (1992) Release of ATP from human erythrocytes in response to a brief period of hypoxia and hypercapnia. *Cardiovasc. Res.* **26:**40–47

Best J.D., Taborsky G.J. Jr., Flatness D.E., Halter J.B. (1984) Effect of Pentobarbital Anesthesia on Plasma Norepinephrine Kinetics in Dogs. *Endocrinology.* **115:**3853-857

Campbell W.B., Gebremedhin D., Pratt P.F., Harder D.R. (1996) Identification of epoxyeicosatrienoic acids as endothelium derived hyperpolarizing factors. *Circ. Res.* **78:** 415–423

Carvalho H., Pittman, R.N. (2008) Longitudinal and radial gradients of PO_2 in the hamster cheek pouch microcirculation. *Microcirculation.***15:**215–224

Collins D.M., McCullough W.T., and Ellsworth M.L. (1998) Conducted vascular responses: communication across the capillary bed. *Microvasc. Res.* **56:**43–53

Cosby K., Partovi K.S., Crawford J.H., Patel R.P., Reiter C.D., Martyr S., Yang B.K., Waclawiw M.A., Zalos G., Xu X., Huang K.T., Shields H., Kim-Shapiro D.B., Schechter A.N., Cannon^{3rd} R.O., Gladwin M.T. (2003) Nitrite reduction to nitric oxide by deoxyhemoglobin vasodilates the human circulation. *Nat. Med.* **9:** 1498–1505

Dietrich H.H. (1989) Effect of locally applied epinephrine and norepinephrine on blood flow and diameter in capillaries of rat. *Microvasc. Res.* **38:**125–135

Dietrich H.H., Ellsworth M.L., Sprague R.S., Dacey R.G. Jr. (2000) Red blood cell regulation of microvascular tone through adenosine triphosphate. Am. J. Physiol. Heart. Circ. Physiol. **278:**H1294–H1298

Dietrich H.H., Horiuchi T., Xiang C., Falck J.R., Hongo K., Dacey R.G. Jr. (2008) Mechanism of ATP-induced local and conducted vasomotor responses in isolated rat cerebral penetrating arterioles. *J. Vasc. Res.* **46:**253–264

Dietrich H.H., Tyml K. (1992a) Microvascular flow response to localized application of norepinephrine on capillaries in rat and frog skeletal muscle. *Microvasc. Res.* **43**: 73-86

Dietrich H.H., Tyml K. (1992b) Capillary as a communicating medium in the microvasculature. *Microvasc. Res.* **43**: 87-99

Duling B. (1974) Oxygen sensitivity of vascular smooth muscle. II. In vivo studies. *Am. J. Physiol.* **227:**42–49

Duling B.R., Berne R.M. (1970) Longitudinal gradients in periarteriolar oxygen tension. A possible mechanism for the participation of oxygen in local regulation of blood flow. *Circ. Res.* **27:**669-678.

Ellis C.G., Bateman R.M., Sharpe M.D., Sibbald W.J., Gill R. (2002) Effect of a maldistribution of microvascular blood flow on capillary O2 extraction in sepsis. *Am. J. Physiol. Heart. Circ. Physiol.* **282:**156–164

Ellis C.G., Ellsworth M.L., Pittman R.N. (1990) Determination of red blood cell oxygenation in vivo by dual video densitometric image analysis. *Am. J. Physiol. Heart. Circ. Physiol.* **258:** H1216–H1223

Ellis C.G., Ellsworth M.L., Pittman R.N., Burgess W.L. (1992) Application of image analysis for evaluation of red blood cell dynamics in capillaries. *Microvasc. Res.* **44:** 214–225

Ellis C.G., Goldman D., Hanson M., Stephenson A.H., Milkovich S., Benlamri A., Ellsworth M.L., Sprague R.S. (2010) Defects in oxygen supply to skeletal muscle of prediabetic ZDF rats. Am. J. Physiol. Heart. Circ. Physiol. **298:**1661–1670

Ellis C.G., Milkovich S.L., Goldman D. (2012) What is the efficiency of ATP signaling from erythrocytes to regulate distribution of O_2 supply within the microvasculature? *Microcirculation*. **5**:440-450

Ellis C.G., Wrigley S.M., Groom A.C. (1994) Heterogeneity of red blood cell perfusion in capillary networks supplied by a single arteriole in resting skeletal muscle. *Circ Res.* **75:**357-368.

Ellsworth M.L., Ellis C.G., Goldman D., Stephenson A.H., Dietrich H.H., Sprague R.S. (2009) Erythrocytes: oxygen sensors and modulators of vascular tone. *Physiology*. **24:** 107–116

Ellsworth M.L., Ellis C.G., Popel A.S., Pittman R.N. (1994) Role of microvessels in oxygen-supply to tissue. *News Physiol Sci.* **9:**119-123.

Ellsworth M.L., Forrester T., Ellis C.G., and Dietrich H.H. (1995) The erythrocyte as a regulator of vascular tone. *Am. J. Physiol. Heart. Circ. Physiol.* **269:**H2155–H2161

Ellsworth M.L., Pittman R.N. (1986) Evaluation of photometric methods for quantifying convective mass transport in microvessels. *Am. J. Physiol. Heart. Circ. Physiol.* **251:**H869–H879

Ellsworth M.L., Pittman R.N., Ellis C.G. (1987) Measurement of hemoglobin oxygen saturation in capillaries. *Am. J. Physiol.* **252:**H1031–H1040

Forsyth A.M.,Wan J., Owrutsky P.D., Abkarian M., Stone H.A. (2011). Multiscale approach to link red blood cell dynamics, shear viscosity, and ATP release. *Proc. Natl. Acad. Sci. U. S. A.* **108**:10986–10991.

Fukao M., Mason H.S., Kenyon J.L., Horowitz B., Keef K.D. (2001) Regulation of BK(Ca) channels expressed in human embryonic kidney 293 cells by epoxyeicosatrienoic acid. *Mol. Pharmacol.* **59:**16–23

Ghonaim N.W., Lau L.W.M., Goldman D., Ellis C.G., Yang J. (2011) A micro-delivery approach for studying microvascular responses to localized oxygen delivery. *Microcirculation*. **18:**646–654

Ghonaim N.W., Fraser G.M., Ellis C.G., Yang J., and Goldman D. (2013) Modeling steady state SO_2-dependent changes in capillary ATP concentration using novel O_2 micro-delivery methods. *Front. Physiol.* **4:**260

Gladwin M.T., Crawford J.H., Patel R.P. (2004) The biochemistry of nitric oxide, nitrite, and hemoglobin: role in blood flow regulation. *Free. Radic. Biol. Med.* **36:**707-717

Goldman D., Bateman R.M., Ellis C.G. (2004) Effect of sepsis on skeletal muscle oxygen consumption and tissue oxygenation: interpreting capillary oxygen transport data using a mathematical model. *Am. J. Physiol. Heart. Circ. Physiol.* **287(6):**H2535-44.

Golub A.S., Pittman R.N. (2012) Oxygen dependence of respiration in rat spinotrapezius muscle in situ. *Am. J. Physiol. Heart. Circ. Physiol.* **303:**H47-H56

Horiuchi T., Dietrich H.H., Tsugane S., Dacey R.G. Jr. (2001) Analysis of purine- and pyrimidine-induced vascular responses in the isolated rat cerebral arteriole. *Am. J. Physiol. Heart. Circ. Physiol.* **280:**H767–H776

Ilie M., Foglietti V., Cianci E., Minotti A. (2003) Optimized deep wet etching of borosilicate glass through Cr-Au-resist mask. *SPIE.* **5227:**318–322

Jackson DN, Moore AW, Segal SS. (2010) Blunting of rapid onset vasodilatation and blood flow restriction in arterioles of exercising skeletal muscle with ageing in male mice. *J Physiol*. **588:**2269–2282.

Jackson W.F. (1987) Arteriolar oxygen reactivity: where is the sensor. *Am. J. Physiol. Heart. Circ. Physiol.* **253:**H1120–H1126

Jackson W.F., Duling B.R. (1983) The oxygen sensitivity of hamster cheek pouch arterioles. In vitro and in situ studies. *Circ Res.* **53:**515–525

Jagger J.E., Bateman R.M., Ellsworth M.L., Ellis C.G. (2001) Role of erythrocyte in regulating local O2 delivery mediated by hemoglobin oxygenation. *Am. J. Physiol. Heart. Circ. Physiol*. **280:**H2833–H2839

Japee S.A., Ellis C.G., Pittman R.N. (2004) Flow visualization tools for image analysis of capillary networks. *Microcirculation.* **11:**39–54

Japee S.A., Pittman R.N., Ellis C.G. (2005) A new video image analysis system to study red blood cell dynamics and oxygenation in capillary networks. *Microcirculation.* **12:**489–506

Jia L., Bonaventura C., Bonaventura J., Stamler J.S. (1996) S-nitrosohaemoglobin: a dynamic activity of blood involved in vascular control. *Nature.* **380:**221–226

Patel R.P., Hogg N., Spencer N.Y., Kalyanaraman B., Matalon S., Darley-Usmar V.M. (1999) Biochemical characterization of human Snitrosohemoglobin. Effects on oxygen binding and transnitrosation. *J. Biol. Chem.* **274:**15487-15492

Pries A.R., Secomb T.W., Gaehtgens P. (1996) Biophysical aspects of blood flow in the microvasculature. *Cardiovasc. Res.* **32:**654-667.

Segal S.S., Damon D.N., Duling B.R. (1989) Propagation of vasomotor responses coordinates arteriolar resistances. *Am. J. Physiol. Heart. Circ. Physiol.* **256:**H832–H837

Segal S.S., Duling B.R. (1989) Conduction of vasomotor responses in arterioles: a role for cell-to-cell coupling? *Am. J. Physiol. Heart. Circ. Physiol.* **256:**H838–H845

Song H., Tyml K. (1993) Evidence for sensing and integration of biological signals by the capillary network. *Am. J. Physiol.* **265**: H1235-H1242

Sprague R.S., Bowles E.A., Hanson M.S., DuFaux E., Sridharan M., Adderley S., Ellsworth M.L., Stephenson A.H. (2008) Prostacyclin analogues stimulate receptor-mediated cAMP synthesis and ATP release from rabbit and human erythrocytes. *Microcirculation.* **15**:461–471.

Sprague R.S., Ellsworth M.L. (2012) Erythrocyte-derived ATP and perfusion distribution: Role of intracellular and intercellular communication. *Microcirculation.* **5:**430-439

Sprague R.S., Ellsworth M.L., Stephenson A.H., Kleinhenz M., Lonigro A. (1998) Deformation-induced ATP release from red blood cells requires cystic fibrosis

transmembrane conductance regulator activity. *Am. J. Physiol. Heart. Circ. Physiol.* **275:**H1726–H1732

Sprague R.S., Ellsworth M.L., Stephenson A.H., Lonigro A.J. (2001) Participation of cAMP in a signal-transduction pathway relating erythrocyte deformation to ATP Release. *Am. J. Physiol. Cell. Physiol.* **281**:C1158–C1164

Sprague R.S., Stephenson A.H., Bowles E.A., Stumpf M.S., and Lonigro A.J. (2006) Reduced expression of Gi in erythrocytes of humans with Type 2 Diabetes is associated with impairment of both cAMP generation and ATP release. *Diabetes.* **55**: 3588-359

Sridharan M., Sprague R.S., Adderley S.P., Bowles E.A., Ellsworth M.L., Stephenson A.H. (2010b). Diamide decreases deformability of rabbit erythrocytes and attenuates low oxygen tension-induced ATP release. *Exp. Biol. Med. (Maywood).* **235**:1142–1148.

Srivastava N., Davenport R.D., Burns M.A. (2005) Nanoliter viscometer for analyzing bloodplasma and other liquid samples. *Anal. Chem.* **77:**383–392

Stamler J.S., Jia L., Eu J.P., McMahon T.J., Demchenko I.T., Bonaventura J., Gernert K., Piantadosi C.A. Blood flow regulation by S-nitrosohemoglobin in the physiological oxygen gradient. *Science.* **276:**2034–2037

Stein J.C., Ellis C.G., Ellsworth M.L. (1993) Relationship between capillary and systemic venous PO_2 during nonhypoxic and hypoxic ventilation. *Am. J. Physiol.* **265:**H537-H542

Swain D.P., Pittman R.N. (1989) Oxygen exchange in the microcirculation of hamster retractor muscle. *Am J Physiol Heart Circ Physiol.* **256:**H247-H255

Tsai A.G., Johnson P.C., Intaglietta M. (2003) Oxygen gradients in the microcirculation. *Physiol. Rev.***83:**933-963.

Tyml K., Budreau C.H. (1991) A new preparation of rat extensor digitorum longus muscle for intravital investigation of the microcirculation. *Int. J. Microcirc. Clin. Exp.* **10:**335–343

Tyml K., Ellis C.G., Safranyos R.G., Fraser S., Groom A.C. (1981) Temporal and spatial distributions of red cell velocity in capillaries of resting skeletal muscle, including estimates of red cell transit times. *Microvasc. Res.* **22:**14-31.

Wan J., Ristenpart W.D., Stone H.A. (2008) Dynamics of shear-induced ATP release from red blood cells. Proc. Natl. Acad. Sci. USA. **105:**16432–16437

Wilson, D.F., Harrison, D.K., Vinogradov S.A. (2012) Oxygen, pH, and mitochondrial oxidative phosphorylation. *J. Appl. Physiol.* **113:**1838-1845

You J.P., Johnson T.D., Marrelli S.P., Bryan R.M. Jr. (1999) Functional heterogeneity of endothelial P2 purinoceptors in the cerebrovascular tree of the rat. *Am. J. Physiol. Heart. Circ. Physiol*. **277:**H893–H900

Chapter 5

5 General Discussion

5.1 Summary of results and conclusions

5.1.1 Developing a technology for investigating SO_2 – dependent micro-vascular responses

In Chapter 2, we described an O_2 micro-delivery device developed for localized O_2 exchange to the micro-vascular bed (Ghonaim et al. 2011). This novel technology, which is based on the full gas exchange chamber setup (Jagger et al. 2005, Ellis et al. 2010; 2012, Ghonaim et al. 2011), allows for altering erythrocyte SO_2 in selected capillaries *in vivo*. Unlike the use of superfusion solutions for O_2 exchange from tissue (Duling 1974, Jackson and Duling 1983), our device delivers O_2 in a gas mixture. This ensures more effective diffusion of O_2 to the tissue and resolves the limitation of poor O_2 solubility in saline superfusion solutions. The use of micro-fabrication techniques to pattern O_2 exchange micro-outlets of desired dimensions is unique and versatile. Delivering O_2 form the micro-outlet to tissue surface in direct interface is more effective than traditional micro-pipetting technique employed for local delivery of substances. Both *in vitro* and *in vivo* testing as well as our modeling data indicate the radial diffusion away from the outlet is limited which better localizes and emphasizes of the signal (Ghonaim et al. 2011). In contrast, the use of micro-pipetting technique, also referred to as Pico-spritzing

(Riemann et al. 2010), results in tissue concentration of substances to be less than that in the pipette. Also, the delivery of substances in liquid form may result in washing away important signaling molecules from tissue surface. The results presented in Chapter 2 describe an effective and novel methodology that allowed for first time examination of micro-vascular responses emerging from the capillary bed due to highly localized stimulus.

5.1.2 Computational modeling of localized PO_2 perturbations on total ATP magnitude in a 3D capillary network

Prior to examining micro-vascular response to altering erythrocyte SO_2 in selected capillaries using the O_2 exchange system, it was critical that we have initial predictions on the relationship between the number of affected capillaries and the magnitude of the SO_2-dependent signal. Chapter 3 describes the development of a computational model to investigate the effect of limited O_2 exchange at the surface of a tissue with an idealized parallel capillary array on total ATP concentration (Ghonaim et al. 2013). Modeling local O_2 exchange through various sized micro-outlets indicated that a rectangular micro-slit (200 µm long x 1000 µm wide) has the optimal dimensions for altering hemoglobin SO_2 in sufficient number capillaries to generate effective changes in total [ATP]. These results suggested there is a threshold for the minimum number of capillaries that need to be stimulated *in vivo* by low tissue PO_2 to induce a conducted micro-vascular response. Modeling SO_2 changing in arterioles and their possible contribution to the net change in

[ATP] indicated the effect of the arteriole is minimal. However, the data also indicated the arterioles would act as O_2 sources thus influencing the O_2 distribution. The modeling data presented in Chapter 3 provide important insights into the use of our novel O_2 micro-delivery device in studying micro-vascular O_2 regulation in the capillaries *in vivo* (Ghonaim et al. 2013).

5.1.3 Examining SO_2-dependent micro-vascular response using our developed technology *in vivo*

Chapter 4 investigated conducted micro-vascular signalling and response to varying SO_2 in selected capillaries on the micro-vascular bed *in vivo*. O_2 availability to specific capillary networks at the surface of muscle tissue (rat Extensor Digitorum Longus) was controlled using our novel O_2 micro-delivery approach. Based on our modelling data presented in Chapter 3 (Ghonaim et al. 2013), a rectangular micro-slit (1000 μm wide x 200 μm long) patterned in ultrathin glass/plastic sheet using state-of-the-art microfabrication techniques was used as the micro-outlet of optimal dimension for O_2 exchange. Combining our novel technology with existing dual wavelength *in vivo* video microscope (DλIVVM) techniques allowed for oscillating O_2 levels at tissue surface while simultaneously measuring and recording blood flow responses. Digitized video sequences were then processed for changes in capillary hemodynamic parameters and erythrocyte SO_2. Our *in vivo* results confirmed our modelling data presented in chapter 3 and indicated there is a threshold for the minimum number of capillaries that need to be

stimulated by local PO_2 perturbations in order to induce a conducted micro-vascular response. Although erythrocyte SO_2 level can be measured in single capillaries flowing over an O_2 micro-outlet down to 100 μm in diameter, at least 3-4 capillaries need to be stimulated within a branching capillary network in order to induce a micro-vascular response. Micro-vascular responses originate from a capillary network positioned directly over the outlet with the feeding arteriolar end positioned upstream of the O_2 micro-outlet, which suggests the responses are conducted. The results presented in chapter 4 indicate we have successfully designed an effective and novel tool for limiting O_2 exchange to specific capillaries on the micro-vascular bed to understand fundamental mechanisms of micro-vascular O_2 regulation.

By careful selection of the minimum PO_2 in the chamber and using fixed levels of CO_2 and temperature, the observed flow responses are due solely to the microvascular response to varying O_2 levels and not to changes in tissue metabolism. Although the maximum PO_2 in the chamber is higher than most tissues would experience, the resulting changes in erythrocyte SO_2 in these capillaries are within the normal physiological range. Hence, the rectangular micro-outlet used in these studies does mimic a crossing arteriole or venule and does demonstrate that the capillary bed is capable of signaling its local O_2 environment to the upstream arterioles to appropriately regulate O_2 supply (Ellis et al. 2012).

5.2 Future Directions

The micro-delivery approach for localized O_2 exchange presented and verified in my thesis serves as promising tool for investigating the fundamental mechanisms for regulating micro-vascular O_2 supply. Our results support the hypothesis that capillaries are able to signal upstream arterioles for changes in erythrocyte supply rate in response to changes in capillary erythrocyte SO_2. The strong relationship between erythrocyte SO_2 changes and supply rate supports the role of the erythrocyte in SO_2-depndent release of signaling molecules. The next step would be to unravel the details of the signaling mechanisms mediating the observed vasomotor responses. The involvement of SO_2-dependent ATP release and endothelium hyperpolarization could be indirectly examined using transgenic mice expressing Ca^{2+} reporter genes in the capillary endothelium (Bagher et al. 2011). However, the possible role of other erythrocyte derived vasodilators as well as signalling from other cell types surrounding the capillaries of interest must also be examined. Currently, computational modelling and *in vitro* testing is conducted at Dr. Ellis' laboratory to investigate the dynamics of ATP release from erythrocyte due to low O_2 (Sove et al. 2013). The findings would elucidate the possible contribution of time scales involved in ATP release to the observed response delay to low O_2. The use of transgenic mice would also help examine the association between the number of activated endothelial cells and the onset of supply rate responses by visualizing the Ca^{2+} release *in vivo*.

The effectiveness of our novel micro-delivery system can be extended to allow for precise and accurate delivery of substances in liquid form (e.g. drugs) in addition to gaseous substances (e.g. O_2, CO). In an *in vivo* experimental setup, in which substances are delivered to interfaced live tissue or cell culture, localized responses can be stimulated. The novel use of our micro-delivery system in conjunction with existing DλIVVM and analysis techniques would provide greater insight into the underlying physiological mechanisms in normal and disease models. The micro-delivery system is a versatile tool with wide range of applications. The system can be used to provide localized stimulus to tissue or cell culture *in vivo*. Also, the developed micro-delivery system could be modified to be used as a diagnostic tool. By placing sensor films over the micro-slit, biological fluids (e.g. plasma, blood, urine...etc) flowing through chamber could be assayed for the presence or release of certain substances.

5.3 References

Bagher P., Davis M.J., Segal S.S. (2011) Visualizing calcium responses to acetylcholine convection along endothelium of arteriolar networks in Cx40 ^{BAC}-GCaMP2 transgenic mice. *Am. J .Physiol. Heart. Circ. Physiol.* **301:**H794-H802A

Duling B. (1974) Oxygen sensitivity of vascular smooth muscle. II. In vivo studies. *Am. J. Physiol.* **227:**42–49

Ellis C.G., Goldman D., Hanson M., Stephenson A.H., Milkovich S., Benlamri A., Ellsworth M.L., Sprague R.S. (2010) Defects in oxygen supply to skeletal muscle of prediabetic ZDF rats. Am. J. Physiol. Heart. Circ. Physiol. **298:**1661-1670

Ellis C.G., Milkovich S.L., Goldman D. (2012) What is the efficiency of ATP signaling from erythrocytes to regulate distribution of O_2 supply within the microvasculature? *Microcirculation*. **5**:440-450

Ghonaim N.W., Lau L.W.M., Goldman D., Ellis C.G., Yang J. (2011) A micro-delivery approach for studying microvascular responses to localized oxygen delivery. *Microcirculation.* **18:**646–654

Ghonaim N.W., Fraser G.M., Ellis C.G., Yang J., and Goldman D. (2013) Modeling steady state SO_2-dependent changes in capillary ATP concentration using novel O_2 micro-delivery methods. *Front. Physiol.* **4:**260

Jagger J.E., Ellis C.G. (2005) Effect of varying oxygen levels on hemodynamic and oxygen transport parameters in the EDL muscle of the rat. *FASEB. J.* **19 (suppl 4):**A731-A731

Riemann M., Rai A., Ngo A.T., Dziegiel M.H., Holstein-Rathlou N-H., Torp-Pedersen C. (2010). Oxygen-dependant vasomotor responses are conducted upstream in the mouse cremaster microcirculation. *J. Vac. Res.* **48:**79-89.

Sove R.J., Ghonaim N.W., Goldman D., Ellis C.G. (2013) A Computational Model of a Microfluidic Device to Measure Oxygen-Dependent ATP Release from Erythrocytes. *PLOS ONE.* Manuscript submitted for publication.

.

APPENDIX A

Western

AUP Number: 2008-066-06

PI Name: Ellis, Christopher G

AUP Title: Characterization Of The Dynamics Of The Local O2 Regulatory System And Role Of The Red Blood Cell In Situ

Approval Date: 08/08/2012

Official Notice of Animal Use Subcommittee (AUS) Approval: Your new Animal Use Protocol (AUP) entitled "Characterization Of The Dynamics Of The Local O2 Regulatory System And Role Of The Red Blood Cell In Situ

" has been APPROVED by the Animal Use Subcommittee of the University Council on Animal Care. This approval, although valid for four years, and is subject to annual Protocol Renewal.2008-066-06::5

This AUP number must be indicated when ordering animals for this project.

Animals for other projects may not be ordered under this AUP number.

Purchases of animals other than through this system must be cleared through the ACVS office. Health certificates will be required.

The holder of this Animal Use Protocol is responsible to ensure that all associated safety components (biosafety, radiation safety, general laboratory safety) comply with institutional safety standards and have received all necessary approvals. Please consult directly with your institutional safety officers.

Submitted by: Copeman, Laura

on behalf of the Animal Use Subcommittee

University Council on Animal Care

APPENDIX B

JOHN WILEY AND SONS LICENSE
TERMS AND CONDITIONS

Jul 10, 2013

This is a License Agreement between Nour Ghonaim ("You") and John Wiley and Sons ("John Wiley and Sons") provided by Copyright Clearance Center ("CCC"). The license consists of your order details, the terms and conditions provided by John Wiley and Sons, and the payment terms and conditions.

All payments must be made in full to CCC. For payment instructions, please see information listed at the bottom of this form.

License Number	3175131400554
License date	Jun 23, 2013
Licensed content publisher	John Wiley and Sons
Licensed content publication	Microcirculation
Licensed content title	A Micro-Delivery Approach for Studying Microvascular Responses to Localized Oxygen Delivery
Licensed copyright line	© 2011 John Wiley & Sons Ltd
Licensed content author	NOUR W. GHONAIM,LEO W. M. LAU,DANIEL GOLDMAN,CHRISTOPHER G. ELLIS,JUN YANG
Licensed content date	Nov 18, 2011
Start page	646
End page	654
Type of use	Dissertation/Thesis
Requestor type	Author of this Wiley article
Format	Print and electronic
Portion	Full article
Will you be translating?	No

JOHN WILEY AND SONS LICENSE
TERMS AND CONDITIONS

Jun 24, 2013

This is a License Agreement between Nour Ghonaim ("You") and John Wiley and Sons ("John Wiley and Sons") provided by Copyright Clearance Center ("CCC"). The license consists of your order details, the terms and conditions provided by John Wiley and Sons, and the payment terms and conditions.

All payments must be made in full to CCC. For payment instructions, please see information listed at the bottom of this form.

License Number	3175140849955
License date	Jun 24, 2013
Licensed content publisher	John Wiley and Sons
Licensed content publication	Journal of Physiology
Licensed content title	Regulation of blood flow distribution in skeletal muscle: role of erythrocyte-released ATP
Licensed copyright line	© 2012 The Authors. The Journal of Physiology © 2012 The Physiological Society
Licensed content author	Mary L. Ellsworth,Randy S. Sprague
Licensed content date	Oct 15, 2012
Start page	4985
End page	4991
Type of use	Dissertation/Thesis
Requestor type	University/Academic
Format	Print and electronic
Portion	Figure/table
Number of figures/tables	1
Original Wiley figure/table number(s)	Figure 1
Will you be translating?	No

Curriculum Vitae

Name:	Nour Ghonaim
Post-secondary Education and Degrees:	Western University London, Ontario, Canada 2004-2008 B.M.Sc.
	Western University London, Ontario, Canada Started M.E.Sc. in 2008, transferred to Ph.D. in 2009 2009-2013 Ph.D.
Honours and Awards:	Western Graduate Research Scholarship (WGRS) 2008-2013
	Natural Sciences and Engineering Research Council of Canada (NSERC) Alexander Graham Bell Canada Graduate Scholarship 2008-2012
	Ontario Graduate Scholarship (OGS)-*Declined* 2008-2012
	The Microcirculatory Society, Inc. Graduate Student Travel Award July 2012

The University of Western Ontario Entrance Continuing Scholarship
2004-2008

Queen Elizabeth II Aiming for the Top Scholarship
2004-2008

Andrew and Sarah Hamilton Scholarship
2005-2008

Dean's Honor List
2004-2008

The University of Western Ontario Gold Medal-Scholar's Electives Program
2008

The University of Western Ontario, Department of Biochemistry, Fourth Year Course Awards
2008
Kaney Ebisuzaki Award for Biochemistry 410a course.
William R. Litchfield Award for Biochemistry 430b course
Fourth year course prize for Biochemistry 465a course
Fourth year course prize for Biochemistry 440a course

Natural Sciences and Engineering Research Council of Canada (NSERC) Undergraduate Student Research Award (USRA)
May 2006-August 2006, May 2007-August 2007

Surface Science Western (SSW) best summer project award
August 2006

Related Work Experience:

Teaching Assistant
Western University
January 2009- May 2009, September 2009- December 2009

Student Research Fellowship
Western University, Department of Biochemistry
May2008 - August 2008

Publications:

Sove R.J., Ghonaim N.W., Goldman D., Ellis C.G. A Computational Model of a Microfluidic Device to Measure Oxygen-Dependent ATP Release from Erythrocytes. PLOS ONE. Manuscript submitted for publication. 2013.

Ghonaim N.W., Fraser G.M., Ellis C.G., Yang J., and Goldman D. (2013) Modeling steady state SO_2-dependent changes in capillary ATP concentration using novel O_2 micro-delivery methods. Frontiers in Physiology. **4:**260

Ghonaim, N. W., Lau, W. M., Goldman, D., Ellis, C.G., and Yang, J. (2011) A micro-delivery approach for studying microvascular responses to localized oxygen delivery. Microcirculation. 18(8), 646-654

Nieradko, M., Ghonaim, N.W., Xi, L., Nie, H.-Y., Francis, J., Grizzi, O., Yeung, K.K.C, Lau, W.M. (2007) Primary ion fluence dependence in time-of-flight SIMS of a self-assembled monolayer of octadecylphosphonic acid molecules on mica discussion of static limit. Canadian Journal of Chemistry. 85(12), 1075–1082

Ghonaim, N.W., Nieradko, M., Xi, L., Nie, H.-Y., Francis, J.T., Grizzi, O., Yeung, K.K.C., and Lau, W.M. (2008). Primary ion fluence dependence in time-of-flight SIMS of self-assembled monolayer of alkyl thiol molecules on Au(111)—Discussion of static limit. Applied Surface Science. 255, 1029-1032

Invited Talks:

Ghonaim, N. W., Lau, W. M., Goldman, D., Ellis, C.G., and Yang, J. (2012) Local Oxygen Signaling: ATP and the Conducted Vasomotor Response. The 3rd Annual Smooth Muscle Underground Conference (SMUG). Westin Hotel, 400 West Broadway, San Diego, California. April 20, 2012 (International Meeting)

Conference Presentations:

Ghonaim, N. W., Lau, W. M., Goldman, D., Ellis, C.G., and Yang, J. (2012) Local Oxygen Signaling: ATP and the Conducted Vasomotor Response. Poster Presented at The Joint Meeting of the British Microcirculation Society and The Microcirculatory Society, Keble College, University of Oxford, Oxford, United Kingdom. July 4, 2012 (International Conference)

Ghonaim, N. W., Lau, W. M., Goldman, D., Ellis, C.G., and Yang, J. (2011) Conducted microvascular response to localized oxygen delivery using a novel micro-delivery approach. Poster Presented at The Joint Meeting of the European Society for Microcirculation (ESM) and the German Society of Microcirculation and Vascular

Biology (GfMVB)**,** Ludwig-Maximilians-University, Munich, Germany. October 14, 2011 (International Conference)

Ghonaim, N. W., Lau, W. M., Goldman, D., Ellis, C.G., and Yang, J. (2010) Evaluating microvascular response to localized oxygen level variations by *in vivo* video microscopy. Poster Presented at The 9th World Congress for Microcirculation, Maison de la Chimie, Paris, France. September 27, 2010 (International Conference). Abstract published in Microcirculation.

Ghonaim, N. W., Lau, W. M., Goldman, D., Ellis, C.G., and Yang, J. (2009) Evaluating microvascular response to localized oxygen level variations by *in vivo* video microscopy. Poster Presented at The fall meeting of the Microcirculatory Society "Frontiers in Microcirculation: Control Processes and Clinical Applications", University of Missouri, Colombia, USA. October 17, 2009 (Regional Conference). Abstract published in Microcirculation.

Ghonaim, N.W., Nieradko, M., Xi, L., Nie, H.-Y., Francis, J.T., Grizzi, O., Yeung, K.K.C., and Lau, W.M. (2008) Primary ion fluence dependence in time-of-flight SIMS of self-assembled monolayer of alkyl thiol molecules on Au(111)—Discussion of static limit. Poster Presented at the Secondary Ion Mass Spectrometry (SIMS) XVI International Conference, Kanazawa, Japan. October 29, 2007.